Discrete Dynamics in Nature and Society

Recent Trends in Dynamical Systems on Time Scales

Special Issue Editor in Chief: Youssef N. Raffoul
Guest Editors: Jeffrey Neugebauer, Cemil Tunç, and George Eid

Recent Trends in Dynamical Systems on Time Scales

Discrete Dynamics in Nature and Society

Recent Trends in Dynamical Systems on Time Scales

Special Issue Editor in Chief: Youssef N. Raffoul
Guest Editors: Jeffrey Neugebauer, Cemil Tunç, and George Eid

Editorial Board

Contents

Hindawi
Discrete Dynamics in Nature and Society
Volume 2018, Article ID 2176510, 2 pages
https://doi.org/10.1155/2018/2176510

Editorial

Recent Trends in Dynamical Systems on Time Scales

George Eid,[1] Jeffry Neugebauer,[2] Youssef Naim Raffoul,[3] and Cemil Tunç[4]

[1]*Faculty of Natural & Applied Sciences, Notre Dame University-Louaize, Lebanon*
[2]*Eastern Kentucky University, Department of Mathematics, USA*
[3]*University of Dayton, Department of Mathematics, Dayton Ohio 45469-2316, USA*
[4]*Department of Mathematics, Faculty of Sciences, Yuzuncu Yil University, Turkey*

Correspondence should be addressed to Youssef Naim Raffoul; yraffoul1@udayton.edu

Received 20 June 2018; Accepted 20 June 2018; Published 19 July 2018

The theory of time scales was created to unify continuous and discrete analysis. Difference and differential equations can be studied simultaneously by studying dynamic equations on time scales. Recently, there has been much interest in the study of dynamical systems on time scales due to their applications to real world problems, such as electric circuits and insect populations. Many application problems can be studied more precisely using dynamical systems on time scales. Subjects such as existence and uniqueness of solutions, stability, Floquet theory, periodicity, stability, and boundedness of solutions can be studied more precisely and generally by utilizing dynamical systems on time scales. Recently, many researchers have been looking at the applications of time scales in various economics models utilizing optimal control theory and developing more realistic models in economics and population dynamics using time scales.

This special issue places its emphasis on the study of the applications of dynamical system on time scales; such applications include economics models utilizing optimal control theory, fractional calculus, and the development of new population models.

All manuscripts submitted to this special issue went through a thorough peer-refereeing process. Based on the reviewers' reports, we collected 5 original research articles by more than 17 active international researchers on dynamical systems.

To be more comprehensive, we give a description of each article in this special issue by providing a short editorial note summarizing each paper.

W. Kumam et al. established sufficient conditions for existence of solutions to the coupled systems of higher-order hybrid fractional differential equations with three-point boundary conditions. They apply the coupled fixed point theorem of Krasnoselskii type to form adequate conditions for existence of solutions to the proposed system. They provided a nice example as an application.

Z. Wang et al. proposed a new docking system that is more efficient and requires less makespan. A cross-docking system is proposed with multiple receiving and shipping dock doors. Their objective is to find the best door assignments and the sequences of trucks in the principle of products distribution to minimize the total makespan of cross-docking. To solve the problem that is regarded as a mixed integer linear programming (MILP) model, three metaheuristics, namely, harmony search (HS), improved harmony search (IHS), and genetic algorithm (GA), are proposed. Furthermore, the fixed parameters are optimized by Taguchi experiments to improve the accuracy of solutions further. Finally, they ended the paper with several numerical examples to evaluate the performances of proposed algorithms.

Z. Liu et al. proposed a new fractional two-dimensional triangle function combination discrete chaotic map (2D-TFCDM) with the discrete fractional difference. Bifurcation behaviors, drawing the bifurcation diagrams, the largest Lyapunov exponent plot, and the phase portraits of the proposed map, were studied. On the application side, they apply the proposed discrete fractional map into image encryption with the secret keys ciphered by Menezes-Vanstone Elliptic Curve Cryptosystem (MVECC). Finally, the image encryption algorithm is analyzed in four main aspects that indicate that the proposed algorithm is better than others.

Z. Wei et al. studied the dynamics of a stochastic modified Bazykin predator-prey system with Lévy jumps. First, they show that the system has a unique global positive solution and

discovered new properties of solutions. Then, some sufficient conditions for persistence and extinction are derived by Itô formula and some inequalities on stochastic analysis. Numerical simulations are provided to check the main results.

Z. Li and D. Tan established an analytical framework studying the optimal dynamic pricing and advertising strategies for online providers; it shows how the strategies are influenced by the videos available time and the viewers' emotional factor. They create the two-stage strategy of revenue models involving a single fee mode and a mixed fee-free mode and find out the optimal fee charge and advertising level of online video services. According to the results, the optimal video price and ads volume dynamically vary over time. The viewer's aversion level to advertising has direct effects on both the volume of ads and the number of viewers who have selected low-quality content. The optimal volume of ads decreases with the increase of ads-aversion coefficient, while it increases as the quality of videos increases. The results also indicate that, in the long run, a pure fee mode or free mode is the optimal strategy for online providers.

Acknowledgments

We would like to thank the editorial board members of this journal, for their support in making this special issue a reality.

George Eid
Jeffrey Neugebauer
Youssef Naim Raffoul
Cemil Tunç

Hindawi
Discrete Dynamics in Nature and Society
Volume 2018, Article ID 8479101, 7 pages
https://doi.org/10.1155/2018/8479101

Research Article

Persistence and Extinction of a Stochastic Modified Bazykin Predator-Prey System with Lévy Jumps

Zhangzhi Wei,[1,2] Zheng Wu,[1] Ling Hu,[1] and Lianglong Wang[1]

[1]*School of Mathematical Sciences, Anhui University, Hefei 230601, China*
[2]*School of Mathematics and Statistics, Suzhou University, Suzhou 234000, China*

Correspondence should be addressed to Lianglong Wang; wangll@ahu.edu.cn

Received 7 December 2017; Accepted 12 March 2018; Published 29 April 2018

Academic Editor: Jeffrey Neugebauer

This paper is devoted to the dynamics of a stochastic modified Bazykin predator-prey system with Lévy jumps. First, we show that the system has a unique global positive solution and give some properties of solutions. Then, some sufficient conditions for persistence and extinction are derived by Itô formula and some inequalities on stochastic analysis. At last, some simulations are provided to check the main results.

1. Introduction

In population biology, construction of models and relevant qualitative analysis are popular fields [1, 2]. In the last few decades, many predator-prey models with functional and numerical responses have been proposed and studied extensively. Particularly, ratio-dependent functional response is common in some classical literature [3–5].

Alexeev and Bazykin firstly proposed a Bazykin system [1]

$$\begin{aligned}\dot{x}(t) &= x(t)\left(a - bx(t) - \frac{cy(t)}{1 + Ax(t)}\right),\\ \dot{y}(t) &= y(t)\left(-g - hy(t) + \frac{fx(t)}{1 + Ax(t)}\right),\end{aligned} \tag{1}$$

where $x(t)$ and $y(t)$ are the size of prey and predator at time t. a, b, c, f, g, and m are positive constants (some details refer to [1]).

Considering the ratio effect in hunting process of predation, Haque built a modified Bazykin system [2]

$$\begin{aligned}\dot{x}(t) &= x(t)\left(a - bx(t) - \frac{cy(t)}{y(t) + Ax(t)}\right),\\ \dot{y}(t) &= y(t)\left(-g - hy(t) + \frac{fx(t)}{y(t) + Ax(t)}\right),\end{aligned} \tag{2}$$

of which dynamical behavior near equilibrium point and bifurcation are observed. System (2) is more reasonable and many researchers began to pay more attention on it. Its generalized forms have been investigated and a lot of results were obtained [6–8].

However, in the natural world, environmental noise is everywhere, and the growth rate of the populations is not constants. In this case, many systems are described by stochastic differential equations driven by Brownian motion of the actual research. For example, [9] studied the following stochastic modified Bazykin system:

$$\begin{aligned}dx(t) &= x(t)\left(a - bx(t) - \frac{cy(t)}{y(t) + Ax(t)}\right)dt\\ &\quad + \alpha x(t)\,dw_1(t),\\ dy(t) &= y(t)\left(-g - hy(t) + \frac{fx(t)}{y(t) + Ax(t)}\right)dt\\ &\quad + \beta y(t)\,dw_2(t),\end{aligned} \tag{3}$$

where $w_1(t)$ and $w_2(t)$ are two independent Wiener processes defined on a complete probability space $(\Omega, \mathcal{F}, \{\mathcal{F}_t\}_{t\geq 0}, P)$ and α and β stand for the level of the white noises. Some sufficient conditions for persistence and extinction are obtained.

Recently, the stochastic differential equation driven by jump has drawn more and more researchers' attention [10–17]. This is mainly according to sudden perturbation of environment, such as toxic contamination of water, torrential flood, and hurricane. Motivated by the above, this paper considers the following stochastic modified Bazykin system with Lévy jumps:

$$\begin{aligned} dx(t) &= x(t^-)\left(a - bx(t) - \frac{cy(t)}{y(t) + Ax(t)}\right)dt \\ &\quad + \alpha x(t)\, dw_1(t) \\ &\quad + \int_Z \gamma(u)\, x(t^-)\, \widetilde{N}(dt, du), \\ dy(t) &= y(t^-)\left(-g - hy(t) + \frac{fx(t)}{y(t) + Ax(t)}\right)dt \\ &\quad + \beta y(t)\, dw_2(t) \\ &\quad + \int_Z \eta(u)\, y(t^-)\, \widetilde{N}(dt, du), \end{aligned} \tag{4}$$

where $x(t^-)$, $y(t^-)$ represent the left limit of $x(t)$, $y(t)$. $\widetilde{N}(dt, du) = N(dt, du) - \lambda(du)dt$, N is a Poisson random measure, and λ is the characteristic measure of N on a measurable subset $Z \subset R^+ = (0, +\infty)$ with $\lambda(Z) < +\infty$.

The rest of this paper is organized as follows. In Section 2, some properties of positive solutions to system (4) are discussed. In Section 3, the main results for persistence and extinction are given. Finally, the simulation results show the validity of our results.

2. Properties of Positive Solutions

Throughout this paper, we require that $w_1(t)$, $w_2(t)$, and N are independent and

$$\begin{aligned} &(H_1) \quad \max\left\{\int_Z (\gamma(u))^p \lambda(du), \int_Z (\eta(u))^p \lambda(du)\right\} < +\infty, \quad p > 0 \\ &(H_2) \quad \max\left\{\int_Z (\ln(1 + \gamma(u)))^2 \lambda(du), \int_Z (\ln(1 + \eta(u)))^2 \lambda(du)\right\} < +\infty \end{aligned} \tag{5}$$

with $\min\{1 + \gamma(u), 1 + \eta(u)\} > 0$, $u \in Z$.

First, we present the global existence of positive solutions.

Lemma 1. *For any given value $(x_0, y_0) \in R^2_+$, system (4) has a unique positive solution $X(t) = (x(t), y(t))$ on $t \geq 0$ and the solution will be in R^2_+ a.s. (almost surely).*

Proof. Let $u(t) = \ln x(t)$, $v(t) = \ln y(t)$, then we consider the following system:

$$\begin{aligned} du(t) &= \left[a - be^{u(t)} - \frac{ce^{v(t)}}{e^{v(t)} + Ae^{u(t)}} - \frac{\alpha^2}{2}\right. \\ &\quad \left. - \int_Z (\gamma(u) - \ln(1 + \gamma(u)))\lambda(du)\right]dt \\ &\quad + \alpha dw_1(t) + \int_Z \ln(1 + \gamma(u))\widetilde{N}(dt, du), \\ dv(t) &= \left[-g - he^{v(t)} + \frac{fe^{u(t)}}{e^{v(t)} + Ae^{u(t)}} - \frac{\beta^2}{2}\right. \\ &\quad \left. - \int_Z (\eta(u) - \ln(1 + \eta(u)))\lambda(du)\right]dt \\ &\quad + \beta(t)\, dw_2(t) + \int_Z \ln(1 + \eta(u))\widetilde{N}(dt, du) \end{aligned} \tag{6}$$

with initial date $u(0) = \ln x_0, v(0) = \ln y_0$ on $t \geq 0$. Since the coefficients of system (6) are locally Lipschitz continuous, then there is a unique local solution on $[0, T]$ a.s., where T is blow-up time. Then $x = e^{u(t)}$, $y = e^{v(t)}$ is the unique positive local solution to system (4) with initial data $x_0 > 0$, $y_0 > 0$. We will show that $T = +\infty$, and this mean the solution is global.

Consider the following equations:

$$\begin{aligned} dX_1(t) &= X_1(t)(a - c - bX_1(t))\, dt + \alpha X_1(t)\, dw_1(t) \\ &\quad + \int_Z X_1(t)\gamma(u)\widetilde{N}(dt, du), \\ X_1(0) &= x_0, \\ dX_2(t) &= X_2(t)(a - bX_2(t))\, dt + \alpha X_2(t)\, dw_1(t) \\ &\quad + \int_Z X_2(t)\gamma(u)\widetilde{N}(dt, du), \\ X_2(0) &= x_0, \\ dY_1(t) &= Y_1(t)\left[-g + \frac{f}{A} - \left(h + \frac{f}{A^2 X_1(t)}\right)Y_1(t)\right]dt \\ &\quad + \beta Y_1(t)\, dw_2(t) \\ &\quad + \int_Z Y_1(t)\eta(u)\widetilde{N}(dt, du), \\ Y_1(0) &= y_0, \end{aligned}$$

$$
\begin{aligned}
dY_2(t) &= Y_2(t)\left(-g + \frac{f}{A} - hY_2(t)\right)dt \\
&\quad - \beta Y_2(t)\, dw_2(t) \\
&\quad + \int_Z Y_2(t)\,\eta(u)\,\widetilde{N}(dt, du), \\
Y_2(0) &= y_0.
\end{aligned} \tag{7}
$$

By the comparison theorem of stochastic differential equation, we conclude that

$$
\begin{aligned}
X_1(t) \le x(t) \le X_2(t), \\
Y_1(t) \le y(t) \le Y_2(t)
\end{aligned} \tag{8}
$$

a.s.

According to [10], we can give

$$
\begin{aligned}
X_1(t) &= \frac{\exp\{(a - c - \rho_1)t + \alpha w_1(t) + \kappa_1(t)\}}{x_0^{-1} + b\int_0^t \exp\{(a - c - \rho_1)s + \alpha w_1(s) + \kappa_1(s)\}\,ds}, \\
X_2(t) &= \frac{\exp\{(a - \rho_1)t + \alpha w_1(t) + \kappa_1(t)\}}{x_0^{-1} + b\int_0^t \exp\{(a - \rho_1)s + \alpha w_1(s) + \kappa_1(s)\}\,ds}, \\
Y_1(t) &= \frac{\exp\{(-g + f/A - \rho_2)t + \beta w_2(t) + \kappa_2(t)\}}{y_0^{-1} + \int_0^t (h + f/A^2 X_1(t)) \exp\{(f/A - g - \rho_2)s + \beta w_2(s) + \kappa_2(s)\}\,ds}, \\
Y_2(t) &= \frac{\exp\{(-g + f/A - \rho_2)t + \beta w_2(t) + \kappa_2(t)\}}{y_0^{-1} + h\int_0^t \exp\{(f/A - g - \rho_2)s + \beta w_2(s) + \kappa_2(s)\}\,ds},
\end{aligned} \tag{9}
$$

where

$$
\begin{aligned}
\rho_1 &= 0.5\alpha^2 + \int_Z [\gamma(u) - \ln(1 + \gamma(u))]\,\lambda(du), \\
\rho_2 &= 0.5\beta^2 + \int_Z [\eta(u) - \ln(1 + \eta(u))]\,\lambda(du), \\
\kappa_1(t) &= \int_0^t \int_Z \ln(1 + \gamma(u))\,\widetilde{N}(dt, du), \\
\kappa_2(t) &= \int_0^t \int_Z \ln(1 + \eta(u))\,\widetilde{N}(dt, du).
\end{aligned} \tag{10}
$$

Because $t \ge 0$ is the existence range of solutions $X_1(t)$, $X_2(t)$, $Y_1(t)$, $Y_2(t)$, that means $T = +\infty$. □

Next, we will show the asymptotic property of the solution to system (4).

Theorem 2. *The solutions of system (4) are bounded in mean.*

Proof. Let $V_1 := V_1(t, x) = e^t x^p$ $(p > 0)$. Direct computation, by the formula $EV_1(t, x(t)) - EV_1(0, x_0) = E\int_0^t LV(s)ds$ [18], now leads to

$$
E\left(e^t x^p\right) = x^p(0) + E\int_0^t LV_1 ds, \tag{11}
$$

where

$$
\begin{aligned}
LV_1 &= e^t x^p + e^t p x^p \left[a - bx + 0.5(p - 1)\alpha^2\right. \\
&\quad \left. - \frac{cy}{y + Ax} + \int_Z \left[(1 + \gamma(u))^p - 1\right]\lambda(du)\right] \le e^t x^p \\
&\quad + e^t p x^p \left[a - bx + 0.5(p - 1)\alpha^2\right. \\
&\quad \left. + \int_Z \left((1 + \gamma(u))^p - 1\right)\lambda(du)\right].
\end{aligned} \tag{12}
$$

From actual meanings of parameters and assumption (H_1), we get that

$$
\begin{aligned}
x^p + p x^p &\left[a - bx + 0.5(p - 1)\alpha^2\right. \\
&\left. + \int_Z \left[(1 + \gamma(u))^p - 1\right]\lambda(du)\right]
\end{aligned} \tag{13}
$$

is bounded. There exists a constant $K_1 > 0$, such that

$$
Ee^t x^p(t) \le x_0^p + \int_0^t K_1 e^s ds \tag{14}
$$

when $1 + x^p + px^p[a - bx + 0.5(p - 1)\alpha^2 \int_Z [(1 + \gamma(u))^p - 1]\lambda(du)] > 0$; otherwise $Ee^t x^p(t) \le x_0^p$. Let $K_2 = \max\{K_1, 0\}$; we have $Ee^t x^p(t) \le x_0^p + K_2 e^t$. Denote $K = K_2 + x_0^p$, then $Ex^p(t) \le K < +\infty$. Similarly, $Ey^p(t) \le K$. □

3. Persistence and Extinction

In this section, some properties of the solutions of system (4) are investigated. Some sufficient conditions for persistence and extinction are shown. To proceed, some definitions and lemma are as follows.

Definition 3 (see [19]). (1) The population x is called to be extinct if $x(t) \to 0$ $(t \to \infty)$ a.s.

(2) The population x is called to be persistent if $\lim\inf_{t\to\infty}(1/t)\int_0^t x(s)ds > 0$ a.s.

(3) System (4) is called to be persistent if populations x and y are all persistent a.s.

Lemma 4 (see [20]). *Under (H_1) and (H_2), suppose $Y(t) \in C(\Omega \times [0,+\infty), R^+)$.*

(1) If there exist three positive T, k, k_0 such that

$$\ln Y(t) \le kt - k_0 \int_0^t Y(s)\,ds + \sum_{i=1}^n k_i w_i(t) + \sum_{i=1}^n c_i \int_0^t \int_Z \ln\left(1+\gamma(u)\right)\widetilde{N}(ds,du) \quad a.s. \tag{15}$$

for all $t > T$, where k_i, c_i are constants, then

$$\limsup_{t\to\infty} \frac{1}{t}\int_0^t Y(s)\,ds \le \frac{k}{k_0} \quad a.s. \tag{16}$$

If $k < 0$ and other conditions are the same, then $\lim_{t\to\infty} Y(t) = 0$ a.s.

(2) If there exist three positive T, k, k_0 such that

$$\ln Y(t) \ge kt - k_0 \int_0^t Y(s)\,ds + \sum_{i=1}^n k_i w_i(t) + \sum_{i=1}^n c_i \int_0^t \int_Z \ln\left(1+\gamma(u)\right)\widetilde{N}(ds,du) \quad a.s. \tag{17}$$

for all $t > T$, where k_i, c_i are constants, then

$$\liminf_{t\to\infty} \frac{1}{t}\int_0^t Y(s)\,ds \ge \frac{k}{k_0} \quad a.s. \tag{18}$$

Now, the main results about persistence and extinction of system (4) are as follows.

Theorem 5. *(1) The populations x and y are extinct if $a-\rho_1 < 0$ a.s.*

(2) The population x is persistent and y is extinct if $a - c - \rho_1 > 0$, $f/A - g - \rho_2 < 0$ a.s.

(3) The populations x and y are persistent if $a - c - \rho_1 > 0$, $f/A - g - \rho_2 > 0$ a.s.

Proof. (1) By using the Itô formula, the following formulas are hold:

$$\begin{aligned} d\ln x(t) &= \left(a - bx(t) - \frac{cy(t)}{y(t)+Ax(t)} - \rho_1\right)dt + \alpha dw_1(t) + \int_Z \ln\left(1+\gamma(u)\right)\widetilde{N}(dt,du), \\ d\ln y(t) &= \left(-g - hy(t) + \frac{fx(t)}{y(t)+Ax(t)} - \rho_2\right)dt + \beta dw_2(t) + \int_Z \ln\left(1+\eta(u)\right)\widetilde{N}(dt,du). \end{aligned} \tag{19}$$

Calculated by integral, we have the following form:

$$\begin{aligned} \ln x(t) - \ln x(0) &= \left(a-\rho_1\right)t + \alpha w_1(t) - \int_0^t bx(s)\,ds - \int_0^t \frac{cy(s)}{y(s)+Ax(s)}ds + \kappa_1(t) \\ &\le \left(a-\rho_1\right)t - b\int_0^t x(s)\,ds + \alpha w_1(t) + \kappa_1(t). \end{aligned} \tag{20}$$

Then by Lemma 4, note that $a < \rho_1$, and therefore $x(t) \to 0$ $(t \to \infty)$ (population x is extinct) a.s. Then, for arbitrarily small $\varepsilon > 0$, there exist a sufficiently large T, when $t > T$, and we have $x(t) < \varepsilon$ and

$$d\ln y(t) \le \left(-g - hy(t) + \varepsilon - \rho_2\right)dt + \beta dw_2(t) + \int_Z \ln\left(1+\eta(u)\right)\widetilde{N}(dt,du), \tag{21}$$

where $-g - \varepsilon - \rho_2 < 0$. It is clear that $y(t) \to 0$ $(t \to \infty)$ (population y is extinct) a.s. Thus (1) is correct.

(2) From (1), the following forms are clear.

$$\begin{aligned} \ln x(t) - \ln x(0) &= \left(a-\rho_1\right)t + \alpha w_1(t) - \int_0^t bx(s)\,ds - \int_0^t \frac{cy(s)}{y(s)+Ax(s)}ds + \kappa_1 \\ &\le \left(a-\rho_1\right)t - b\int_0^t x(s)\,ds + \alpha w_1(t) + \kappa_1, \\ \ln x(t) - \ln x(0) &= \left(a-\rho_1\right)t + \alpha w_1(t) - \int_0^t bx(s)\,ds - \int_0^t \frac{cy(s)}{y(s)+Ax(s)}ds + \kappa_1 \\ &\ge \left(a-c-\rho_1\right)t - b\int_0^t x(s)\,ds + \alpha w_1(t) + \kappa_1. \end{aligned} \tag{22}$$

Then by Lemma 4, we have

$$\frac{a-c-\rho_1}{b} \le \liminf_{t\to\infty}\frac{1}{t}\int_0^t x(s)\,ds \le \limsup_{t\to\infty}\frac{1}{t}\int_0^t x(s)\,ds \le \frac{a-\rho_1}{b} \quad \text{a.s.} \tag{23}$$

Therefore the population x is persistent in mean. For population y, we have

$$d\ln y(t) \le \left(-g - hy(t) + \frac{f}{A} - \rho_2\right)dt + \beta dw_2(t) + \int_Z \ln\left(1+\eta(u)\right)\widetilde{N}(dt,du). \tag{24}$$

From Lemma 4 and condition $f/A - g - \rho_2 < 0$, we know that $y(t) \to 0$ $(t \to \infty)$ (i.e., population y is extinct) a.s.

(3) In view of above, we can conclude the following when $a - c - \rho_1 > 0$, $g/A - g - \rho_2 > 0$, and

$$\begin{aligned} \ln y(t) - \ln y(0) &\geq \left(-g + \frac{f}{A} - \rho_2\right) t \\ &\quad - \left(h + \frac{f}{A^2 X_{1*}}\right) \int_0^t y(s)\, ds \\ &\quad + \beta w_2(t) + \kappa_2(t). \end{aligned} \tag{25}$$

Then, we have

$$\begin{aligned} \frac{f/A - g - \rho_2}{h + f/A^2 X_{1*}} &\leq \liminf_{t\to\infty} \frac{1}{t} \int_0^t y(s)\, ds \\ &\leq \limsup_{t\to\infty} \frac{1}{t} \int_0^t y(s)\, ds \\ &\leq \frac{f/A - g - \rho_2}{h}, \quad \text{a.s.}, \end{aligned} \tag{26}$$

where X_{1*} is the minimum of $X_1(t) > 0$.

It is clear that population y is persistent. □

Remark 6. For (1) in Theorem 5, it implies that the population x of extinction a.s. leads to the extinction of population y a.s. As shown in Figure 2, the simulations also affirm this point. In Figure 2, we can see that population x becomes extinct, and after a while, population y becomes extinct.

4. Numerical Simulations

We will demonstrate our results with the help of numerical simulations by using the Euler-Maruyama scheme [21, 22]. In numerical simulation, randomly selected parameters are as follows $a = 0.55$, $b = 0.21$, $c = 0.15$, $f = 0.93$, $h = 0.11$, $A = 1.23$, $\alpha = 0.75$, $\beta = 0.73$, $Z = (0, +\infty)$, and $\lambda(Z) = 1$, with simulation time span $T = 50$ and step size $\Delta t = T/N$, where $N = 2^{12}$. The initial data is $(x_0, y_0) = (0.3, 0.11)$ in Figure 2, and others are $(3, 1)$.

(1) As illustrated in Figure 1, we choose $\gamma(u) = 0.99$, $\eta(u) = 0.85$, then $\rho_1 = a - 0.5\alpha^2 - \int_Z (\gamma(u) - \ln(1 + \gamma(u)))\lambda(du) = 0.58312$, $\rho_2 = a - 0.5\beta^2 - \int_Z (\eta(u) - \ln(1 + \eta(u)))\lambda(du) = 0.50126$, and $a - \rho_1 = -0.03312 < 0$, $f/A - g - \rho_2 = -0.09517 < 0$. By Theorem 5, the populations x and y are extinct a.s. Numerical experiments verify the correctness of (1) in Theorem 5.

(2) As illustrated in Figure 2, we choose $\gamma(u) = 0.99$, $\eta(u) = 0.05$, then $\rho_1 = a - 0.5\alpha^2 - \int_Z (\gamma(u) - \ln(1 + \gamma(u)))\lambda(du) = 0.58312$, $\rho_2 = a - 0.5\beta^2 - \int_Z (\eta(u) - \ln(1 + \eta(u)))\lambda(du) = 0.26766$, and $a - \rho_1 = -0.03312 < 0$, $f/A - g - \rho_2 = 0.13844 > 0$. By Theorem 5, the populations x and y are extinct a.s. Numerical experiments also verify the correctness of (1) in Theorem 5.

(3) As shown in Figure 3, we choose $\gamma(u) = 0.15$, $\eta(u) = 0.91$, then $\rho_1 = a - 0.5\alpha^2 - \int_Z (\gamma(u) - \ln(1 + \gamma(u)))\lambda(du) = 0.29149$, $\rho_2 = a - 0.5\beta^2 - \int_Z (\eta(u) - \ln(1 + \eta(u)))\lambda(du) = 0.52935$, and $a - c - \rho_1 = 0.048512 > 0$, $f/A - g - \rho_2 = -0.12325 < 0$. By Theorem 5, the population x is persistent a.s. and population y is extinct a.s. The correctness of (2) in Theorem 5 is verified.

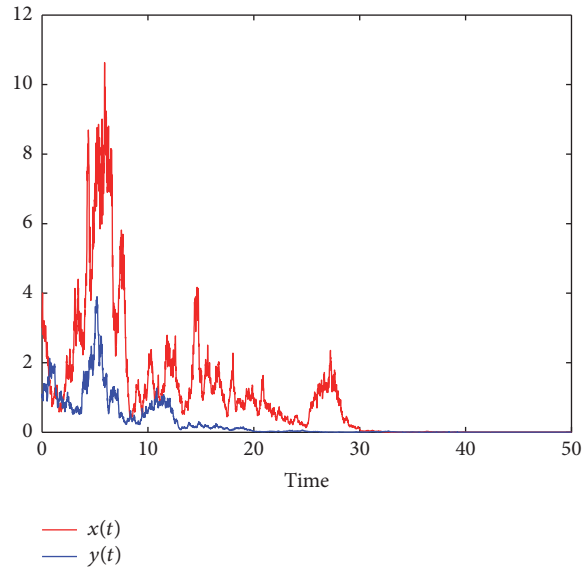

Figure 1

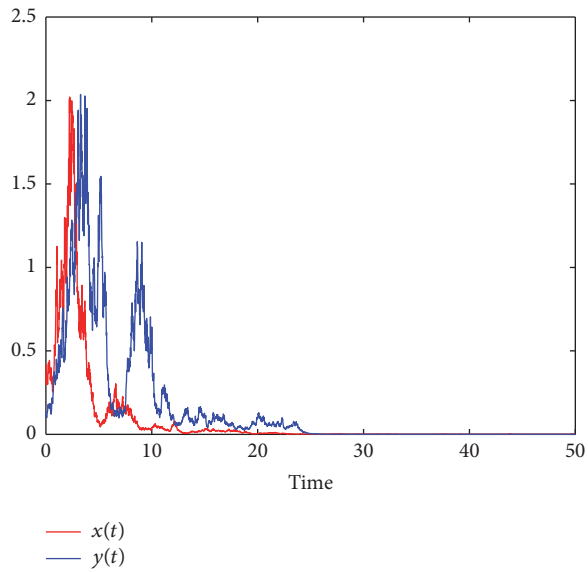

Figure 2

(4) As shown in Figure 4, we choose $\gamma(u) = 0.15$, $\eta(u) = 0.05$, then $\rho_1 = a - 0.5\alpha^2 - \int_Z (\gamma(u) - \ln(1 + \gamma(u)))\lambda(du) = 0.29149$, $\rho_2 = a - 0.5\beta^2 - \int_Z (\eta(u) - \ln(1 + \eta(u)))\lambda(du) = 0.52935$, and $a - c - \rho_1 = 0.048512 > 0$, $f/A - g - \rho_2 = 0.13844 > 0$. By Theorem 5, the populations x and y are persistent a.s. The validity of correctness of (3) in Theorem 5 is verified.

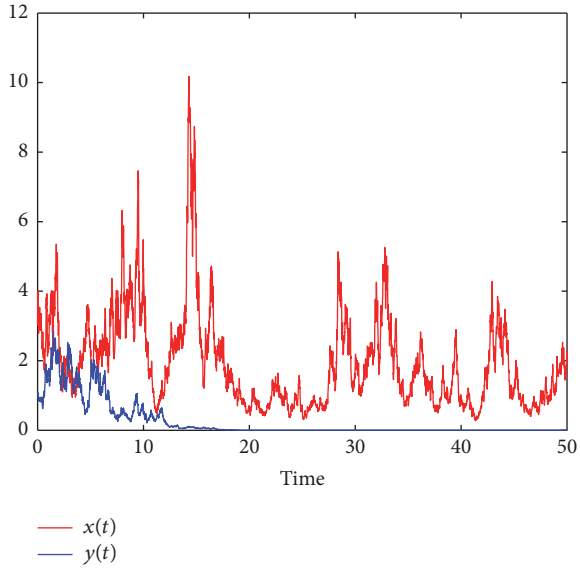

Figure 3

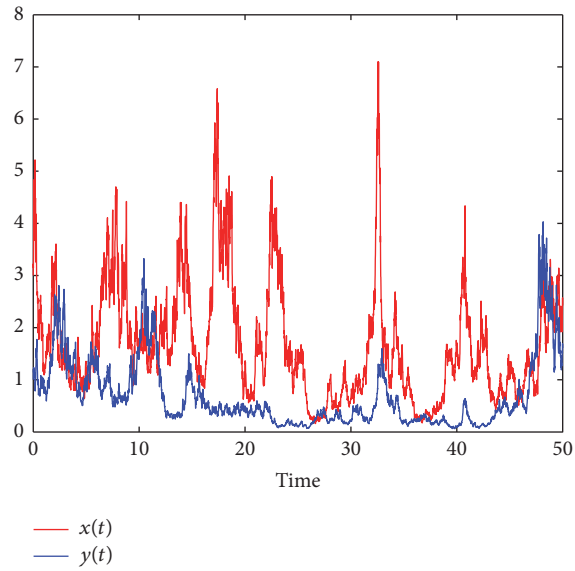

Figure 4

5. Conclusions

In this paper, a stochastic modified Bazykin system with Lévy jumps is discussed. Firstly, the existence of global positive solutions is investigated, and boundedness in mean is also given. Further, under related assumption, we obtain the sufficient conditions for the stochastic permanence and extinction of system (4). There are some interesting topics which deserve further discussion. For example, many authors consider the stationary distribution for stochastic predator-prey model with harvesting and delays [23–25], epidemic model with regime switching [26], impulsive stochastic model [27], and budworm growth model with Markovian switching [28]. The above investigations are left for future work.

Conflicts of Interest

The authors declare that there are no conflicts of interest regarding the publication of this manuscript.

Acknowledgments

This work is supported by National Natural Science Foundation of China (nos. 11771001, 11471015, and 11401002), Nature Science Foundation of Anhui Province (no. 1508085QA01 and no. 1508085MA10), Natural Science Foundation of Anhui Colleges (no. KJ2014A010), Program for Excellent Young Talents in University of Anhui Province (no. gxyq2017092), and Anhui Province Workshop of Prestigious Teacher (no. 2016msgzs006).

References

[1] A. D. Bazykin, *Nonlinear Dynamics of Interacting Populations*, vol. 11 of *World Scientific Series on Nonlinear Science, Series A*, World Scientific, River Edge, NJ, USA, 1998.

[2] M. Haque, "Ratio-dependent predator-prey models of interacting populations," *Bulletin of Mathematical Biology*, vol. 71, no. 2, pp. 430–452, 2009.

[3] Y. Kuang and E. Beretta, "Global qualitative analysis of a ratio-dependent predator-prey system," *Journal of Mathematical Biology*, vol. 36, no. 4, pp. 389–406, 1998.

[4] D. Xiao and S. Ruan, "Global dynamics of a ratio-dependent predator-prey system," *Journal of Mathematical Biology*, vol. 43, no. 3, pp. 268–290, 2001.

[5] Y. Xiao and L. Chen, "Modeling and analysis of a predator-prey model with disease in the prey," *Mathematical Biosciences*, vol. 171, no. 1, pp. 59–82, 2001.

[6] S. Sarwardi, M. Haque, and P. . Mandal, "Ratio-dependent predator-prey model of interacting population with delay effect," *Nonlinear Dynamics*, vol. 69, no. 3, pp. 817–836, 2012.

[7] S. Sarwardi, M. Haque, and P. . Mandal, "Persistence and global stability of Bazykin predator-prey model with BEDdington-DeAngelis response function," *Communications in Nonlinear Science and Numerical Simulation*, vol. 19, no. 1, pp. 189–209, 2014.

[8] M. Haque, "A detailed study of the Beddington-DeAngelis predator-prey model," *Mathematical Biosciences*, vol. 234, no. 1, pp. 1–16, 2011.

[9] J. Lv, K. Wang, and D. Chen, "Analysis on a stochastic two-species ratio-dependent predator-prey model," *Methodology and Computing in Applied Probability*, vol. 17, no. 2, pp. 403–418, 2015.

[10] J. Bao and C. Yuan, "Stochastic population dynamics driven by Lévy noise," *Journal of Mathematical Analysis and Applications*, vol. 391, no. 2, pp. 363–375, 2012.

[11] M. Liu and C. Bai, "Dynamics of a stochastic one-prey two-predator model with Lévy jumps," *Applied Mathematics and Computation*, vol. 284, pp. 308–321, 2016.

[12] Q. Liu, D. Jiang, N. Shi, T. Hayat, and A. Alsaedi, "Stochastic mutualism model with Lévy jumps," *Communications in Nonlinear Science and Numerical Simulation*, vol. 43, pp. 78–90, 2017.

[13] W. Mao, L. Hu, and X. Mao, "The existence and asymptotic estimations of solutions to stochastic pantograph equations with diffusion and Lévy jumps," *Applied Mathematics and Computation*, vol. 268, pp. 883–896, 2015.

[14] X. Zhang, D. Jiang, T. Hayat, and B. Ahmad, "Dynamics of a stochastic SIS model with double epidemic diseases driven by Lévy jumps," *Physica A: Statistical Mechanics and its Applications*, vol. 471, pp. 767–777, 2017.

[15] X. Meng and X. Wang, "Stochastic predator-prey system subject to Lévy jumps," *Discrete Dynamics in Nature and Society*, Article ID 5749892, 13 pages, 2016.

[16] Q. Zhu, "Razumikhin-type theorem for stochastic functional differential equations with Lévy noise and Markov switching," *International Journal of Control*, vol. 90, no. 8, pp. 1703–1712, 2017.

[17] L. Guo and Q. Zhu, "Stability analysis for stochastic Volterra-Levin equations with Poisson jumps: fixed point approach," *Journal of Mathematical Physics*, vol. 52, no. 4, Article ID 042702, 042702, 15 pages, 2011.

[18] X. Mao, *Stochastic Differential Equations and Their Applications*, Horwood, Chichester, UK, 1997.

[19] M. Liu and K. Wang, "Dynamics of a two-prey one-predator system in random environments," *Journal of Nonlinear Science*, vol. 23, no. 5, pp. 751–775, 2013.

[20] M. Liu and K. Wang, "Stochastic Lotka-Volterra systems with Lévy noise," *Journal of Mathematical Analysis and Applications*, vol. 410, no. 2, pp. 750–763, 2014.

[21] D. J. Higham, X. Mao, and A. M. Stuart, "Strong convergence of Euler-type methods for nonlinear stochastic differential equations," *SIAM Journal on Numerical Analysis*, vol. 40, no. 3, pp. 1041–1063, 2002.

[22] L. Wang, *Numerical Solutions of Stochastic Differential Equations*, 2016.

[23] M. Liu, X. He, and J. Yu, "Dynamics of a stochastic regime-switching predator-prey model with harvesting and distributed delays," *Nonlinear Analysis: Hybrid Systems*, vol. 28, pp. 87–104, 2018.

[24] H. Qiu and W. Deng, "Optimal harvesting of a stochastic delay tri-trophic food-chain model with Lévy jumps," *Physica A: Statistical Mechanics and its Applications*, vol. 492, pp. 1715–1728, 2018.

[25] J. Yu and M. Liu, "Stationary distribution and ergodicity of a stochastic food-chain model with Lévy jumps," *Physica A: Statistical Mechanics and its Applications*, vol. 482, pp. 14–28, 2017.

[26] X. Zhang, D. Jiang, A. Alsaedi, and T. Hayat, "Stationary distribution of stochastic SIS epidemic model with vaccination under regime switching," *Applied Mathematics Letters*, vol. 59, pp. 87–93, 2016.

[27] M. Liu, C. Du, and M. Deng, "Persistence and extinction of a modified Leslie-Gower Holling-type II stochastic predator-prey model with impulsive toxicant input in polluted environments," *Nonlinear Analysis: Hybrid Systems*, vol. 27, pp. 177–190, 2018.

[28] M. Liu and Y. Zhu, "Stability of a budworm growth model with random perturbations," *Applied Mathematics Letters*, vol. 79, pp. 13–19, 2018.

Hindawi
Discrete Dynamics in Nature and Society
Volume 2018, Article ID 7913256, 15 pages
https://doi.org/10.1155/2018/7913256

Research Article

Improved Harmony Search Algorithm for Truck Scheduling Problem in Multiple-Door Cross-Docking Systems

Zhanzhong Wang, Yue Lu, Liying Zhao, and Ningbo Cao

College of Transportation, Jilin University, No. 5988 Renmin Street, Changchun, Jilin, China

Correspondence should be addressed to Liying Zhao; 791950198@qq.com

Received 8 December 2017; Revised 22 February 2018; Accepted 7 March 2018; Published 24 April 2018

Academic Editor: Youssef N. Raffoul

The key of realizing the cross docking is to design the joint of inbound trucks and outbound trucks, so a proper sequence of trucks will make the cross-docking system much more efficient and need less makespan. A cross-docking system is proposed with multiple receiving and shipping dock doors. The objective is to find the best door assignments and the sequences of trucks in the principle of products distribution to minimize the total makespan of cross docking. To solve the problem that is regarded as a mixed integer linear programming (MILP) model, three metaheuristics, namely, harmony search (HS), improved harmony search (IHS), and genetic algorithm (GA), are proposed. Furthermore, the fixed parameters are optimized by Taguchi experiments to improve the accuracy of solutions further. Finally, several numerical examples are put forward to evaluate the performances of proposed algorithms.

1. Introduction

Cross docking is a process of logistics, of which the products are unloaded from the inbound trucks and then sorted and loaded into outbound trucks without warehousing. In a traditional distribution center, there are four major functions of warehousing that can be distinguished: receiving, storage, order picking, and shipping. Since the major costs of warehousing are operations of storage and order picking, and the cross docking can successfully eliminate them to considerably decrease distribution costs, cross docking is nowadays used by many companies, such as Wal Mart, Goodyear GB Ltd., Toyota, Eastman Kodak Co., and Dots and LLC [1].

There are several problems that researchers are passionate about, such as layout design, location, network, and vehicle routing problems. For example, Bartholdi III and Gue [2] introduced an efficient design of the cross-docking layout, whose objective was to minimize the transfer time, material handling, and congestion. Dondo and Cerdá [3] presented a new monolithic MILP formulation which integrated the pickup/delivery vehicle routing and scheduling with the assignment of dock doors. Nevertheless, two of the most important factors that affect the efficiency of cross docking are door assignment and truck scheduling. A proper sequence of trucks can significantly decrease the makespan and improve the efficiency. The problems of door assignment and truck scheduling are always considered together to optimize the procedure of the cross docking.

The layout of the cross-docking terminal is in many forms, such as the number of dock doors and whether there is a temporary storage. Yu and Egbelub [4] proposed a truck scheduling model with one inbound door and one outbound door. Boloori Arabani et al. [5] put forward metaheuristic algorithms to solve the same problem. Forouharfard and Zandieh [6] proposed an integer programming (IP) model to solve the problem of single receiving and shipping door. Besides, a genetic algorithm was applied to solve the model. In addition, Yu [7] dealt with truck scheduling problem with multiple dock doors to find the best sequence for trucks as well as assignments for trucks to doors and at the same time determine the unloading sequences, product routing, and routing sequences. Madani-Isfahani et al. [8] considered a truck scheduling model with multiple doors and then designed two metaheuristics, namely, simulated

annealing and firefly algorithm to solve the offered model. Assadi and Bagheri [9] considered a cross-docking terminal with multiple doors and temporary storage, assuming the ready time of inbound trucks were uncertain. Assadi and Bagheri [10] proposed two algorithms, namely, differential evolution and population-based simulated annealing to solve the multiple-door cross-docking system.

The objective functions of truck scheduling are about time, number of products transferred to temporary storage, customer satisfaction, and so on. The makespan of cross docking as well as the total earliness and total tardiness of trucks is discussed more often. Wisittipanich and Hengmeechai [11] and Boloori Arabani et al. [12] proposed a truck scheduling model with objective of minimizing the total earliness and tardiness simultaneously. Lee et al. [13] established a mathematical model to maximize the number of products shipped in a given working horizon. Ladier and Alpan [14] proposed an objective of minimizing both total number of pallets put in storage and the dissatisfaction of transportation providers to evaluate the quality of cross-docking system.

The operation forms of cross docking may be different, the times of a truck moves in and out can be once or more. Vahdani et al. [15] presented a truck scheduling model with no temporary storage in the cross-docking terminal. Both inbound and outbound trucks can move in and out of the docks during their tasks repetitively. Two known metaheuristics named genetic algorithm and electromagnetism-like algorithm were applied to minimize the total flow time. Mohtashami [16] dealt with a model that the outbound trucks can repetitively move; however the inbound trucks can move in only once.

Truck scheduling problems could be divided into two categories, which are the scheduling of both inbound and outbound trucks as well as the scheduling of inbound trucks only. Boysen et al. [17] dealt with scheduling of inbound trucks only, assuming outbound trucks left at fixed sequence and then proposed decomposition procedures and simulated annealing to minimize total lost profit. Rahmanzadeh Tootkaleh et al. [18] proposed an inbound truck scheduling model based on fixed outbound trucks' departure times.

This paper proposes a truck scheduling model at a cross-docking system with multiple inbound and outbound doors to minimize the total makespan. The inbound and outbound trucks are all available at time zero, so it is necessary to schedule all the trucks and make proper door assignments as well as truck sequences. Furthermore, it is assumed that outbound trucks load products from temporary storages first and then from inbound trucks, in case that the temporary storages get filled up. An inbound truck enters the inbound platform when the predecessor leaves and leaves the inbound platform when none of the outbound trucks at the outbound platforms need its products. It is worth noting that its leaving time is no less than the start time plus the unloading time due to the waiting time existing. In addition, three metaheuristics are proposed, namely, HS, IHS, and GA, to solve the model in order to find the best sequence.

The remainder of this paper is organized as follows: The next section describes the assumptions, mixed integer programming model for the truck scheduling problem, and the process of the cross docking. Section 3 presents three metaheuristics: harmony search, improved harmony search, and genetic algorithm. In Section 4, the performances of the metaheuristic algorithms are evaluated over the tests about truck scheduling. Finally, conclusions are drawn and future work is shortly expressed.

2. Problem Description

The studied problem in this paper is a mathematical model based on mixed integer programming working on trucks scheduling problems in a cross-docking system with multiple doors. Figure 1 shows the layout of the cross-docking terminal; in the terminal, temporary storages are designed besides the inbound doors, which are extremely large but limited. The outbound trucks load products from temporary storages first and then from inbound trucks in the inbound doors to avoid filling up the temporary storages. The objective function is minimizing the total makespan in order to reduce the waiting time and improve the efficiency of cross-docking system.

2.1. Assumptions

(1) There are multiple receiving doors and shipping doors in cross-docking system.

(2) The shipping time is related to the distance.

(3) Every outbound truck leaves until satisfying its needs.

(4) Every inbound truck leaves until unloading its products.

(5) Every truck is available at time zero.

(6) The quantities and categories the inbound trucks load are equal to the quantities and categories the outbound trucks need.

(7) There is no preemption of any truck.

(8) The capacity of each truck is different, each inbound truck loads specific types of products, and outbound truck needs specific types of products.

(9) There is a temporary storage next to each receiving door which is with a large volume but limited.

(10) The changeover time of trucks is equal.

(11) The time of loading and unloading is in direct proportion to the quantity of products.

(12) The processes of sorting and labeling are not considered.

(13) The outbound truck loads products from inbound trucks, when there are no more products that the outbound truck needs in the temporary storages.

(14) The order of loading and unloading of products is not considered.

(15) The products can be exchanged; that is, the products on a certain inbound truck can be loaded into any outbound trucks, which need them.

(16) There is only one chance for each inbound and outbound truck to move in. The inbound truck unloads the rest of the products to the temporary storage and leaves when the inbound truck on the inbound platform cannot fill any outbound trucks on the outbound platforms. An outbound truck leaves when it fills all the products needed.

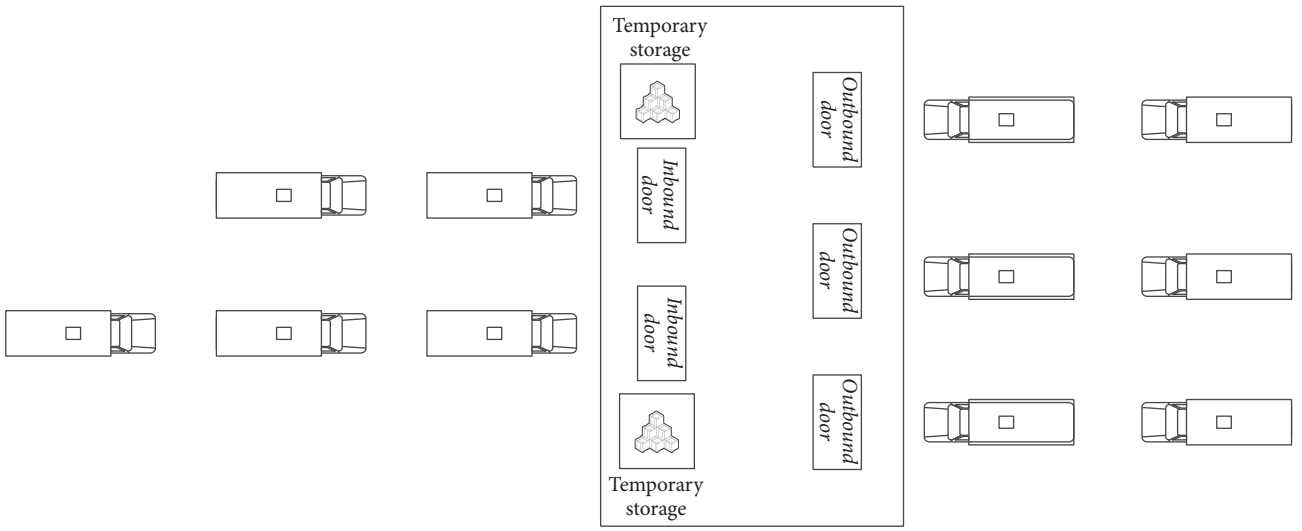

Figure 1: The layout of cross-docking terminal.

2.2. Notations

R: number of inbound trucks ($i = 1, 2, \ldots, I$).

S: number of outbound trucks ($j = 1, 2, \ldots, O$).

P: number of product types.

k: index for product type ($k = 1, 2, \ldots, P$).

I: number of doors at receiving door ($m = 1, 2, \ldots, R$).

O: number of doors at shipping door ($n = 1, 2, \ldots, S$).

DT: changeover time of trucks.

M: a positive big number.

T: loading or unloading time per product unit.

r_{ik}: number of units of product type k that is initially loaded in inbound truck i.

s_{jk}: number of units of product type k that is initially needed for outbound truck j.

t_{mn}: transfer time per unit of product type k from inbound door m to outbound door n.

c_i: time at which inbound truck i enters the receiving door.

C_i: time at which inbound truck i leaves the receiving door.

l_j: time at which outbound truck j enters the shipping door.

L_j: time at which outbound truck j leaves the shipping door.

$L\text{previous}_j$: time at which the predecessor of outbound truck j leaves the outbound door.

x_{ijk}: number of units of product type k transferred from inbound truck i to outbound truck j.

LX_{ijk}: number of units of product type k transferred from temporary storage to outbound truck j, which the products have been transferred from inbound truck i to temporary storage.

C_{ij}: time at which outbound truck j starts to load products from inbound truck i.

$C_{ij_{\text{last}}}$: time at which the last outbound truck j starts to load products from inbound truck i.

D_j: time at which outbound truck j starts to load products from temporary storage.

v_{ij}: if any products are transferred from inbound truck i to outbound truck j directly: 1, otherwise: 0.

y_{im}: if inbound truck i is assigned to receiving door m: 1, otherwise: 0.

z_{jn}: if outbound truck j is assigned to shipping door n: 1, otherwise: 0.

p_{ij}: if inbound trucks i and j are assigned to the same receiving door and i is a predecessor of truck j: 1, otherwise: 0.

q_{ij}: if outbound trucks i and j are assigned to the same shipping door and i is a predecessor of truck j: 1, otherwise: 0.

2.3. The Mathematical Model. The mathematical model for the problem is given as follows:

$$\min \quad T \tag{1}$$

$$\text{S.t:} \quad T \geq L_j, \quad j = 1, 2, \ldots, S \tag{2}$$

$$\sum_{m=1}^{I} y_{im} = 1, \quad i = 1, 2, \ldots, R \tag{3}$$

$$\sum_{n=1}^{O} z_{jn} = 1, \quad j = 1, 2, \ldots, S \tag{4}$$

$$\sum_{j=1}^{S} x_{ijk} = r_{ik}, \quad i = 1, 2, \ldots, R, \ k = 1, 2, \ldots, P \tag{5}$$

$$\sum_{i=1}^{R} x_{ijk} = s_{jk}, \quad i = 1, 2, \ldots, S, \ k = 1, 2, \ldots, P \tag{6}$$

$$p_{ij} + p_{ji} \le 1, \quad i \ne j, \ i, j = 1, 2, \ldots, R \tag{7}$$

$$q_{ij} + q_{ji} \le 1, \quad i \ne j, \ i, j = 1, 2, \ldots, S \tag{8}$$

$$y_{im} + y_{jm} - 1 \le p_{ij} + p_{ji}, \quad i, j = 1, 2, \ldots, R, \ i \ne j, \ m = 1, 2, \ldots, I \tag{9}$$

$$z_{in} + z_{jn} - 1 \le q_{ij} + q_{ji}, \quad i, j = 1, 2, \ldots, S, \ i \ne j, \ n = 1, 2, \ldots, O \tag{10}$$

$$C_i + DT - M * \left(1 - p_{ij}\right) \le c_j, \quad i, j = 1, 2, \ldots, R \tag{11}$$

$$C_i \ge C_{ij_{\text{last}}} + \sum_{k=1}^{P} x_{ijk} - M * \sum_{j=1}^{S} v_{ij}, \quad i = 1, 2, \ldots, R, \ j = 1, 2, \ldots, S, \ k = 1, 2, \ldots, P \tag{12}$$

$$C_i \ge C_l + DT + \sum_{k=1}^{P} r_{ik} - M * \left(1 - p_{li}\right) - M * \sum_{j=1}^{S} v_{ij}, \quad i, l = 1, 2, \ldots, R, \ k = 1, 2, \ldots, P, \ j = 1, 2, \ldots, S \tag{13}$$

$$C_{ij} \ge \max\left(c_i, \left(l_j + T\sum_{i=1}^{R}\sum_{k=1}^{P} LX_{ijk}\right)\right) - M * \left(1 - V_{ij}\right), \quad i = 1, 2, \ldots, R, \ j = 1, 2, \ldots, S, \ k = 1, 2, \ldots, P \tag{14}$$

$$D_j \ge L_i + DT - M * \left(1 - q_{ij}\right), \quad i, j = 1, 2, \ldots, S, \ i \ne j \tag{15}$$

$$L_i + DT - M * \left(1 - q_{ij}\right) \le l_j, \quad i, j = 1, 2, \ldots, S, \ i \ne j \tag{16}$$

All variables ≥ 0.

Constraint (3) guarantees that the makespan is greater than or equal to the time the last outbound truck leaves the outbound door. Constraints (4)-(5) ensure every inbound truck or outbound truck is allowed to be assigned to one of the inbound doors or outbound doors. Constraint (6) ensures the total number of products of type k from inbound truck i to all outbound trucks is equal to the number of products of type k that unloaded from the inbound truck i. Constraint (7) ensures the total number of products of type k from all inbound trucks to outbound truck j is equal to the number of products of type k that loaded to the outbound truck j. Constraints (8)-(9) guarantee the inbound truck or outbound truck occurs only once. Constraint (10) confirms the relationship between y_{im} and p_{ij}; similarly, the relationship between z_{jn} and q_{ij} is ensured by constraint (11). Constraint (12) ensures that the start time of the next inbound truck j is equal to the finished time of the former inbound truck i plus the delay time of truck change. Constraint (13) is the condition of the finished time of inbound truck, in the case that there is any outbound truck loading products directly from the inbound truck i. Constraint (14) is the condition of the finished time of inbound truck i, in the case that there is no outbound truck loading products directly from the inbound truck i. Constraint (15) assures the time at which outbound truck j starts to load products from inbound truck i. Constraint (16) assures the time at which outbound truck j starts to load products from temporary storages. Constraint (17) ensures that the start time of the next outbound truck j is equal to the finished time of the former outbound truck i plus the delay time of truck change.

2.4. The Process of Cross Docking. The temporary storage is extremely large but not without a limit, so the outbound trucks on the outbound docks load products from temporary storages first and then load products from inbound trucks on the inbound docks, if the outbound trucks are still not full. The inbound trucks will stay at the inbound docks if there are any outbound trucks full and leaving the outbound dock; if not, leave the docks and unload the rest of the products to the temporary storages. The process of cross docking will be finished when all outbound trucks are full, and no truck remains. The specific flow diagram of the process of cross docking is shown in Figure 2.

There are multiple inbound doors and outbound doors in cross-docking system; more than two trucks operate at the same time at the inbound and outbound docks. Formulate the unloading and loading principles in order to assure that the cross-docking system moves smoothly and efficiently. Here are two principles as follows:

(1) Which outbound truck at outbound docks is chosen by the inbound truck to transfer products to is decided by the distance between the docks. The products from one inbound truck are loaded to the outbound truck that are the nearest from the inbound truck. For the outbound truck, if the nearest inbound truck cannot satisfy it, the far inbound trucks at other inbound docks will be considered.

(2) If there are two inbound trucks constituting the products that the outbound truck needs and the two inbound trucks are equally far from the outbound truck, the outbound truck will choose one inbound truck first randomly and then the other.

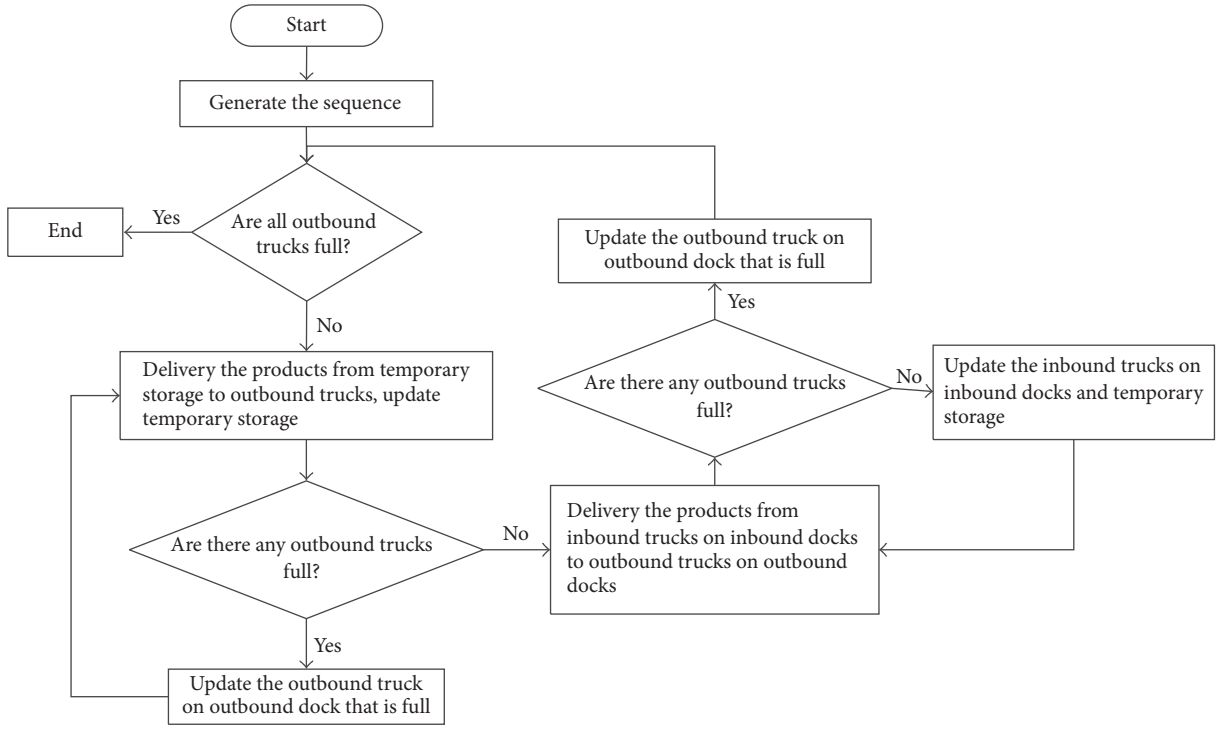

Figure 2: The process of cross docking.

3	4	1	2	5	4	2	6	1	5	3
1	2	1	1	2	1	3	2	2	3	1

Figure 3: Scheme of a solution.

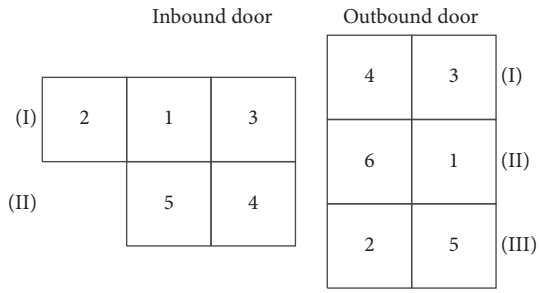

Figure 4: Sequences of trucks.

3. Solution Methods

This paper proposes three algorithms, namely, harmony search, improved harmony search, and genetic algorithm. It is necessary to design the representation scheme of the solution, which will be used in further work. The solution consists of two layers of arrays, the first layer expresses the codes of the inbound and outbound trucks, and the second layer represents the codes of the inbound and outbound doors. The length of a solution is decided by the total number of inbound and outbound trucks. As shown in Figure 3, it is a cross-docking terminal with two inbound doors and three outbound doors; besides there are five inbound trucks and six outbound trucks in it. The left five columns represent the inbound trucks as well as the dock doors they belong to; therefore, the right six columns represent the outbound trucks. Figure 4 demonstrates unloading and loading sequences of inbound and outbound trucks. For example, inbound truck 3 is the first truck to unload in inbound door 1.

3.1. Improved Harmony Search

3.1.1. Harmony Search Algorithm. Harmony search was first proposed by Geem et al. in 2001 [19]; it is a novel intelligent algorithm, which simulates the principle of the music play. In the music performance, the musicians adjust the tones of their instruments repeatedly through the memory to achieve a beautiful harmony.

3.1.2. Initialize the Problem and Parameters. The objective function of this paper is to minimize the total makespan of the cross-docking system. The parameters in harmony search are HMS, HMCR, PAR, and BW. HMS represents the number of solution vectors in the harmony memory. HMCR expresses the harmony memory considering rate. PAR indicates the pitch adjusting rate. BW means bandwidth for each generation. In addition, the harmony memory (HM) is an array that contains all the solution vectors.

3.1.3. Initialize the Solution Set. Generate HMS sets of solutions randomly in HM matrix; the format of the solution is the same as in Figure 3. A solution consists of two levels, the first level are the codes of trucks and the second level are the codes of the doors. The solution set HM consists of HMS sets of solutions, and the number of rows in the array is $2 * \text{HMS}$. The sum of the inbound trucks and outbound trucks is equal to the number of columns in the array. The left R columns of HM represent the codes of inbound trucks, and the right S columns of HM represent the codes of outbound trucks.

$$\text{HM} = \begin{bmatrix} T_1^1 & T_2^1 & \cdots & T_R^1 & T_{R+1}^1 & T_{R+2}^1 & \cdots & T_{R+S}^1 \\ D_1^1 & D_2^1 & \cdots & D_R^1 & D_{R+1}^1 & D_{R+2}^1 & \cdots & D_{R+S}^1 \\ T_1^2 & T_2^2 & \cdots & T_R^2 & T_{R+1}^2 & T_{R+2}^2 & \cdots & T_{R+S}^2 \\ D_1^2 & D_2^2 & \cdots & D_R^2 & D_{R+1}^2 & D_{R+2}^2 & \cdots & D_{R+S}^2 \\ \vdots & \vdots & \vdots & \vdots & \vdots & \vdots & \vdots & \vdots \\ T_1^{\text{HMS}-1} & T_2^{\text{HMS}-1} & \cdots & T_R^{\text{HMS}-1} & T_{R+1}^{\text{HMS}-1} & T_{R+2}^{\text{HMS}-1} & \cdots & T_{R+S}^{\text{HMS}-1} \\ D_1^{\text{HMS}-1} & D_2^{\text{HMS}-1} & \cdots & D_R^{\text{HMS}-1} & D_{R+1}^{\text{HMS}-1} & D_{R+2}^{\text{HMS}-1} & \cdots & D_{R+S}^{\text{HMS}-1} \\ T_1^{\text{HMS}} & T_2^{\text{HMS}} & \cdots & T_R^{\text{HMS}} & T_{R+1}^{\text{HMS}} & T_{R+2}^{\text{HMS}} & \cdots & T_{R+S}^{\text{HMS}} \\ D_1^{\text{HMS}} & D_2^{\text{HMS}} & \cdots & D_R^{\text{HMS}} & D_{R+1}^{\text{HMS}} & D_{R+2}^{\text{HMS}} & \cdots & D_{R+S}^{\text{HMS}} \end{bmatrix}. \tag{17}$$

3.1.4. Generate a New Solution Randomly. A new solution is generated based on three rules: (1) memory consideration, (2) pitch adjustment, and (3) random selection. Each value of the variable of the solution is selected from the historical values stored in the HM with possibility HMCR. That is to say, in the memory consideration, the value of the first variable (T_1') in the first level of the solution is selected randomly from values in the specified HM range ($T_1'^1$–$T_1'^{\text{HMS}}$), and the value of the first variable (D_1') in the second level of the solution is selected randomly from values in the HM range ($D_1'^1$–$D_1'^{\text{HMS}}$) with possibility HMCR. Otherwise, select a value from the possible range of values with possibility (1 − HMCR). Values of other variables in the solution are selected in the same manner.

$$T_i' = \begin{cases} T_i' \in \left\{T_i^1, T_i^2, \ldots, T_i^{\text{HMS}}\right\} & \text{with probability HMCR} \\ T_i' \in T & \text{with probability } (1 - \text{HMCR}) \end{cases}$$
$$D_i' = \begin{cases} D_i' \in \left\{D_i^1, D_i^2, \ldots, D_i^{\text{HMS}}\right\} & \text{with probability HMCR} \\ D_i' \in D & \text{with probability } (1 - \text{HMCR}). \end{cases} \tag{18}$$

T and D in formulas (18) represent all possible values of T_i' and D_i', respectively, which are discrete variables determined by the number of inbound and outbound trucks and the number of inbound and outbound doors.

If the value of a variable is obtained by memory consideration, it should be determined whether to be pitch-adjusted with probability PAR.

$$\text{Pitch adjusting decision for } T_i' = \begin{cases} \text{Yes} & \text{with probability PAR,} \\ \text{No} & \text{with probability } (1 - \text{PAR}). \end{cases}$$
$$\text{Pitch adjusting decision for } D_i' = \begin{cases} \text{Yes} & \text{with probability PAR,} \\ \text{No} & \text{with probability } (1 - \text{PAR}). \end{cases} \tag{19}$$

The value will be adjusted if the pitch adjusting decision is yes, and the adjusting formulas are as follows:

$$T_i' = T_i' \pm \text{rand}() * \text{BW}$$
$$D_i' = D_i' \pm \text{rand}() * \text{BW}. \tag{20}$$

3	3	1	5	5	4	6	6	3	5	3
1	2	1	1	2	1	3	2	2	3	1

Figure 5: A new solution of HS.

3	2	1	5	4	4	6	2	3	5	1
1	2	1	1	2	1	3	2	2	3	1

Figure 6: A modified solution of HS.

Here, rand( ) is a random number between 0 and 1.

The new solution may not meet the model requirements after the generating rules, so some corrections are needed. As shown in Figure 5, there are repeated 3 and repeated 5 in the inbound truck codes at the first level of the solution. It could not be real for the reasonable solution. The position of the second 3 should be replaced by the missing number 2 or 4 randomly, and the position of the second 5 should be replaced by the rest missing number. As for the outbound truck codes, the same approach should be applied to. Figure 6 represents a modified solution that may occur.

3.1.5. Update the Solution Set. Considering the objective function value, replace the worst solution by the new solution, if the new solution is better than the worst in the HM; otherwise, remain the worst and generate a new solution again.

3.1.6. Check Stopping Criterion. The maximum cycle time is defined; the loop will continue until it meets the stopping criterion.

3.1.7. Improved Harmony Search Algorithm. The parameters of basic harmony search are fixed, but parameters perform differently in the every iteration. The algorithm that possesses small parameter of PAR with large parameter of BW performs worse and increases the iteration needed to find the optimum solution. Furthermore, large PAR and small BW will cause great improvement in final generations with algorithm converged to optimal solution vector. Considering the parameter of BW separately, small BW in final generations increase the fine-tuning of solution vectors, but large BW performs better in the early iterations and increases the diversity of solution vectors to search for the best solution.

To eliminate the drawbacks of HS algorithm with fixed values of PAR and BW and improve the performances of them, dynamic values of parameters will be applied to the basic HS algorithm. The formulas of dynamic parameters are defined as follows [20, 21]:

$$\begin{aligned} \mathrm{PAR}(\mathrm{gn}) &= \mathrm{PAR}_{\min} + \frac{(\mathrm{PAR}_{\max} - \mathrm{PAR}_{\min})}{NI} \times \mathrm{gn} \\ \mathrm{BW}(\mathrm{gn}) &= \mathrm{BW}_{\max} \exp(c \times \mathrm{gn}) \\ c &= \frac{\ln(\mathrm{BW}_{\min}/\mathrm{BW}_{\max})}{NI}. \end{aligned} \tag{21}$$

PAR(gn) and BW(gn) are the values of PAR and BW in each generation, $\mathrm{PAR}_{\max}$ and $\mathrm{PAR}_{\min}$ are the maximum and minimum pitch adjusting rate, $\mathrm{BW}_{\max}$ and $\mathrm{BW}_{\min}$ are the maximum and minimum bandwidth, gn represents the generation number, and NI represents the solution vector generations.

3.2. Genetic Algorithm. There are several steps in genetic algorithm, such as population initialization, selection, crossover, and mutation operation. The population initialization process is similar to the initialization of solution sets in harmony search, and the selection method is roulette. So here are some explanations for crossover and mutation operation.

3.2.1. Crossover Design of Chromosomes. The chromosomes of this paper consist of two parts that are inbound trucks codes and outbound trucks codes; the crossover operations need to be done in two parts. As shown in Figure 7, two cross points are generated randomly as 2 and 3, which means the cross point of inbound trucks sequence is between the locations two and three; likewise, cross point of outbound trucks sequence is between the locations three and four. A solution is generated but does not meet the requirements. Therefore, some modified operations like red digits are applied following what HS does.

3.2.2. Mutation Design of Chromosomes. In order to perform the mutation operations for inbound and outbound trucks, swap mutation is applied. As shown in Figure 8, for inbound trucks sequence, the value at mutation point 1 and mutation point 2 will be changed, and the outbound trucks sequence mutates likewise.

4. Parameters Setting

There are several parameters in each algorithm. Meanwhile, each factor varies from different levels. However, the value of each parameter could affect the performances of the algorithms. Hence, several methods should be carried out to find out the best combination of parameters in each algorithm.

Taguchi experiment is a kind of method to design experiments, which decreases the number of experiments but provides an efficient combination of variables. Each

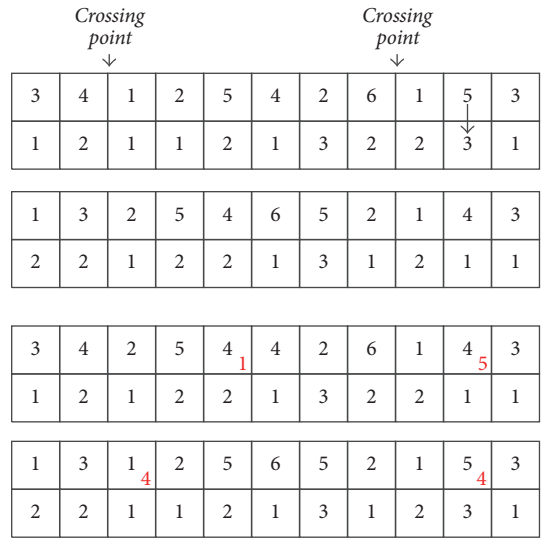

Figure 7: The process of crossover.

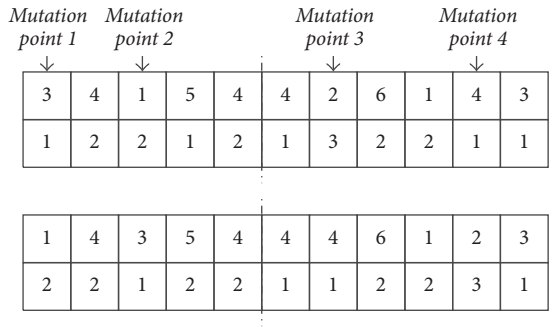

Figure 8: The process of mutation.

Table 1: Levels of parameters for HS.

Parameters	Levels			
	$L1$	$L2$	$L3$	$L4$
HMS	10	20	30	40
HMCR	0.7	0.9	0.95	0.99
PAR	0.2	0.4	0.6	0.7
BW	0.01	0.35	0.7	1

factor can be compared independently with any other factors, which ensures a balanced comparison among all levels of any factors. For the above reasons, Taguchi experiments are widely used in engineering design to determine optimal experimental conditions. The performance of each algorithm is evaluated by the signal to noise (S/N) to search combination of factors with a small amount of variation.

In the Taguchi method, the measured values of searching for the optimal combination of the parameters will be transformed into S/N ratio. The objective of the function in this paper is the small-the-better type, and the formula is as follows:

$$\text{S/N ratio} = -10 \log \frac{1}{n} \left[\sum_{i=1}^{n} \text{objective function}_i^2 \right]. \quad (22)$$

There are four parameters in HS, which are HMS, HMCR, PAR, and BW, each of whom has four levels. Table 1 displays different levels of the parameters, and the best combination is that the values of HMS, HMCR, PAR, and BW are 30, 0.95, 0.6, and 0.7, respectively, as shown in Figure 9.

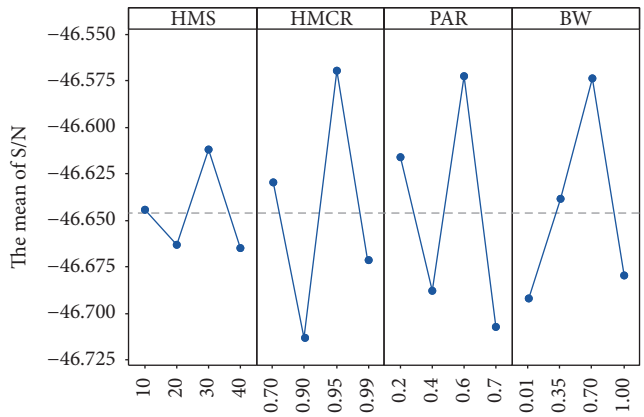

Figure 9: Main effects plot for S/N ratios of HS factors.

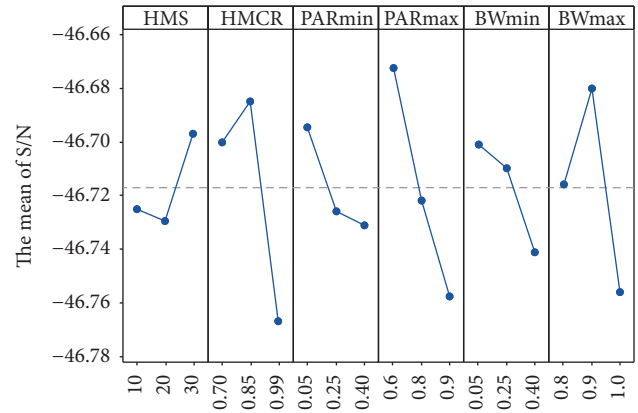

Figure 10: Main effects plot for S/N ratios of IHS factors.

Table 2: Levels of parameters for IHS.

Parameters	Levels		
	*L*1	*L*2	*L*3
HMS	10	20	30
HMCR	0.7	0.85	0.99
PAR_{min}	0.05	0.25	0.4
PAR_{max}	0.6	0.8	0.9
BW_{min}	0.05	0.25	0.4
BW_{max}	0.8	0.9	1

There are six parameters in IHS, which are HMS, HMCR, PAR_{min}, PAR_{max}, BW_{min}, and BW_{max}, each of whom has three levels. Table 2 displays different levels of the parameters, and the best combination is that the values of HMS, HMCR, PAR_{min}, PAR_{max}, BW_{min}, and BW_{max} are 30, 0.85, 0.05, 0.6, 0.05, and 0.9, respectively, as shown in Figure 10.

There are four parameters in GA, which are P_c, P_m, P_s, and POP, representing crossover probability, mutation probability, selection probability, and population size, respectively, each of whom has four levels. Table 3 suggests different levels of the parameters, and the best combination of values for P_c, P_m, P_s, and POP are 0.8, 0.2, 0.5, and 20, respectively, as shown in Figure 11.

5. Computational Results

5.1. Illustrative Examples. The number of inbound doors and outbound doors in the docking system are 2 and 3, respectively. In order to illustrate the performance of each proposed algorithm, several cases have been proposed to be experimented. The problems are divided into nine cases, considering the number of trucks, products, and their types. The subproblems 1–3 are divided due to the number of the products and types, of which subproblem 1 represents the small size, subproblem 2 is on behalf of the medium size, and subproblem 3 represents the large size. In addition, each subproblem is divided further, due to the number of

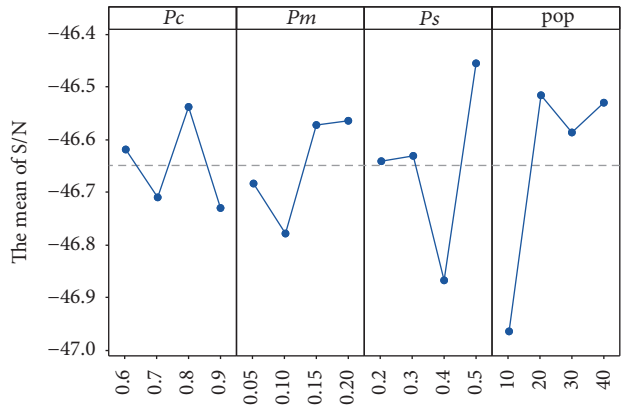

Figure 11: Main effects plot for S/N of GA factors.

Table 3: Levels of parameters for GA.

Parameters	Levels			
	$L1$	$L2$	$L3$	$L4$
P_c	0.6	0.7	0.8	0.9
P_m	0.05	0.1	0.15	0.2
P_s	0.2	0.3	0.4	0.5
POP	10	20	30	40

inbound and outbound trucks. Table 4 displays the detailed information of the nine cases.

It should be mentioned that the moving time of products from the inbound door to the outbound door is related to the distance, which means the moving time is 30, if doors are far apart, otherwise it is 15. And the changeover time of trucks is considered equal to 50 units; furthermore, the loading time is 1 unit, which is the equal to the unloading time; all data is processed by MATLAB 2016.

5.2. Comparison of Solution Procedures. For the experiments, the percentage deviation of the solutions in each method from the optimal solution based on makespan and the computational time are used to evaluate the performances. Percentage deviation of a solution is calculated as follows:

$$\text{Percentage deviation}\,(\%) = \frac{(\text{Evaluative factor for compared solution}) - (\text{Evaluative factor for best solution})}{(\text{Evaluative factor for best solution})} \times 100\%. \tag{23}$$

In order to evaluate performances of the three proposed methods in terms of the optimal value, worst value, average value, and the computational time, each case is tested 20 times and terminates at the iteration of 120. Table 5 shows makespan and computational time of nine tests by the three methods. As can be seen in Table 5, in the aspect of the optimal solution, there are 6 sets of optimal solutions searched by GA, 4 sets by IHS, and, nevertheless, 1 set by HS. In the aspect of the worst solution, IHS performs better, which gets 6 sets of best solutions among the worst solutions. As for average solution, the average values of nine cases calculated by GA are all showing best among the three methods. In terms of computational time, IHS performs best, while GA need much more time than the other methods.

As shown in Table 6, the percentage deviations of the optimal makespan searched by GA from the optimal makespan searched by three methods range from 0% to 6.18% for nine cases and range from 0% to 5.72% for IHS. The percentage deviations of the worst makespan searched by HS from the optimal makespan among the worst solutions searched by three methods range from 0% to 6.18% for nine cases and range from 0% to 11.1% for GA. GA performs best in average makespan; however, the percentage deviations of the average value calculated by HS from the best among the average values calculated by three methods range from 0.18% to 8.8% for nine cases. The percentage deviations of the computational time of GA from the shortest computational time among the three methods rage from 188.39% to 511.59% for nine cases,

Table 4: Nine sets of numerical experiments.

Subproblem 1 (small)						Subproblem 2 (medium)						Subproblem 3 (large)					
Case 1		Case 2		Case 3		Case 4		Case 5		Case 6		Case 7		Case 8		Case 9	
Product	357	Product	370	Product	399	Product	960	Product	1075	Product	1033	Product	1870	Product	1906	Product	1805
Type	5	Type	5	Type	6	Type	10	Type	11	Type	9	Type	13	Type	14	Type	15
Inbound truck	6	Inbound truck	15	Inbound truck	27	Inbound truck	7	Inbound truck	17	Inbound truck	26	Inbound truck	5	Inbound truck	16	Inbound truck	26
Outbound truck	5	Outbound truck	15	Outbound truck	33	Outbound truck	5	Outbound truck	16	Outbound truck	26	Outbound truck	7	Outbound truck	18	Outbound truck	27

Table 5: Makespan and computational time obtained by three methods for the nine test problems.

Problem set	HS				IHS				GA			
	Optimal	Worst	Average	Computational time	Optimal	Worst	Average	Computational time	Optimal	Worst	Average	Computational time
1	198	254	233.2	17.301	187	238	220.4	16.734	196	248	209.9	48.260
2	455	498	477.05	29.280	433	474	456.9	27.611	419	489	441.35	90.881
3	873	964	920.8	29.442	866	937	903.9	26.109	820	1012	869.85	159.679
4	429	467	445.6	23.842	429	471	445.5	24.480	429	465	444.7	97.429
5	687	798	741.65	40.347	647	750	721.35	39.253	687	777	689	141.686
6	922	1010	975.4	36.304	905	984	933.25	38.102	856	983	918.6	176.780
7	791	1011	926.3	31.501	784	979	928.25	32.548	791	922	853.2	109.181
8	1044	1193	1112.1	51.448	963	1093	1044.9	49.160	948	1095	1011	176.188
9	1166	1337	1231.3	50.592	1153	1243	1195.7	49.094	1110	1381	1186.4	268.185

Table 6: Percentage deviation for makespan and computational time between optimal solutions and other solutions.

Problem set	Optimal solution makespan	Optimal worst solution makespan	Optimal average solution makespan	Optimal computational time	RPD for optimal solutions			RPD for worst solutions			RPD for average solutions			RPD for computational time		
					HS	IHS	GA	HS	IHS	GA	HS	IHS	GA	HS	IHS	GA
1	187	238	209.9	16.734	5.88%	0.00%	4.81%	6.72%	0.00%	4.20%	11.10%	5.00%	0.00%	3.39%	0.00%	188.39%
2	419	474	441.35	27.611	8.59%	3.34%	0.00%	5.06%	0.00%	3.16%	8.09%	3.52%	0.00%	6.04%	0.00%	229.15%
3	820	937	869.85	26.109	6.46%	5.61%	0.00%	2.88%	0.00%	8.00%	5.86%	3.91%	0.00%	12.77%	0.00%	511.59%
4	429	465	444.7	23.842	0.00%	0.00%	0.00%	0.43%	1.29%	0.00%	0.20%	0.18%	0.00%	0.00%	2.68%	308.64%
5	647	750	689	39.253	6.18%	0.00%	6.18%	6.40%	0.00%	3.60%	7.64%	4.70%	0.00%	2.79%	0.00%	260.96%
6	856	983	918.6	36.304	7.71%	5.72%	0.00%	2.75%	0.10%	0.00%	6.18%	1.59%	0.00%	0.00%	4.95%	386.94%
7	784	922	853.2	31.501	0.89%	0.00%	0.89%	9.65%	6.18%	0.00%	8.57%	8.80%	0.00%	0.00%	3.32%	246.6%
8	948	1093	1011	49.160	10.13%	1.58%	0.00%	9.15%	0.00%	0.18%	10.00%	3.35%	0.00%	4.65%	0.00%	258.4%
9	1110	1243	1186.4	49.094	5.05%	3.87%	0.00%	7.56%	0.00%	11.10%	3.78%	0.78%	0.00%	3.05%	0.00%	446.27%

Table 7: Makespan and percentage deviation under the operation times 20 s and 40 s.

Problem set	Operation time 20 s						Operation time 40 s					
	IHS		HS		GA		IHS		HS		GA	
	Makespan	PD	Makespan	PD	Makespan	PD	Makespan	PD	Makespan	PD	Makespan	PD
1	235.6	0.00%	240	1.87%	293.6	24.62%	220.8	0.00%	222	0.54%	264.7	19.88%
2	473.7	0.00%	487.3	2.87%	675.9	42.69%	473.8	0.00%	481.4	1.60%	612.2	29.21%
3	924.9	0.00%	945.2	2.19%	1266.1	36.89%	913.4	0.00%	937.1	2.59%	1215.8	33.11%
4	464.4	0.00%	465.3	0.19%	539	16.06%	437.4	0.00%	451.6	3.25%	482.1	10.22%
5	765.6	0.00%	776	1.36%	968.1	26.45%	759.5	0.00%	760.5	0.13%	942.4	24.08%
6	959.1	0.00%	997.8	4.04%	1283.8	33.85%	966.5	0.00%	973.1	0.68%	1198.1	23.96%
7	977.2	3.48%	944.3	0.00%	1077.3	14.08%	937.4	1.32%	925.2	0.00%	1024.5	10.73%
8	1142.5	0.00%	1155.3	1.12%	1393.4	21.96%	1083.7	0.00%	1104.1	1.88%	1351.9	24.75%
9	1298.7	0.00%	1308.6	0.76%	1386.5	6.76%	1235.5	0.00%	1272.1	2.96%	1316.9	6.59%

which show GA performs worst in computational time and needs much more time than other methods.

To evaluate the performances of three algorithms under the same operation time, nine sets of experiments will be terminated at 20 s and 40 s using IHS, HS, and GA, respectively. To improve the accuracy of the results, each experiment will be run 10 times so as to get the average value. As shown in Table 7, for each method, the makespan get shorter, when the operation time is longer. IHS performs best among them for the same running time; however, GA performs worst. The percentage deviations (PD) of the values searched by GA from the best values get smaller when operation time is longer. However, the percentage deviations get larger for HS when operation time is longer.

6. Conclusions

This study has described a truck scheduling model in cross-docking system with multiple doors; furthermore, three algorithms are proposed, namely, HS, IHS, and GA to solve the problem. To evaluate the performances of the methods, these algorithms were applied for 9 sets of different problems divided by the number of products, categories, and trucks to minimize the total makespan of cross-docking procedure. During the analysis, it is proved that IHS performs better than HS in searching for optimal solutions, when dynamic values of parameters are applied. In addition, for the same iteration, both IHS and GA provide satisfactory results. However, GA performs better in providing optimal solutions, while IHS is far superior to GA in computational time. For the same operation time, HS performs best; however GA performs worst. For future studies, new hybrid metaheuristic algorithms will be applied to cross-docking system, instead of the basic algorithms, and the truck scheduling model could be perfect in uncertainty or fuzzy arrival time of trucks.

Conflicts of Interest

There are no conflicts of interest regarding the publication of this paper.

References

[1] J. Van Belle, P. Valckenaers, G. V. Berghe, and D. Cattrysse, "A tabu search approach to the truck scheduling problem with multiple docks and time windows," *Computers & Industrial Engineering*, vol. 66, no. 4, pp. 818–826, 2013.

[2] J. J. Bartholdi III and K. R. Gue, "Reducing labor costs in an LTL crossdocking terminal," *Operations Research*, vol. 48, no. 6, pp. 823–832, 2000.

[3] R. Dondo and J. Cerdá, "A monolithic approach to vehicle routing and operations scheduling of a cross-dock system with multiple dock doors," *Computers & Chemical Engineering*, vol. 63, no. 11, pp. 184–205, 2014.

[4] W. Yu and P. J. Egbelu, "Scheduling of inbound and outbound trucks in cross docking systems with temporary storage," *European Journal of Operational Research*, vol. 184, no. 1, pp. 377–396, 2008.

[5] A. R. Boloori Arabani, S. M. T. Fatemi Ghomi, and M. Zandieh, "Meta-heuristics implementation for scheduling of trucks in a cross-docking system with temporary storage," *Expert Systems with Applications*, vol. 38, no. 3, pp. 1964–1979, 2011.

[6] S. Forouharfard and M. Zandieh, "An imperialist competitive algorithm to schedule of receiving and shipping trucks in cross-docking systems," *The International Journal of Advanced Manufacturing Technology*, vol. 51, no. 9-12, pp. 1179–1193, 2010.

[7] W. Yu, "Truck scheduling for cross docking systems with multiple receiving and shipping docks," *International Journal of Shipping and Transport Logistics*, vol. 7, no. 2, pp. 174–196, 2015.

[8] M. Madani-Isfahani, R. Tavakkoli-Moghaddam, and B. Naderi, "Multiple cross-docks scheduling using two meta-heuristic algorithms," *Computers & Industrial Engineering*, vol. 74, pp. 129–138, 2014.

[9] M. T. Assadi and M. Bagheri, "Scheduling trucks in a multiple-door cross docking system with unequal ready times," *European Journal of Industrial Engineering*, vol. 10, no. 1, pp. 103–125, 2016.

[10] M. T. Assadi and M. Bagheri, "Differential evolution and Population-based simulated annealing for truck scheduling problem in multiple door cross-docking systems," *Computers & Industrial Engineering*, vol. 96, no. 20, pp. 149–161, 2016.

[11] W. Wisittipanich and P. Hengmeechai, "A multi-objective differential evolution for Just-In-Time door assignment and truck scheduling in multi-door Cross docking problems," *Industrial*

Engineering & Management Systems, vol. 14, no. 3, pp. 299–311, 2015.

[12] A. R. Boloori Arabani, S. M. T. Fatemi Ghomi, and M. Zandieh, "A multi-criteria cross-docking scheduling with just-in-time approach," *The International Journal of Advanced Manufacturing Technology*, vol. 49, no. 5-8, pp. 741–756, 2010.

[13] K. Lee, B. S. Kim, and C. M. Joo, "Genetic algorithms for door-assigning and sequencing of trucks at distribution centers for the improvement of operational performance," *Expert Systems with Applications*, vol. 39, no. 17, pp. 12975–12983, 2012.

[14] A.-L. Ladier and G. Alpan, "Crossdock truck scheduling with time windows: earliness, tardiness and storage policies," *Journal of Intelligent Manufacturing*, 2014.

[15] B. Vahdani, R. Soltani, and M. Zandieh, "Scheduling the truck holdover recurrent dock cross-dock problem using robust meta-heuristics," *The International Journal of Advanced Manufacturing Technology*, vol. 46, no. 5-8, pp. 769–783, 2010.

[16] A. Mohtashami, "Scheduling trucks in cross docking systems with temporary storage and repetitive pattern for shipping trucks," *Applied Soft Computing*, vol. 36, pp. 468–486, 2015.

[17] N. Boysen, D. Briskorn, and M. Tschöke, "Truck scheduling in cross-docking terminals with fixed outbound departures," *OR Spectrum*, vol. 35, no. 2, pp. 479–504, 2013.

[18] S. Rahmanzadeh Tootkaleh, S. M. T. Fatemi Ghomi, and M. Sheikh Sajadieh, "Cross dock scheduling with fixed outbound trucks departure times under substitution condition," *Computers & Industrial Engineering*, vol. 92, pp. 50–56, 2016.

[19] Z. W. Geem, J. H. Kim, and G. V. Loganathan, "A new heuristic optimization algorithm: harmony search," *Simulation*, vol. 76, no. 2, pp. 60–68, 2001.

[20] M. Mahdavi, M. Fesanghary, and E. Damangir, "An improved harmony search algorithm for solving optimization problems," *Applied Mathematics and Computation*, vol. 188, no. 2, pp. 1567–1579, 2007.

[21] M. R. Valaei and J. Behnamian, "Allocation and sequencing in 1-out-of-N heterogeneous cold-standby systems: Multi-objective harmony search with dynamic parameters tuning," *Reliability Engineering & System Safety*, vol. 157, pp. 78–86, 2017.

Hindawi
Discrete Dynamics in Nature and Society
Volume 2018, Article ID 4585083, 24 pages
https://doi.org/10.1155/2018/4585083

Research Article

Image Encryption Technology Based on Fractional Two-Dimensional Triangle Function Combination Discrete Chaotic Map Coupled with Menezes-Vanstone Elliptic Curve Cryptosystem

Zeyu Liu,[1] **Tiecheng Xia**,[1,2] **and Jinbo Wang**[2]

[1]*Department of Mathematics, Shanghai University, Shanghai 200444, China*
[2]*Science and Technology on Communication Security Laboratory, Chengdu, Sichuan 610041, China*

Correspondence should be addressed to Tiecheng Xia; xiatc@shu.edu.cn

Received 7 December 2017; Revised 10 February 2018; Accepted 22 February 2018; Published 23 April 2018

Academic Editor: Youssef N. Raffoul

A new fractional two-dimensional triangle function combination discrete chaotic map (2D-TFCDM) with the discrete fractional difference is proposed. We observe the bifurcation behaviors and draw the bifurcation diagrams, the largest Lyapunov exponent plot, and the phase portraits of the proposed map, respectively. On the application side, we apply the proposed discrete fractional map into image encryption with the secret keys ciphered by Menezes-Vanstone Elliptic Curve Cryptosystem (MVECC). Finally, the image encryption algorithm is analysed in four main aspects that indicate the proposed algorithm is better than others.

1. Introduction

Nowadays, image encryption plays a significant role with the development of security technology in the areas of network, communication, and cloud service. Multifarious chaos-based image encryption algorithms have been developed up to now, such as in [1–6]; however a few of them have referred to the image encryption algorithm based on fractional discrete chaotic map accompanied with Elliptic Curve Cryptography (ECC).

The theory of the fractional difference has been developed for decades [7–13]. Recently, Wu et al. [14–16] made a contribution to the application of the discrete fractional calculus (DFC) on an arbitrary time scale, and the theories of delta difference equations were utilized to reveal the discrete chaos behavior.

ECC is a widely used technology in data security and communication security; it can achieve the same level of security with smaller key sizes and higher computational efficiency [17]. Many famous public-key algorithms, such as Diffie-Hellman, EIGamal, and Schnorr, can be implemented by means of elliptic curves over finite fields. MVECC is one of the popular elliptic curve public-key cryptosystems [18] and we adopt it in our cryptosystem.

Many encryption methods based on fractional derivatives have been proposed in recent time, like fractional logistic maps [19], fractional-order chaos systems [20], and fractional form of hyperchaotic system [21].

In [22], a new image encryption algorithm based on one-dimensional fractional chaotic time series within fractional-order difference has been proposed; however, the two-dimensional discrete chaotic map has seldom been used in image encryption except [23, 24].

Our main purpose is to introduce a new two-dimensional discrete chaotic map based on fractional-order difference and apply it in image encryption. The rest of this paper is organized as follows. In Section 2, the definitions and the properties of the DFC are introduced. After that, the definitions and operation of ECC are given. Then, the working principle of MVECC is described in the next section. In Section 5, we give the fractional 2D-TFCDM on time scales from the discrete integral expression. The bifurcation diagrams and the

phase portraits of the map are presented while the difference orders and the coefficients are changing; the largest Lyapunov exponent plots are also displayed. Afterwards, we apply the proposed map into image encryption and show several examples. In Section 7, the performance of the proposed image encryption method is analysed systematically. Finally, we have come to some conclusions.

2. Preliminaries

The definitions of the fractional sum and difference are given as follows. Let $\mathbb{N}_a$ denote the isolated time scale and $\mathbb{N}_a = \{a, a+1, a+2, \ldots\}$ ($a \in \mathbb{R}$ fixed). Within the DFC, the function $f(t)$ is changed as a sequence $f(n)$. The difference operator Δ is defined as $\Delta f(n) = f(n+1) - f(n)$.

Definition 1 (see [25]). Let $u\colon \mathbb{N}_a \to \mathbb{R}$ and $0 < \nu$ be given. The νth fractional sum is defined by

$$\Delta_a^{-\nu} u(t) \coloneqq \frac{1}{\Gamma(\nu)} \sum_{s=a}^{t-\nu} (t-s-1)^{\nu-1} u(s), \quad t \in \mathbb{N}_{a+\nu}. \tag{1}$$

Note that a is the starting point; $t^{(\nu)}$ is the falling function defined as

$$t^{(\nu)} = \frac{\Gamma(t+1)}{\Gamma(t+1-\nu)}. \tag{2}$$

Definition 2 (see [26]). For $0 < \nu$, $\nu \notin \mathbb{N}$, and $u(t)$ defined on $\mathbb{N}_a$, the ν-order Caputo fractional difference is defined by

$$\begin{aligned} {}^{C}\Delta_a^{\nu} u(t) &\coloneqq \Delta_a^{-(m-\nu)} \Delta^m u(t) \\ &= \frac{1}{\Gamma(m-\nu)} \sum_{s=a}^{t-(m-\nu)} (t-s-1)^{(m-\nu-1)} \Delta^m u(s), \\ &\qquad t \in \mathbb{N}_{a+m-\nu}, \ m = [\nu] + 1. \end{aligned} \tag{3}$$

Theorem 3 (see [27]). *For the delta fractional difference equation*

$$\begin{aligned} {}^{C}\Delta_a^{\nu} u(t) &= f(t+\nu-1, u(t+\nu-1)), \\ \Delta^k u(a) &= u_k, \quad m = [\nu]+1, \ k = 0, \ldots, m-1 \end{aligned} \tag{4}$$

the equivalent discrete integral equation is

$$\begin{aligned} x(n) = u_0(t) + \frac{1}{\Gamma(\nu)} \sum_{s=a+m-\nu}^{t-\nu} (t-s-1)^{(\nu-1)} \\ \times f(s+\nu-1, u(s+\nu-1)), \quad t \in \mathbb{N}_{a+m}, \end{aligned} \tag{5}$$

where

$$u_0(t) = \sum_{k=0}^{m-1} \frac{(t-a)^{(k)}}{k!} \Delta^k u(a). \tag{6}$$

The complex difference equation with long-term memory is obtained here. It can reduce to the integer order one with the difference order $\nu = 1$ but the integer one does not hold the discrete memory. From (3) to (5), the domain is shifted from $\mathbb{N}_{a+m-\nu}$ to $\mathbb{N}_{a+m}$ and the function $u(t)$ is preserved to be defined on the isolated time scale $\mathbb{N}_a$ in the fractional sums.

3. Introduction to Elliptic Curve

Definition 4. An elliptic curve (EC) E over a prime field F_p denoted by $E(F_p)$ refers to the set of all points (x, y) that satisfy the equation

$$E : y^2 \equiv x^3 + ax + b \pmod{p}, \tag{7}$$

together with a special point O at infinity, where $a, b \in F_p$, $p \neq 2, 3$ and $4a^3 + 27b^2 \neq 0$ [28, 29].

3.1. Elliptic Curve Operations. If $P = (x_1, y_1)$, $Q = (x_2, y_2) \in E(F_p)$; then if $x_1 = x_2$ but $y_1 \neq y_2$, $P + Q = O$; that is, $Q = -P = (x_1, -y_1)$ [29].

$$P + Q = \begin{cases} R = (x_3, y_3), & P \neq -Q, \\ O, & P = -Q, \end{cases} \tag{8}$$

where

$$\begin{aligned} x_3 &\equiv \left(\lambda^2 - 2x_1\right) \pmod{p}, \\ y_3 &\equiv \left(\lambda(x_1 - x_3) - y_1\right) \pmod{p}, \\ \lambda &= \begin{cases} \dfrac{(y_2 - y_1)}{(x_2 - x_1)}, & P \neq Q, \\ \dfrac{3x_1^2 + a}{2y_1}, & P = Q. \end{cases} \end{aligned} \tag{9}$$

The scalar multiplication over $E(F_p)$ is defined by

$$kP = \underbrace{P + P + \cdots + P}_{k \text{ times}}, \tag{10}$$

where k is an integer.

Definition 5. The order of an EC is defined by the number of points that lie on the EC denoted by $\#E$ [29].

Definition 6. Set $P \in E(F_p)$, and then P is called a generator point if $\mathrm{ord}(P) = \#E$ ($\mathrm{ord}(P)$ is the smallest positive integer n that makes $nP = O$) [29].

4. Menezes-Vanstone Elliptic Curve Cryptosystem (MVECC)

MVECC is one of most significant extensions of ECC; the working principle of MVECC is as follows.

If Andy wants to encrypt and send the message M to Bob, they should do the step as mentioned hereunder:

(1) Andy and Bob make an agreement on an elliptic curve $E(F_p)$ and the base point α.

(2) Bob firstly selects a private key k to compute the public key $\gamma = k \cdot \alpha$ ($0 \leqq k < \mathrm{ord}(\alpha)$).

(3) If Andy wants to send a message $M = (x_1, x_2) \in Z_p^* \times Z_p^*$ to Bob, he firstly chooses a random private key d ($0 \leqq d < \mathrm{ord}(\alpha)$) and then computes his public key $\beta = d \cdot \alpha$. On the other hand, Andy calculates the secret key (c_1, c_2) by

$$(c_1, c_2) = d \cdot \gamma = d \cdot k \cdot \alpha = k \cdot \beta. \tag{11}$$

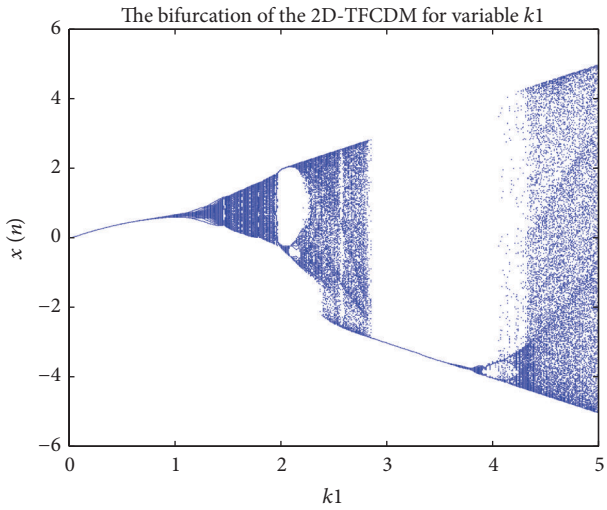

FIGURE 1: The bifurcation diagram of the 2D-TFCDM of variable k_1 for $\nu = 1$.

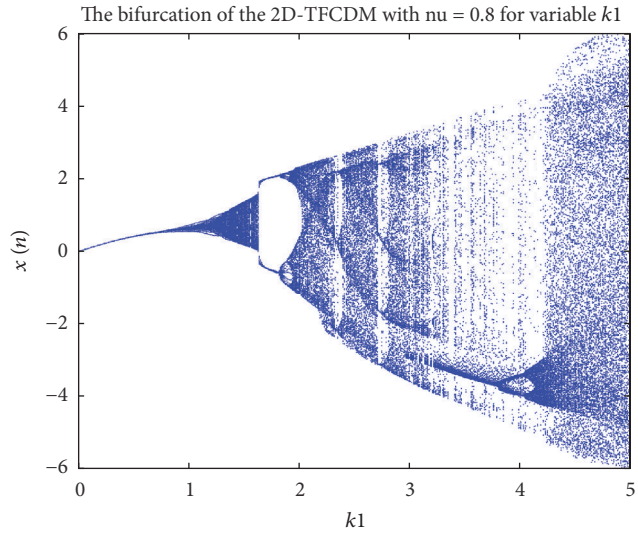

FIGURE 2: The bifurcation diagram of the fractional 2D-TFCDM of variable k_1 for $\nu = 0.8$.

He should compute the ciphered message afterwards by

$$\begin{aligned} y_1 &= x_1 * c_1 \mod p, \\ y_2 &= x_2 * c_2 \mod p. \end{aligned} \tag{12}$$

(4) Then the ciphertext $\{\gamma, (y_1, y_2)\}$ is sent to Bob. When Bob wants to get the plaintext (x_1, x_2), firstly, he computes the secret key $(c_1, c_2) = k \cdot \beta = k \cdot d \cdot \alpha$, and then he computes $M = (x_1, x_2)$ by

$$\begin{aligned} x_1 &= y_1 * c_1^{-1} \mod p, \\ x_2 &= y_2 * c_2^{-1} \mod p, \end{aligned} \tag{13}$$

to get the plaintext [18].

Any adversary that only has β and γ without the private keys d and k very difficultly breaks the MVECC to get the plaintext M. What is more, if $\#E$ have only one big prime divisor, the EC is called a safe EC [29]; then, the MVECC can become an more efficient and secure cryptosystem.

5. Fractional 2D-TFCDM

From [14–16], we notice the application of the DFC in fractional generalizations of the discrete chaotic maps. Recently [30], the following 2D-TFCDM was proposed:

$$\begin{aligned} x_{n+1} &= k_1 \cos(x_n + y_n), \quad k_1 = 8, \\ y_{n+1} &= k_2 \sin(x_n - y_n), \quad k_2 = 0.5. \end{aligned} \tag{14}$$

Now, consider the fractional generalization of $x(n)$; the map was also studied in [31]:

$$\begin{aligned} {}^{C}\Delta_{\alpha}^{\nu} x(t) &= k_1 \cos(x(t+\nu) + y(t+\nu)) - x(t+\nu), \\ &\qquad 0 < \nu < 1, \ t \in N_{a+1-\nu}, \\ y_{n+1} &= k_2 \sin(x_n - y_n), \quad k_2 = 0.5. \end{aligned} \tag{15}$$

From Theorem 3, we have the following equivalent discrete numerical formula for the variable k_1: ($k_2 = 0.5$) with $0 < \nu < 1$:

$$\begin{aligned} x(n) &= x(0) + \frac{1}{\Gamma(\nu)} \sum_{j=1}^{n} \frac{\Gamma(n-j+\nu)}{\Gamma(n-j+1)} \\ &\quad \cdot [k_1 \cos(x(j-1) + y(j-1)) - x(j-1)], \\ y(n) &= k_2 \sin(x(n-1) - y(n-1)), \quad k_2 = 0.5. \end{aligned} \tag{16}$$

Let $\nu = 1$, $x(0) = 0.19$, $y(0) = 0.06$, $n = 200$, and k_1 be fixed. In what follows, Figure 1 is the bifurcation diagram where the step size of k_1 is 0.002. Figure 2 is the same bifurcation diagram except for $\nu = 0.8$.

In Figures 3 and 4, the largest Lyapunov exponent plots are drawn by use of the Jacobian matrix algorithm proposed in [32]. The largest Lyapunov exponent LE is positive somewhere; it is corresponding to the chaotic intervals in Figures 1 and 2.

By choosing 101 different initial values we can plot $y(n)$ versus $x(n)$ in one figure. The phase portraits of the integer map are derived from Figure 5. The cases of $\nu = 0.8$ and $\nu = 0.6$ are plotted in Figures 6 and 7, respectively.

6. Applications

The fractionalized chaotic map can be applied in image encryption. Exploit (16) into an algorithm, and set the initial values x_0, y_0, the order ν, and the coefficients k_1, k_2 of chaotic system as keys. In this paper, we propose the encryption algorithm and divide it into 3 parts.

6.1. Generation of New Keys Based on Elliptic Curve in a Finite Field. Setting $a = 1$, $b = 6$, and $p = 9996887$ in (7), we can get $E(F_{9996887})$. Since $\#E = 10000721$ is a prime number, according to [29], $E(F_{9996887})$ is a safe EC. Let $\alpha = (2, 4)$,

randomly select $d = 9134417$, $k = 1269960 \in [1, \#E]$; then $\beta = d\alpha = (6020909, 7282175)$, $\gamma = k\alpha = (7495358, 7052635)$, and $(c_1, c_2) = k\beta = (3049362, 3915118) = d\gamma$. The initial key $\nu = 0.6026331$, $x_0 = 4.107532$, $\nu_{01} = \nu \times 10^7 = 6026331$, and $x_{01} = x_0 \times 10^6 = 4107532$.

Calculate

$$\begin{aligned} \nu'_{01} &= c_1 * \nu_{01} \mod p = 3049362 \cdot 6026331 \bmod 9996887 = 7123456 \bmod 9996887, \\ x'_{01} &= c_2 \cdot x_{01} \mod p = 3915118 \cdot 4107532 \bmod 9996887 = 190000 \bmod 9996887. \end{aligned} \tag{17}$$

Then, the ciphertext is $((7495358, 7052635), 7123456, 190000)$, the enciphered key is $\nu' = \nu'_{01}/10^7 = 0.7123456$, and $x'_0 = x'_{01}/10^6 = 0.19$.

Make $y_0 = 3.650991$, $k_1 = 0.897029$, and $k_2 = 0.434264$, and compute $y_{01} = y_0 \times 10^6$, $k_{01} = k_1 \times 10^6$, and $k_{02} = k_2 \times 10^6$; then

$$\begin{aligned} y'_{01} &= c_1 \cdot y_{01} \mod p = 3049362 \cdot 3650991 \bmod 9996887 = 60000 \bmod 9996887, \\ k'_{01} &= c_2 \cdot k_{01} \mod p = 3915118 \cdot 897029 \bmod 9996887 = 8000000 \bmod 9996887, \\ k'_{02} &= c_1 \cdot k_{02} \mod p = 3049362 \cdot 434264 \bmod 9996887 = 500000 \bmod 9996887. \end{aligned} \tag{18}$$

Set $y'_0 = y'_{01}/10^6 = 0.06$, $k'_1 = k'_{01}/10^6 = 8$, $k'_2 = k'_{02}/10^6 = 0.5$, and then x'_0, y'_0, ν', k'_1, k'_2 are taken as the keys of Section 6.2.

6.2. Permutation Procedure Based on Fractional 2D-TFCDM. Taking advantage of (16) with the initial values x'_0, y'_0, ν', k'_1, and k'_2 generated in the last section, we can encrypt the image. The next step of encryption is permutation; it is subdivided into 4 steps:

(1) Set x'_0 as $x(1)$; iterate (16) for $MN-1$ times to generate the one-dimensional real number chaotic sequence $x(i)$, $i = 1, 2, \ldots, MN$; here M and N denote the length and width of the original image V, respectively.

(2) Reorder $x(k)$ by the bubble sort and get $x'(k)$, and record the change of the subscript of $x(k)$ as $z(k)$.

(3) Change $M \times N$ original image V into $1 \times MN$ sequence $v(k)$, and rearrange $v(k)$ according to $z(k)$ to get the new sequence $v'(k)$.

(4) Reshape $v'(k)$ into $M \times N$ image as V'; V' is the permutated image we needed.

Reversing the above 4 steps, we can remove the effect of permutation to get the original image.

6.3. Encryption Method Based on Fractional 2D-TFCDM. (1) In Section 6.2 we get the chaotic sequence $x(i)$ and image V'. Reshape $M \times N$ image V' into $1 \times MN$ sequence $u(i)$; that is $i = N(m-1) + n$, $(m = 1, 2, \ldots, M, n = 1, 2, \ldots, N)$. Another $M \times N$ image is used as a key image (K-image). Change the K-image also into $1 \times MN$ sequence $w(i)$.

(2) Set $i = 0$.

(3) Round $x(i) \times 10^8$ as $x_1(i)$, do modulus operation to $x_1(i)$ in (19), and get $x_2(i)$:

$$x_2(i) = \operatorname{mod}\left(x_1(i), 256\right). \tag{19}$$

(4) Do the following operation and get $u'(i)$:

$$u'(i) = u(i) \oplus \operatorname{mod}\left(w(i) + x_2(i), 256\right), \tag{20}$$

where $\oplus$ refers to the Xor operation, and $u'(i)$ is the encrypted pixel value.

The inverse form of (20) is

$$u(i) = u'(i) \oplus \operatorname{mod}\left(w(i) + x_2(i), 256\right). \tag{21}$$

(5) Compute the iteration times $k(i)$ according to

$$k(i) = 1 + \operatorname{mod}\left(u'(i), 256\right). \tag{22}$$

Then, iterate (16) for $k(i)$ times to get $x(i+1)$, circle from step (3) to step (5), until getting $x(MN)$.

(6) Change $u'(i)$ into $M \times N$ image as V'', which is the finally encrypted figure we need.

The decryption procedure is including 2 parts:

(1) Do all steps in encryption process except (20) which is replaced by (21).

(2) Reverse the procedure in Section 6.2. Then the decryption procedure is done.

Figure 8 shows the encryption process described in Sections 6.2 and 6.3 in a flow chart, and Figure 9 illustrates the iteration procedure of S box.

The original, encrypted, and decrypted images are shown in Figures 10–18. The proposed algorithm can encrypt any rectangular image.

The adopted cryptosystem in Section 6.1 is asymmetric; however, the ones in Sections 6.2 and 6.3 are symmetric.

7. Analysis of Results in Applications

7.1. Key Space. In the proposed algorithm, the initial values x_0, y_0, the order ν, and the coefficients k_1, k_2 are taken as the

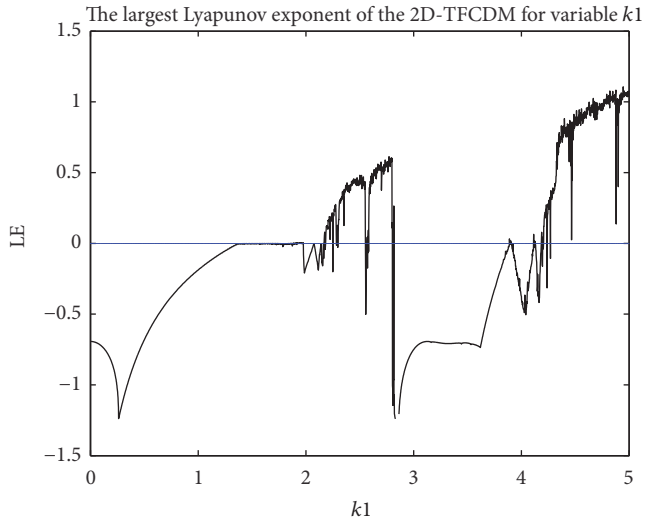

Figure 3: The largest Lyapunov exponent of the 2D-TFCDM of the variable k_1.

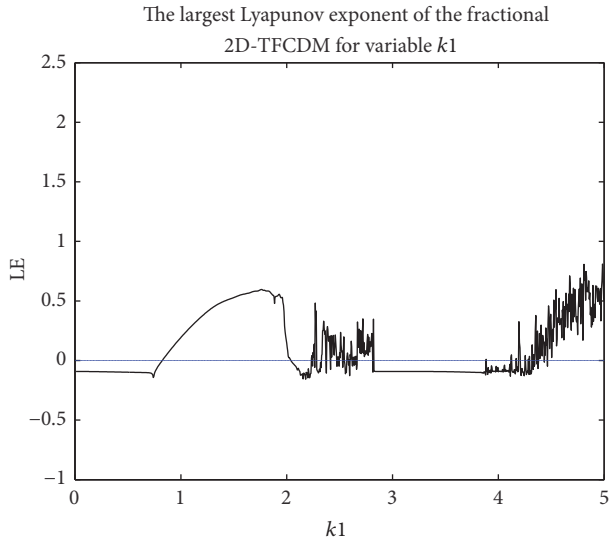

Figure 4: The largest Lyapunov exponent of the fractional 2D-TFCDM of the variable k_1.

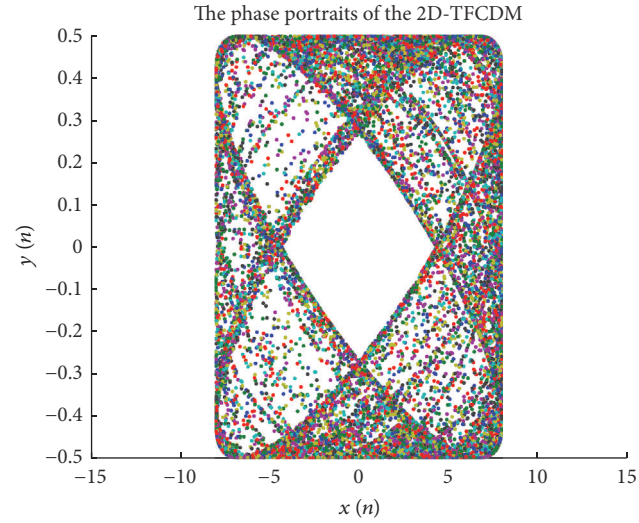

Figure 5: The phase portraits of the 2D-TFCDM for $k_1 = 8$, $k_2 = 0.5$, and $\nu = 1$.

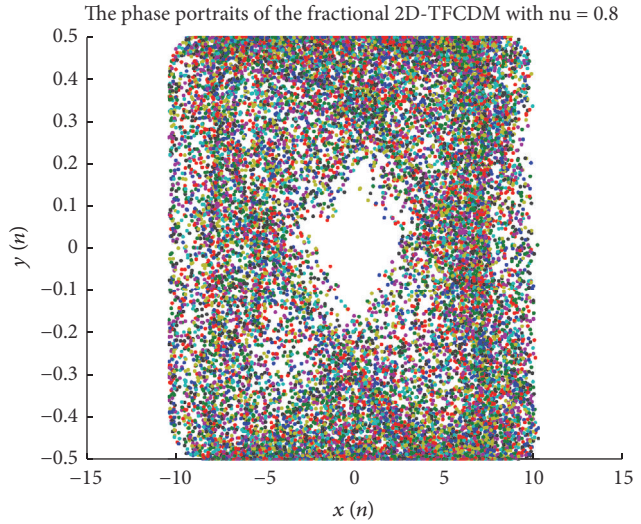

Figure 6: The phase portraits of the fractional 2D-TFCDM for $k_1 = 8$, $k_2 = 0.5$, and $\nu = 0.8$.

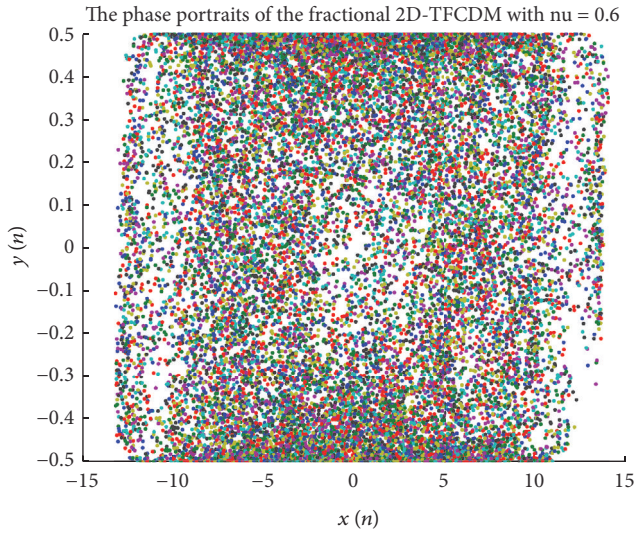

Figure 7: The phase portraits of the fractional 2D-TFCDM for $k_1 = 8$, $k_2 = 0.5$, and $\nu = 0.6$.

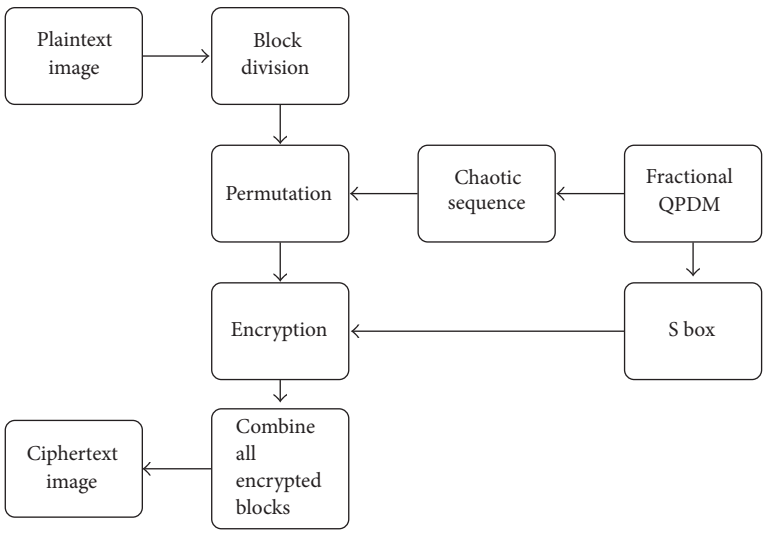

Figure 8: The proposed encryption method.

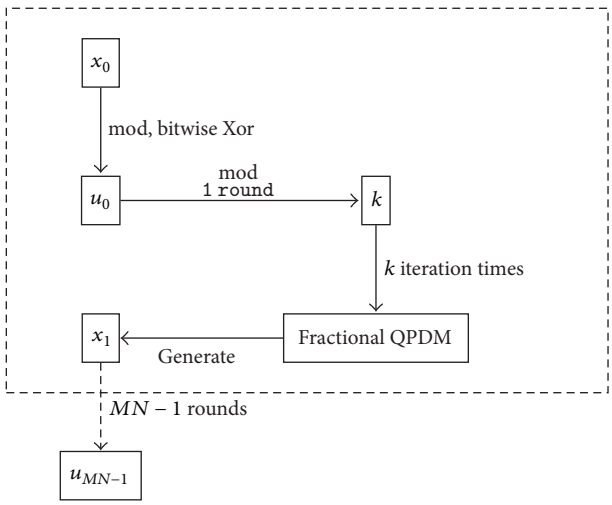

Figure 9: The S box.

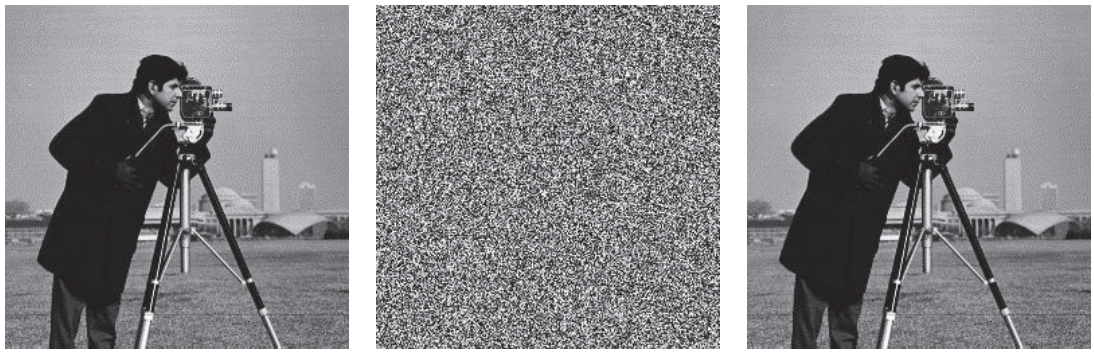

(a) The original figure (b) The encrypted figure (c) The decrypted figure

Figure 10: Cameraman.

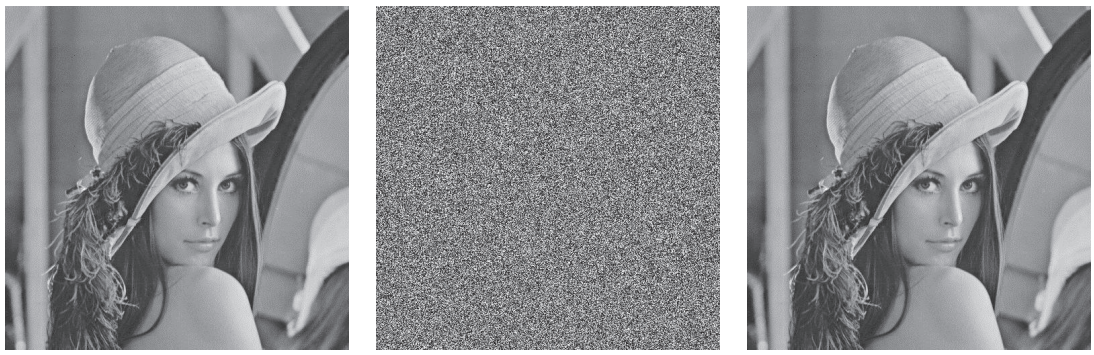

(a) The original figure (b) The encrypted figure (c) The decrypted figure

Figure 11: Lena.

secret keys; consequently there are 5 keys. Assume the precision of x_0, y_0, ν, k_1, and k_2 are $10^{-16}, 3 \times 10^{-17}, 10^{-16}, 10^{-15}$, and 10^{-16}, respectively; then the key's space is $1/3 \times 10^{80} \approx 1.12 \times 2^{264}$. If the size of the plaintext is 512×512, then the key space of K-image is also $512 \times 512 \times 2^8 = 2^{26}$. The total key space of the proposed algorithm is 1.12×2^{290}.

7.2. Statistics Analysis. The quality against any statistical attack is important for a well-designed encryption method; it include 3 aspects as follows.

7.2.1. Correlation of the Plain- and Cipher-Images. In an ordinary image, the adjacent pixels are related; therefore the correlation coefficient of adjacent pixels is usually high. A good


(a) The original figure

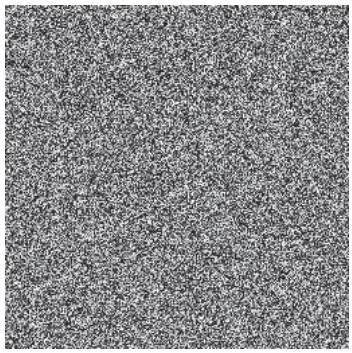
(b) The encrypted figure


(c) The decrypted figure

Figure 12: Peppers.


(a) The original figure

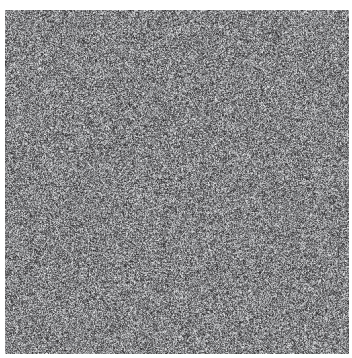
(b) The encrypted figure


(c) The decrypted figure

Figure 13: Lake.

(a) The original figure

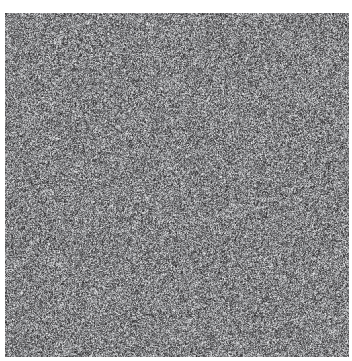
(b) The encrypted figure

(c) The decrypted figure

Figure 14: Dollar.

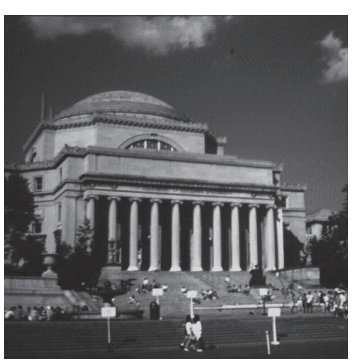
(a) The original figure

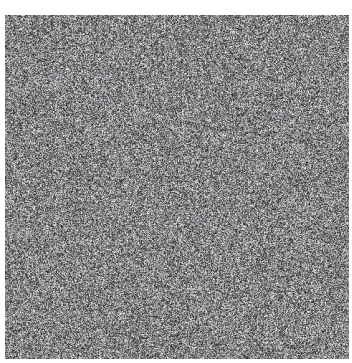
(b) The encrypted figure

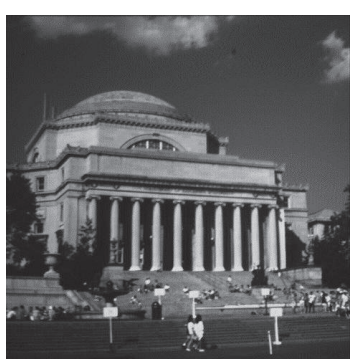
(c) The decrypted figure

Figure 15: Columbia.

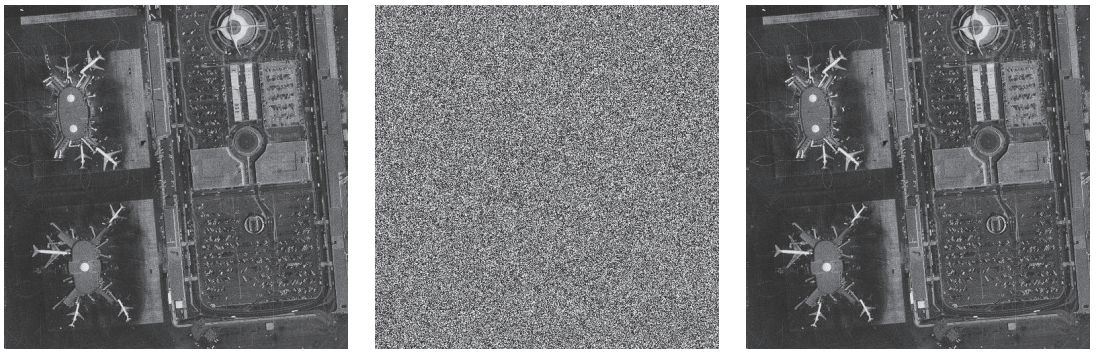

(a) The original figure (b) The encrypted figure (c) The decrypted figure

Figure 16: Lax.

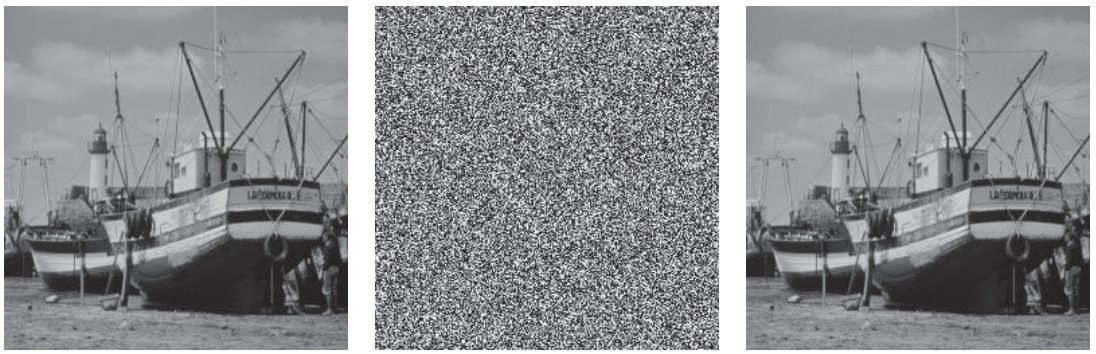

(a) The original figure (b) The encrypted figure (c) The decrypted figure

Figure 17: Boat.

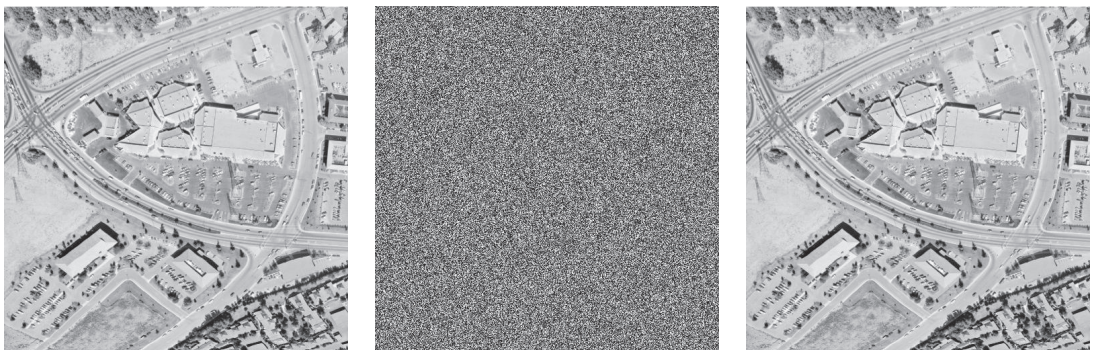

(a) The original figure (b) The encrypted figure (c) The decrypted figure

Figure 18: Aerial.

encryption algorithm should make the correlation coefficients of encrypted image nearly equal to zero. The closer to zero the correlation coefficients is, the better the encryption algorithm is. Formulas (23) calculate the correlation coefficient. The correlations along the x direction of both original and encrypted images are displayed in Figures 19–27 from Cameraman to Aerial. The correlation coefficients are displayed in Table 1.

$$r_{xy} = \frac{\left|\operatorname{cov}(x, y)\right|}{\sqrt{D(x)}\sqrt{D(y)}}$$

$$\operatorname{cov}(x, y) = \frac{1}{N}\sum_{i=1}^{N}\left(x_i - E(x)\right)\left(y_i - E(y)\right)$$

$$E(x) = \frac{1}{N}\sum_{i=1}^{N}x_i$$

$$D(x) = \frac{1}{N}\sum_{i=1}^{N}\left(x_i - E(x)\right)^2. \tag{23}$$

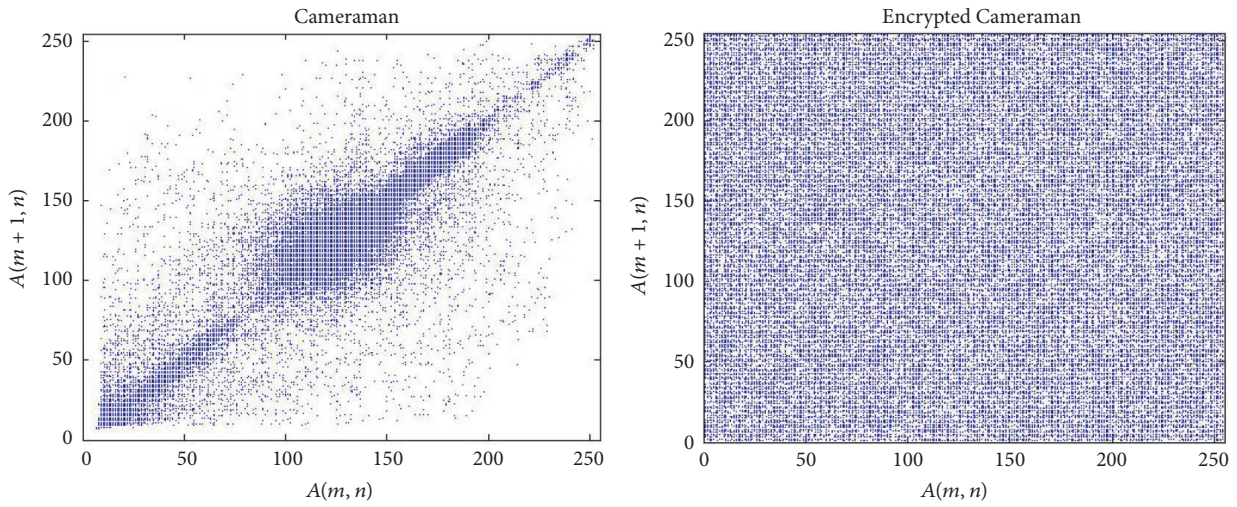

(a) The original figure (b) The encrypted figure

Figure 19: Cameraman.

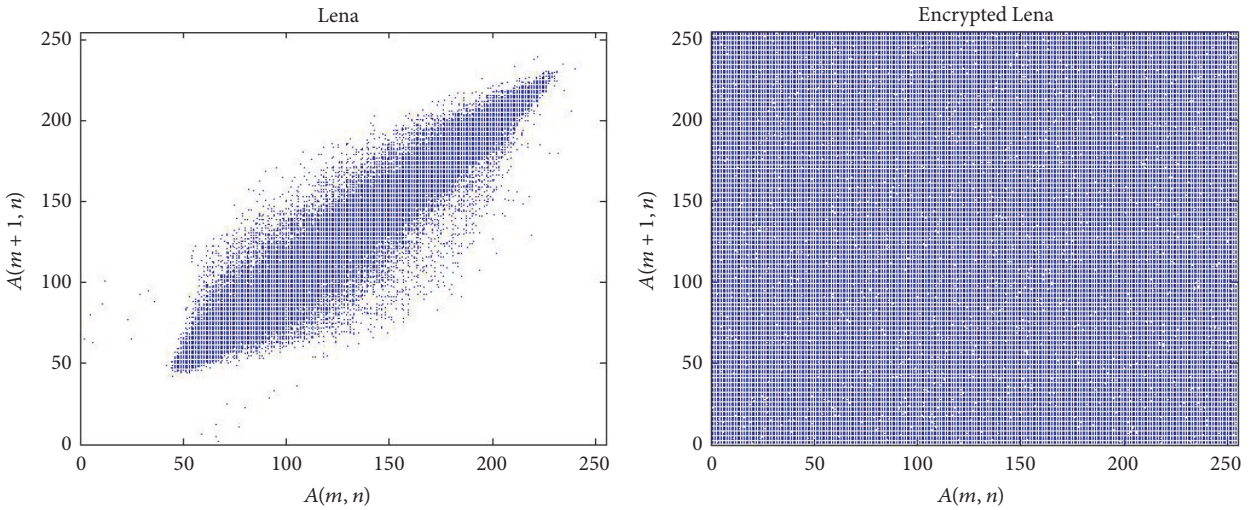

(a) The original figure (b) The encrypted figure

Figure 20: Lena.

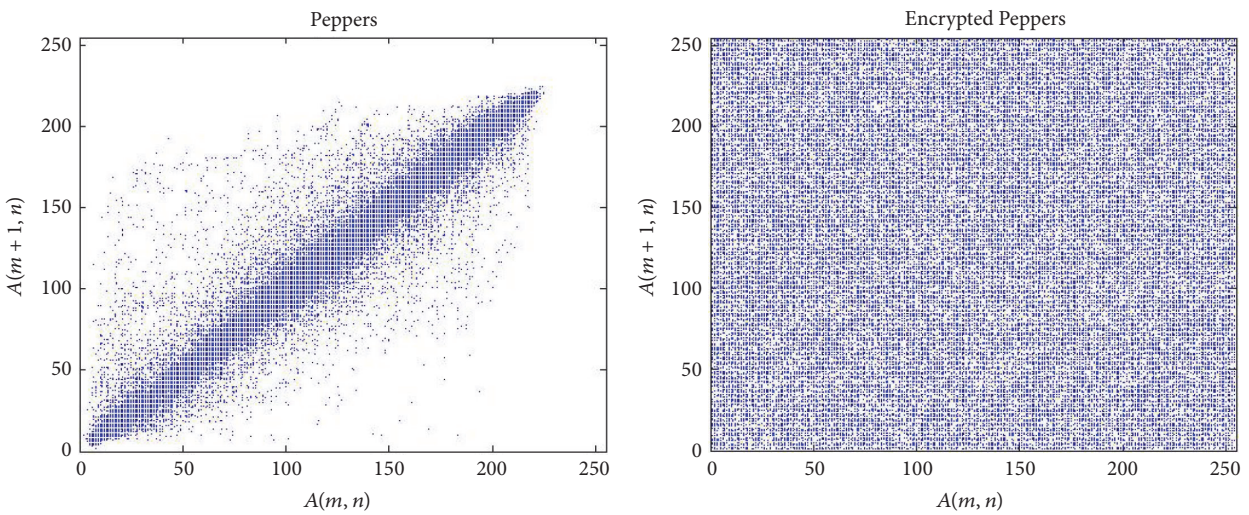

(a) The original figure (b) The encrypted figure

Figure 21: Peppers.

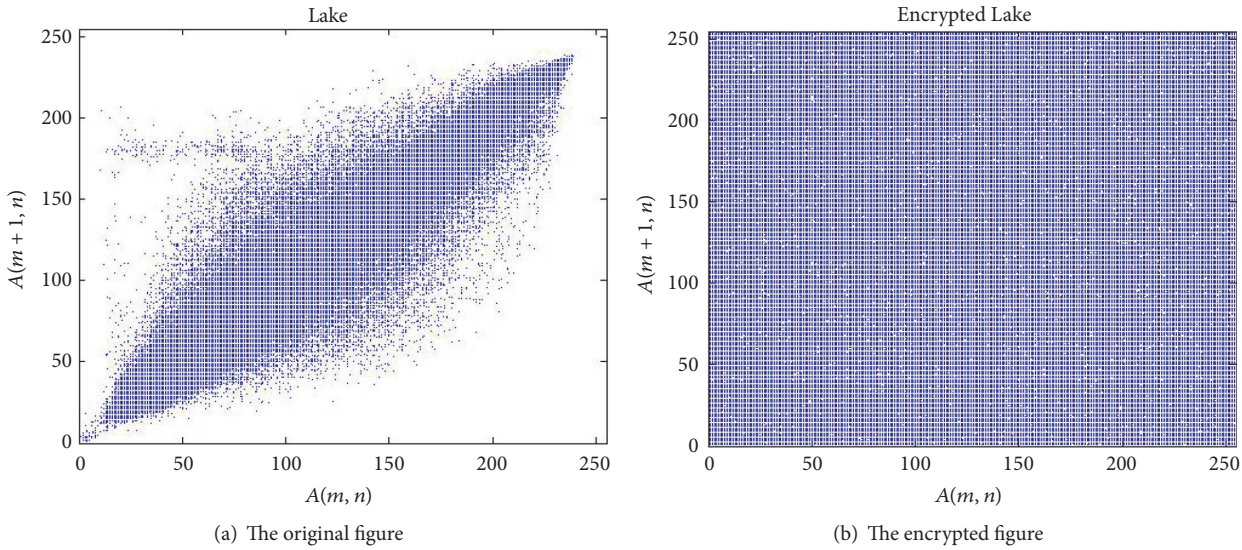

(a) The original figure (b) The encrypted figure

Figure 22: Lake.

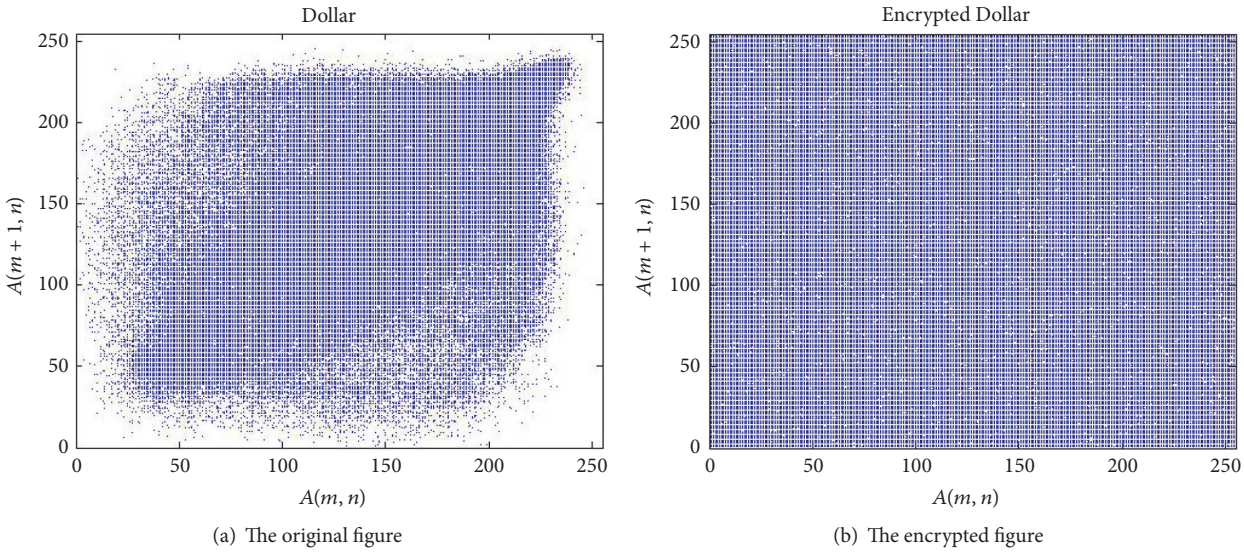

(a) The original figure (b) The encrypted figure

Figure 23: Dollar.

With the sharp contrast of data between original image and encrypted image, Table 1 indicates that the encryption process make pixels of the encrypted image almost independent with each other. Consequently, the encryption algorithm is good at pixel value randomization.

Compared with other algorithm, we can observe that most correlation coefficients of encrypted image are nearer to 0 in Table 2. As a consequence of this, the proposed encryption algorithm is superior to others.

7.2.2. Histogram. Histogram reflects the distribution of colors inside the image. The adversary can get some effective information from the regularity of histogram. Therefore, a well-designed image encryption method should make the pixel value of encrypted image distribute uniformly. Figure 28 shows the histogram of Cameraman. Similarly, the histograms of the other 8 cases are drawn in Figures 29–36. It is illustrated that the proposed encryption method has a good effect on pixel value distribution uniformization.

7.2.3. Information Entropy. Information entropy defines the randomness and the unpredictability of information in an image. It is defined by

$$H(m) = \sum_{i=0}^{2^n-1} p(m_i) \log_2 \frac{1}{p(m_i)}. \tag{24}$$

Here $p(m_i)$ is the probability of m_i; n is the number of bits that is required to represent the symbol m_i. For the pixels values of the image are 0~255, according to (24) the information entropy is 8 bits for an ideally random image. Therefore, the closer to 8 bits the information entropy is, the better

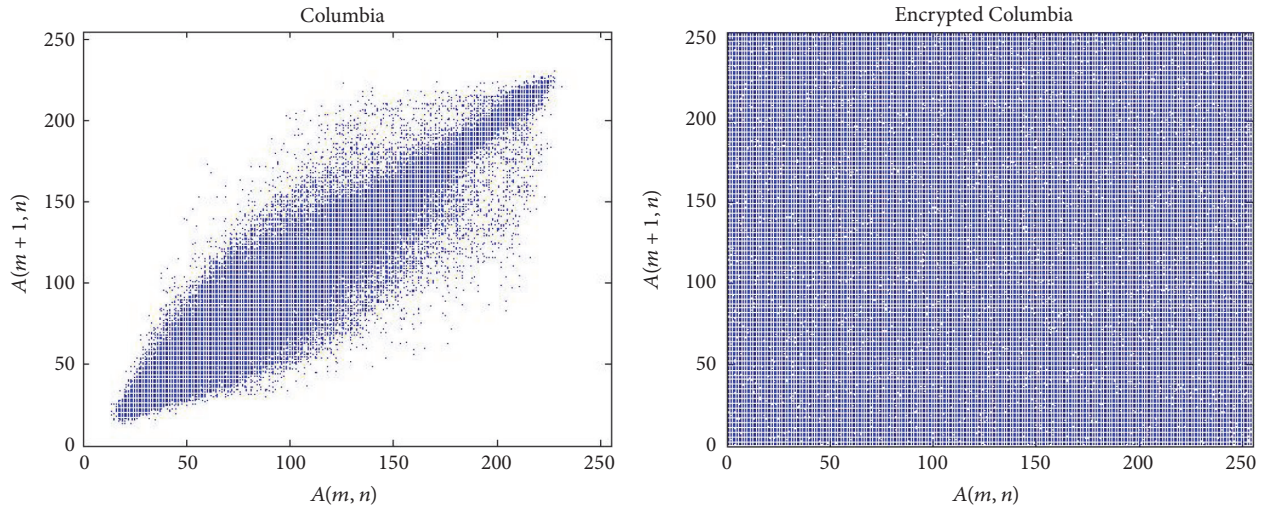

(a) The original figure (b) The encrypted figure

Figure 24: Columbia.

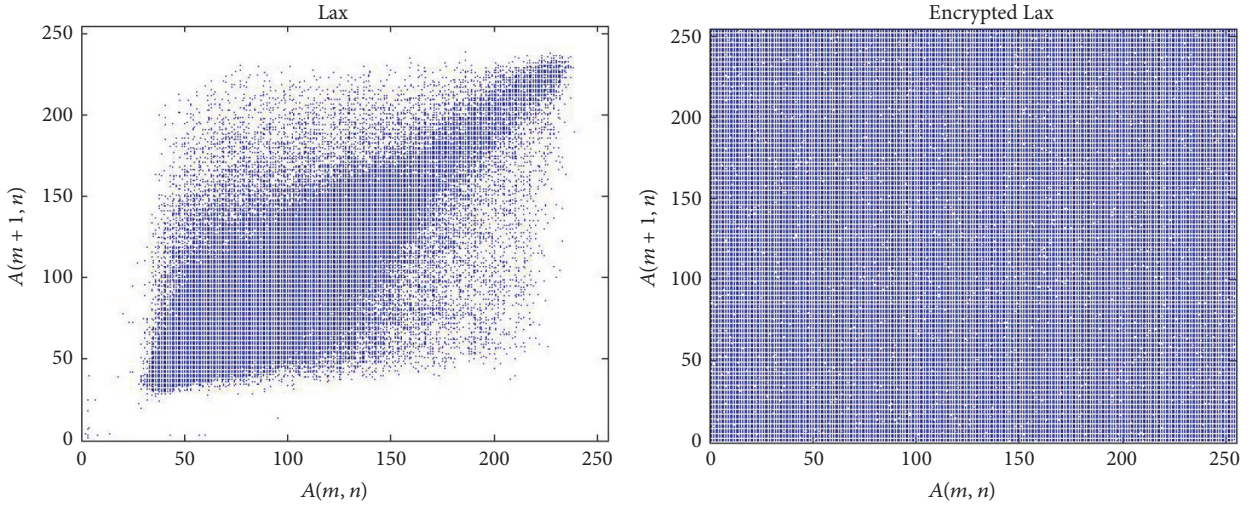

(a) The original figure (b) The encrypted figure

Figure 25: Lax.

Table 1: Correlation coefficients of image.

Image	Original image			Encrypted image		
	Horizontal	Diagonal	Vertical	Horizontal	Diagonal	Vertical
Cameraman	0.9276	0.9120	0.9597	0.0119	−0.0021	−0.0025
Lena	0.9722	0.9527	0.9860	−0.0140	−0.0086	−0.0034
Peppers	0.9667	0.9382	0.9694	−0.0088	0.0080	−0.0054
Lake	0.9768	0.9544	0.9748	−0.0155	0.0101	−0.0088
Dollar	0.8035	0.6952	0.6938	0.0131	−0.0183	0.0263
Columbia	0.9727	0.9403	0.9705	0.0060	−0.0104	−0.0093
Lax	0.7889	0.7151	0.8483	−0.0107	0.0147	0.0107
Boat	0.9407	0.9158	0.9545	0.0169	−0.0074	−0.0077
Aerial	0.9135	0.7952	0.8677	0.0084	−0.0123	−0.0133

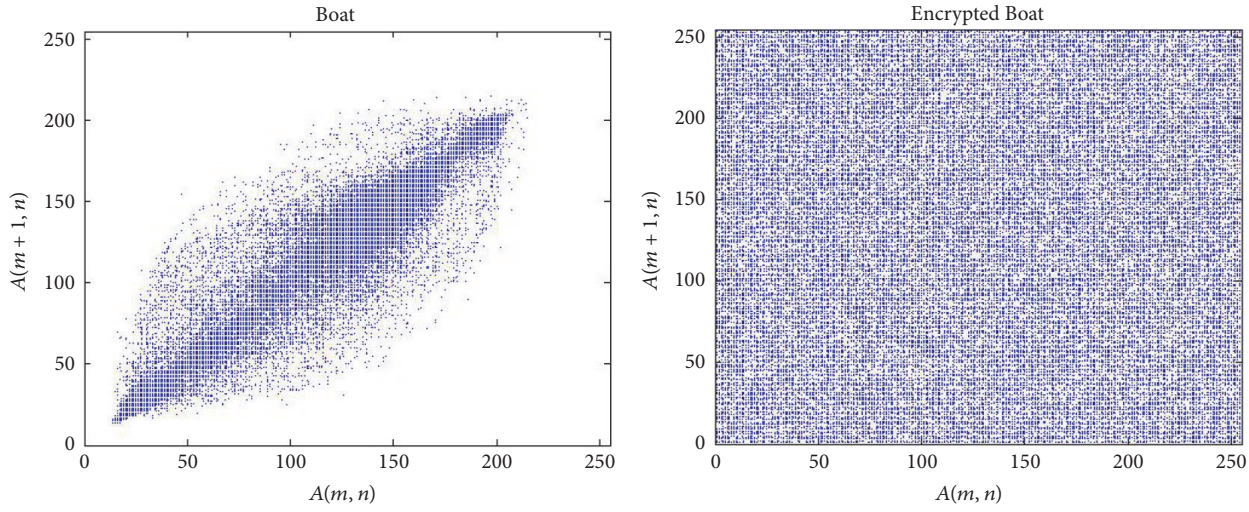

(a) The original figure (b) The encrypted figure

Figure 26: Boat.

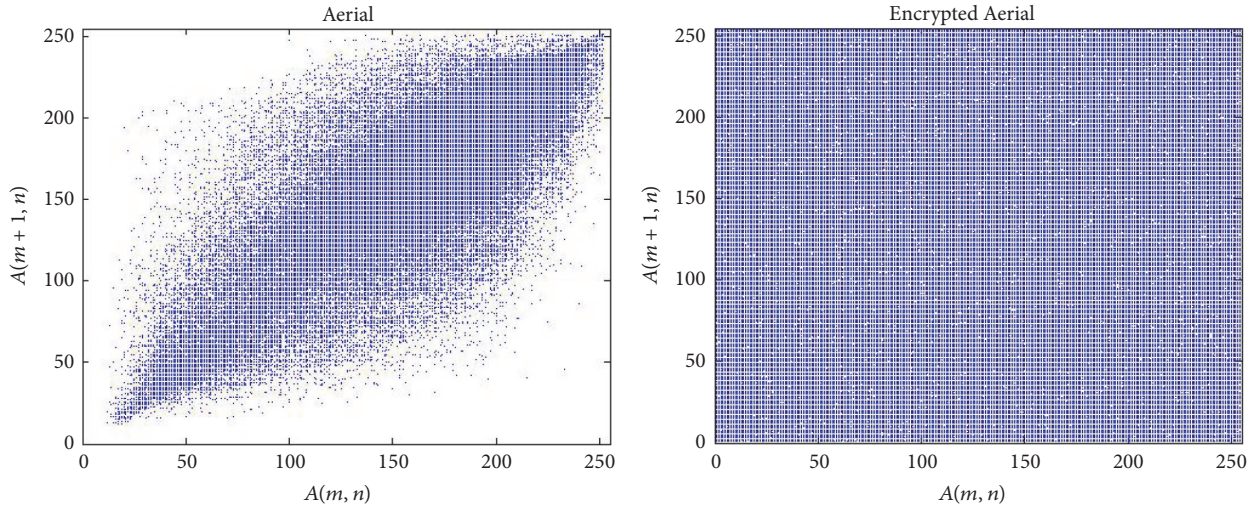

(a) The original figure (b) The encrypted figure

Figure 27: Aerial.

the encryption algorithm is. The information entropy of the 9 cases is gotten in Table 3; it indicates that the encrypted images are very close to the random images.

From Table 4, we can observe that the information entropy of proposed algorithm is nearer to 8 bits than other algorithms.

7.3. Sensitivity Analysis. The different range between two images is measured by two criteria: number of pixels change rate (NPCR) and unified average changing intensity (UACI). They are defined as follows:

$$D(i,j) = \begin{cases} 0, & T_1(i,j) = T_2(i,j), \\ 1, & T_1(i,j) \neq T_2(i,j), \end{cases}$$

$$\text{NPCR} = \frac{\sum_{i=1}^{W}\sum_{j=1}^{H} D(i,j)}{W \times H} \times 100\%$$

$$\text{UACI} = \frac{\sum_{i=1}^{W}\sum_{j=1}^{H} \left|T_1(i,j) - T_2(i,j)\right|}{255W \times H} \times 100\%. \tag{25}$$

Here W and H are the width and the height of T_1 and T_2.

7.3.1. Key Sensitivity. We encrypt the image by the keys $x_0 = 0.19$, $y_0 = 0.06$, $\nu = 0.7123456$, $k_1 = 8$, and $k_2 = 0.5$. Figure 37(a) is the decrypted image with the correct keys. Figure 37(b) represents the decrypted image under 10^{-16} adding to x_0 with other keys unchanged. Similarly, the secret

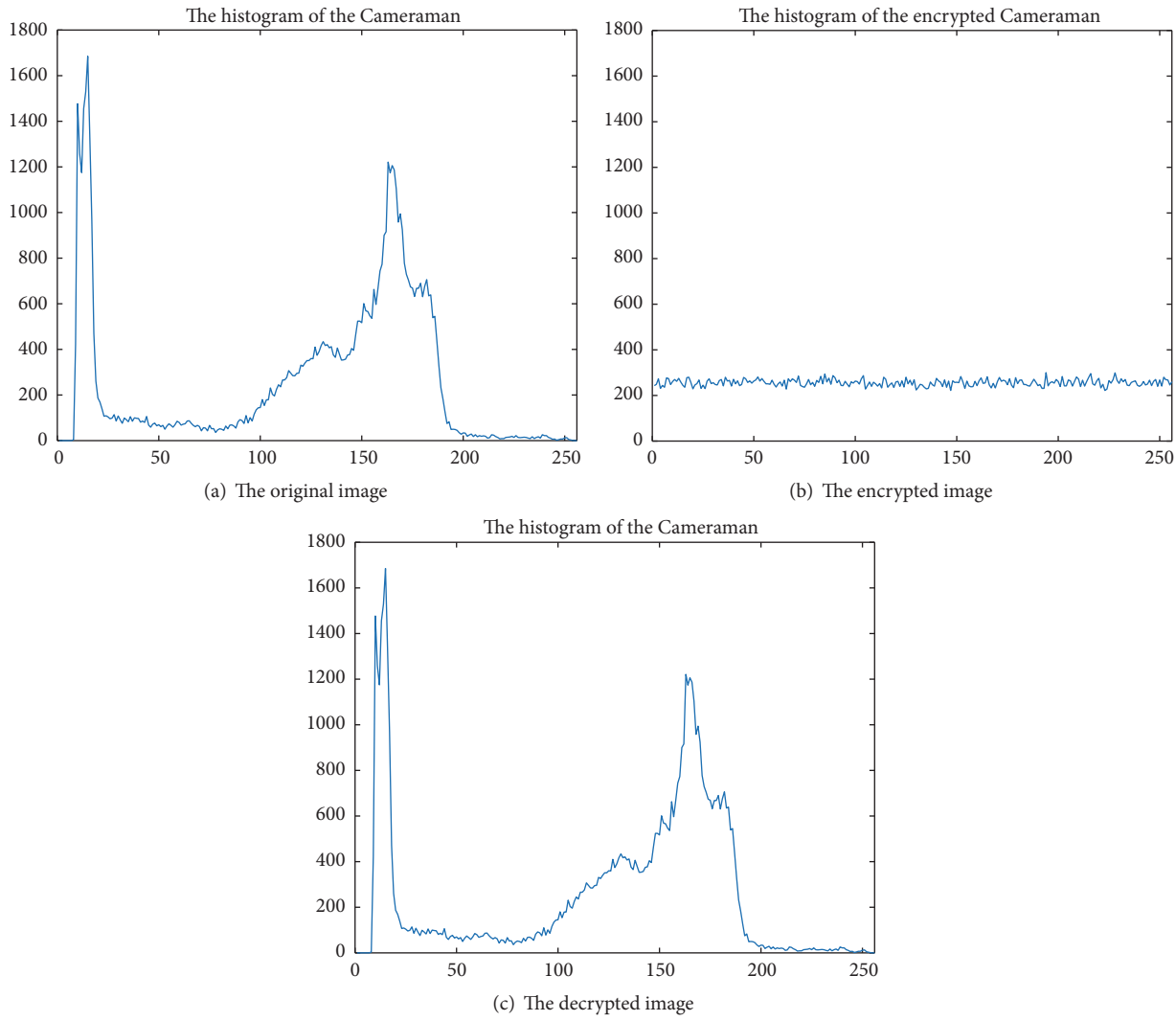

(a) The original image

(b) The encrypted image

(c) The decrypted image

Figure 28: Cameraman.

Table 2: Comparison of correlation coefficients of image.

Algorithm	Image	Original image			Encrypted image		
		Horizontal	Vertical	Diagonal	Horizontal	Vertical	Diagonal
Proposed	Lena	0.9722	0.9527	0.9860	−0.0140	−0.0086	−0.0034
[1]	Lena	0.9503	0.9755	0.9275	−0.0226	0.0041	0.0368
[2]	Lena	0.927970	0.926331	0.839072	−0.010889	−0.018110	−0.006104
[5]	Lena	0.946	0.973	0.921	−0.0055	−0.0075	0.0026
[6]	Lena	0.9569	0.9236	0.9019	0.0042	−0.0043	0.0163

keys y_0, ν, k_1, k_2 are added as $3 \times 10^{-17}, 10^{-16}, 10^{-15}$ and 10^{-16} to decrypt the images separately with other keys unchanged. The results are shown in Figures 37(c)–37(f). The comparison of key space is shown in Table 5 and the NPCR and UACI between Figures 37(a) and 37(b)–37(f) are calculated in Table 6.

In contrast with other algorithm, the key space of proposed algorithm is larger than others.

Most NPCR are near to 99.61% and most of UACI are higher than 30% in Table 6. We cannot recognize the man inside from Figures 37(b)–37(f); therefore the encryption method is sensitive to the keys.

7.3.2. Plaintext Sensitivity. By encrypting two same images with only one pixel difference, the attackers can obtain effective information by comparing the two encrypted

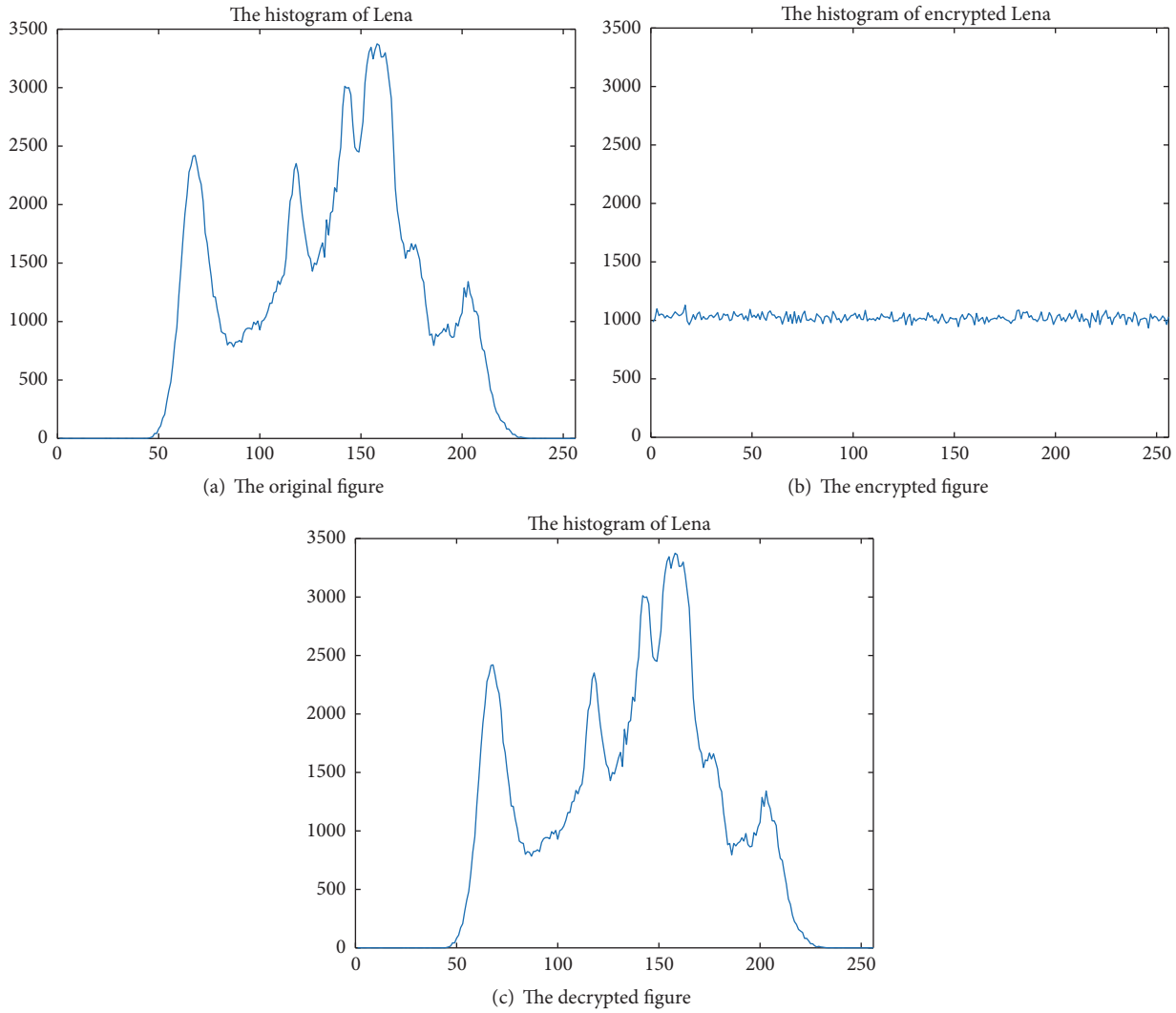

(a) The original figure

(b) The encrypted figure

(c) The decrypted figure

Figure 29: Lena.

Table 3: Information entropy.

Image	Original image	Encrypted image
Cameraman	7.0097	7.9974
Peppers	7.5739	7.9976
Dollar	6.9785	7.9992
Lax	6.8272	7.9993
Aerial	6.9940	7.9992
Lena	7.2185	7.9993
Lake	7.4845	7.9993
Columbia	7.2736	7.9992
Boat	6.9391	7.9972

Table 4: Comparison of information entropy.

Algorithm	Image	Original image	Encrypted image
Proposed	Lena	7.2185	7.9993
[1]	Lena	7.2072	7.9973
[4]	Lena	Undefined	7.9972
[19]	Lena	Undefined	7.987918
[20]	Lena	7.447144	7.988847

Table 5: Comparison of key spaces.

Algorithm	Proposed	[2]	[4]	[6]
Key spaces	$2.23 \times 10^{87}(1.12 \times 2^{290})$	2^{128}	$\approx 2^{273}$	2^{276}

images. Therefore an encryption method designed against differential attack should ensure that the two encrypted images are completely different even if there is only a pixel difference in the original image.

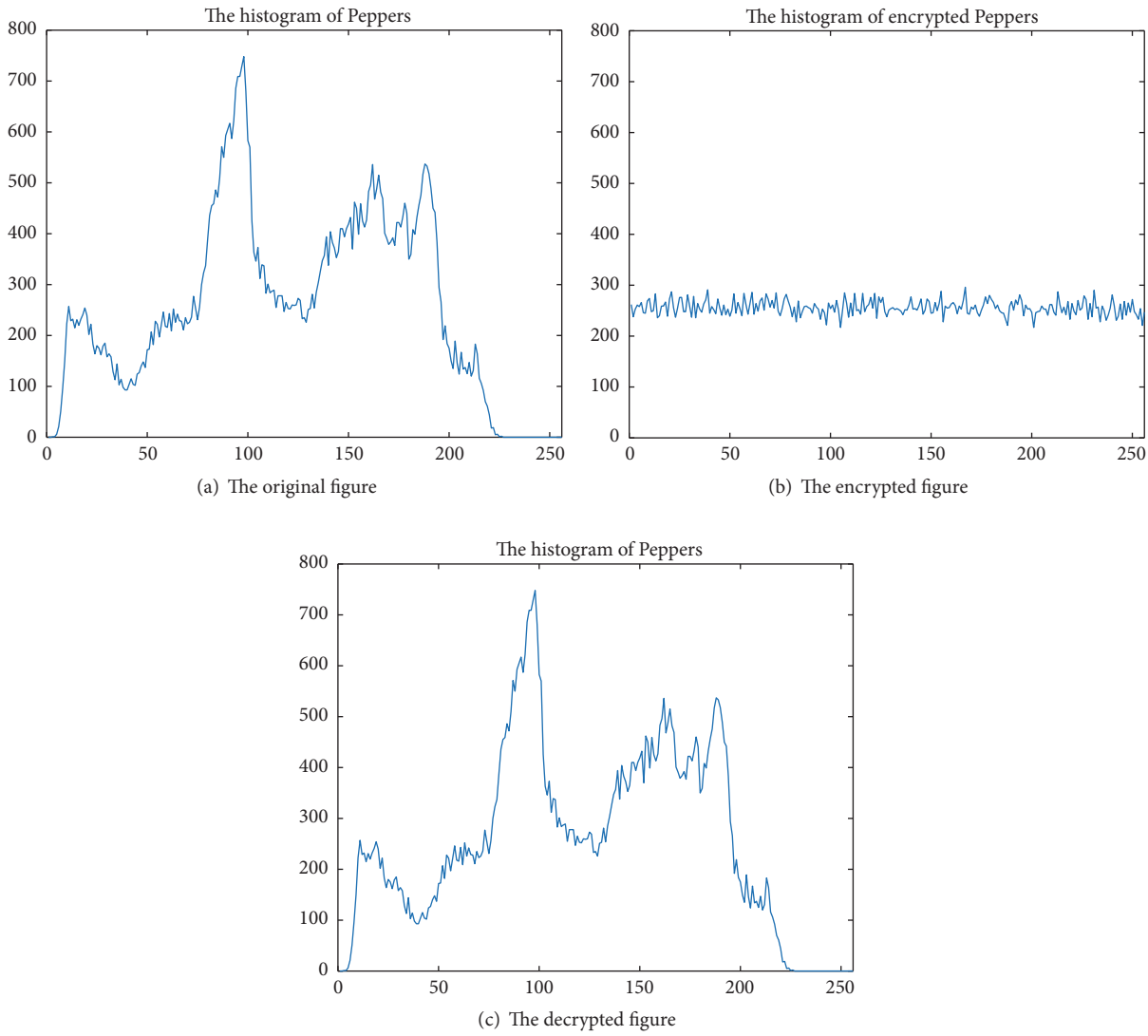

(a) The original figure

(b) The encrypted figure

(c) The decrypted figure

Figure 30: Peppers.

Table 6: NPCR and UACI between Figures 37(a) and 37(b)–37(f).

Image	NPCR and UACI	
	NPCR (%)	UACI (%)
Figure 37(b)	99.61	31.26
Figure 37(c)	97.02	30.23
Figure 37(d)	99.60	31.03
Figure 37(e)	99.61	31.01
Figure 37(f)	99.62	31.27

In Table 7, Figure 10(a)(x, y) is the same as Figure 10(a) except for a pixel locating (x, y). After that, the 2 images are encrypted with the same keys and the NPCR and UACI between the 2 ciphertext images are calculated. Similarly, the data of other 8 cases are obtained in Tables 8–15.

From Table 16, the NPCR and UACI of proposed algorithm after 2-round encryption are nearer to the ideal values 99.61% and 33.46% [33] than others. Therefore the proposed method is better.

7.4. Resistance to Known-Plaintext and Chosen-Plaintext Attacks. In Section 6.3, the iteration times of the next round are decided by the encrypted pixel value of present round. In (20), $x_2(i)$, generated from the fractional 2D-TFCDM, is dependent on $k(i-1)$ and determines $k(i)$. Therefore, the corresponding keystream is different when different plaintext is encrypted. For the resultant information is related to the chosen-images, the attacker cannot get useful information after encrypting some special images. As a result, the attacks proposed in [34–41] become ineffective for our scheme. In a word, the proposed scheme can primely resist the known-plaintext and the chosen-plaintext attacks.

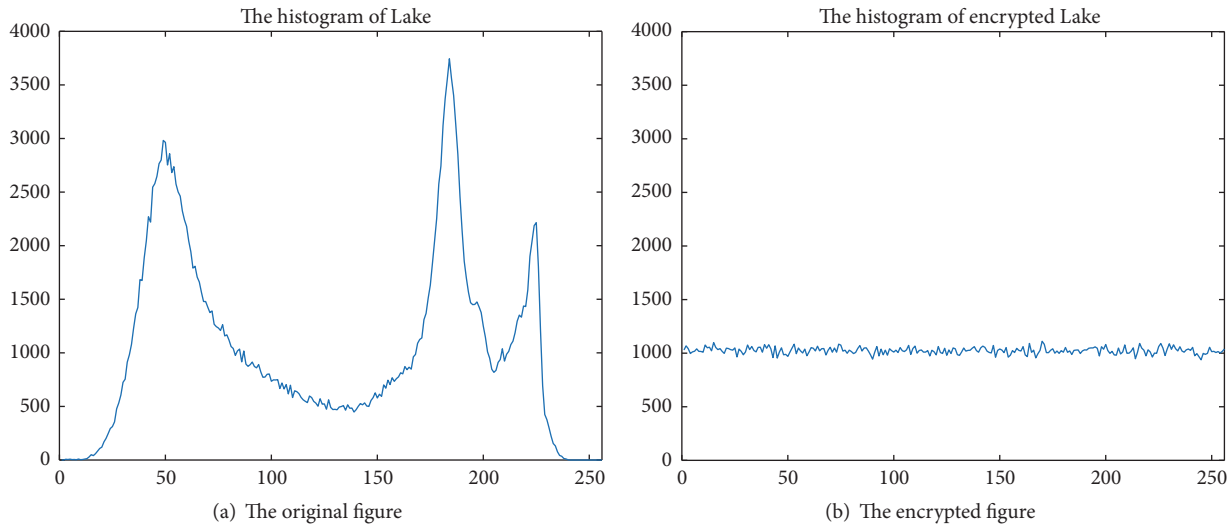

(a) The original figure

(b) The encrypted figure

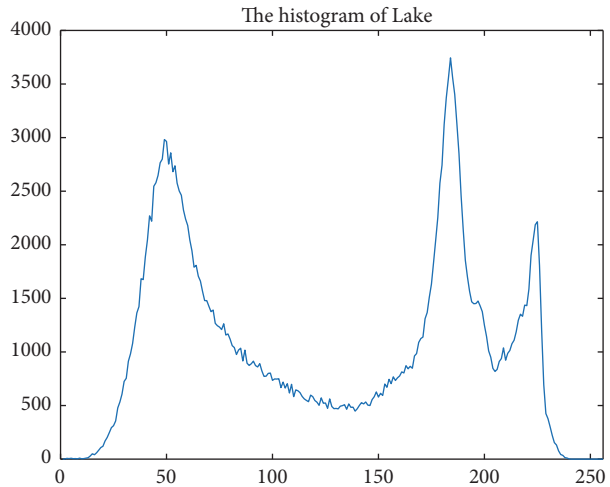

(c) The decrypted figure

Figure 31: Lake.

Table 7: NPCR and UACI between cipher-images with slightly different plain-images.

Image	NPCR and UACI of Cameraman			
	NPCR (1-round %)	UACI (1-round %)	NPCR (2-round %)	UACI (2-round %)
Figure 10(a)(30, 30)	4.84	1.64	99.57	33.61
Figure 10(a)(50, 50)	81.43	27.39	99.62	33.56
Figure 10(a)(80, 80)	80.87	27.19	99.59	33.51
Figure 10(a)(100, 100)	6.82	2.28	99.59	33.46

Table 8: NPCR and UACI between cipher-images with slightly different plain-images.

Image	NPCR and UACI of Lena			
	NPCR (1-round %)	UACI (1-round %)	NPCR (2-round %)	UACI (2-round %)
Figure 11(a)(30, 30)	1.21	0.41	99.59	33.39
Figure 11(a)(50, 50)	95.06	31.93	99.59	33.53
Figure 11(a)(80, 80)	94.90	31.93	99.60	33.48
Figure 11(a)(100, 100)	1.71	0.58	99.63	33.40

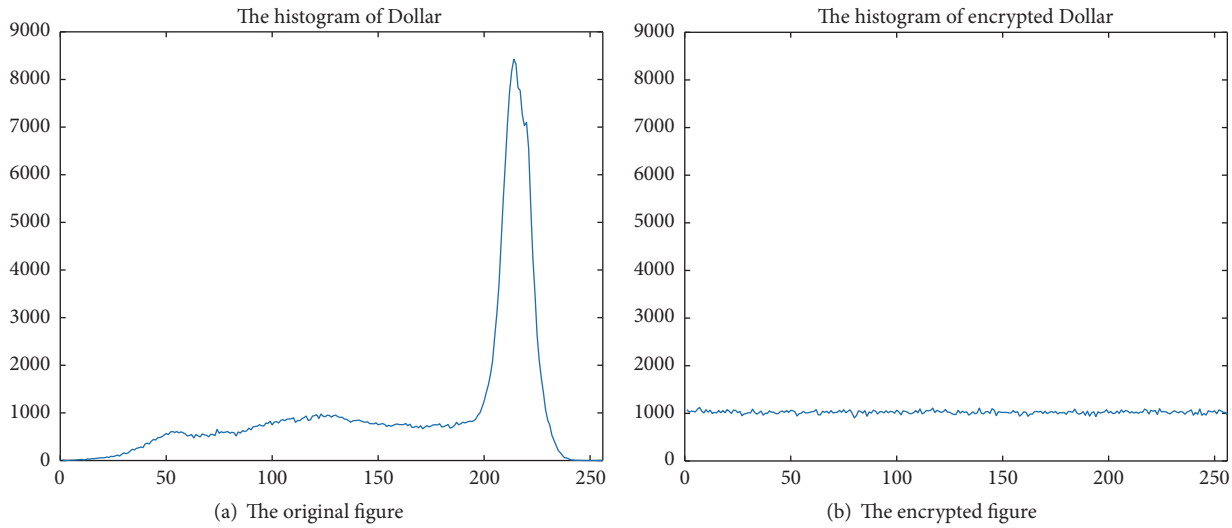

(a) The original figure

(b) The encrypted figure

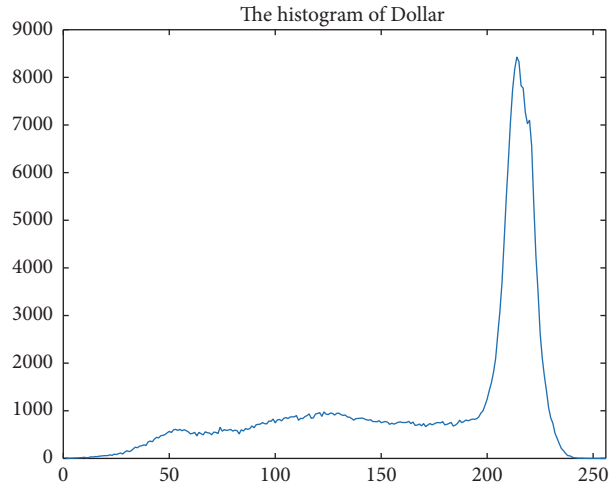

(c) The decrypted figure

Figure 32: Dollar.

Table 9: NPCR and UACI between cipher-images with slightly different plain-images.

Image	NPCR and UACI of Peppers			
	NPCR (1-round %)	UACI (1-round %)	NPCR (2-round %)	UACI (2-round %)
Figure 12(a)(30, 30)	4.83	1.64	99.56	33.44
Figure 12(a)(50, 50)	81.44	27.35	99.62	33.50
Figure 12(a)(80, 80)	6.12	2.03	99.57	33.42
Figure 12(a)(100, 100)	6.83	2.32	99.60	33.50

Table 10: NPCR and UACI between cipher-images with slightly different plain-images.

Image	NPCR and UACI of Lake			
	NPCR (1-round %)	UACI (1-round %)	NPCR (2-round %)	UACI (2-round %)
Figure 13(a)(30, 30)	1.21	0.41	99.61	33.46
Figure 13(a)(50, 50)	95.09	31.88	99.61	33.42
Figure 13(a)(80, 80)	94.92	31.89	99.60	33.46
Figure 13(a)(100, 100)	1.71	0.58	99.59	33.47

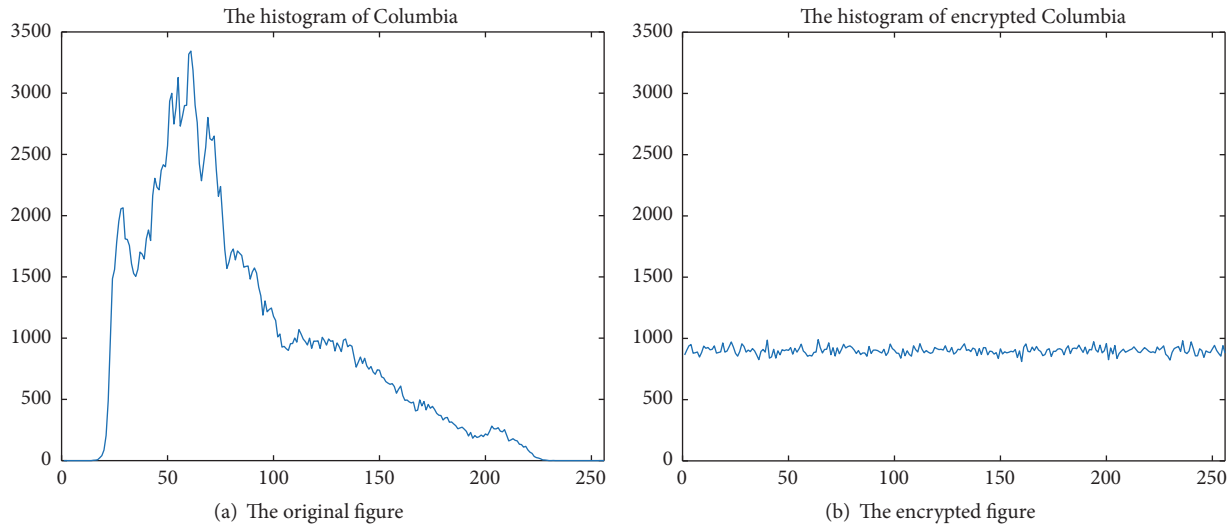

(a) The original figure

(b) The encrypted figure

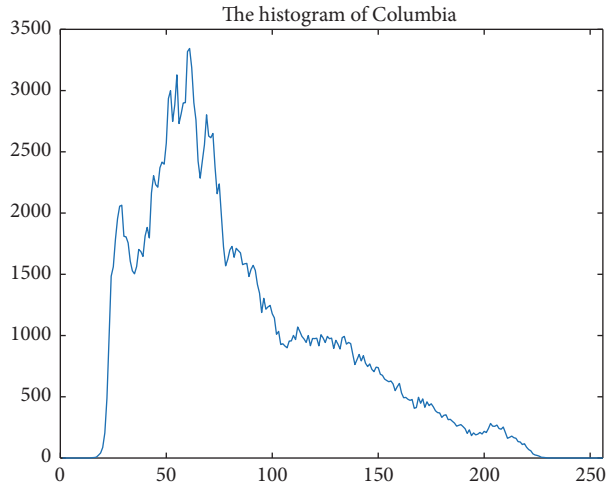

(c) The decrypted figure

Figure 33: Columbia.

Table 11: NPCR and UACI between cipher-images with slightly different plain-images.

Image	NPCR and UACI of Dollar			
	NPCR (1-round %)	UACI (1-round %)	NPCR (2-round %)	UACI (2-round %)
Figure 14(a)(30, 30)	1.21	0.41	99.64	33.42
Figure 14(a)(50, 50)	95.08	32.00	99.60	33.49
Figure 14(a)(80, 80)	94.90	31.93	99.61	33.48
Figure 14(a)(100, 100)	1.71	0.57	99.61	33.41

Table 12: NPCR and UACI between cipher-images with slightly different plain-images.

Image	NPCR and UACI of Columbia			
	NPCR (1-round %)	UACI (1-round %)	NPCR (2-round %)	UACI (2-round %)
Figure 15(a)(30, 30)	94.83	31.96	99.61	33.47
Figure 15(a)(50, 50)	93.48	31.40	99.48	33.36
Figure 15(a)(80, 80)	0.96	0.32	99.60	33.45
Figure 15(a)(100, 100)	1.11	0.38	99.61	33.51

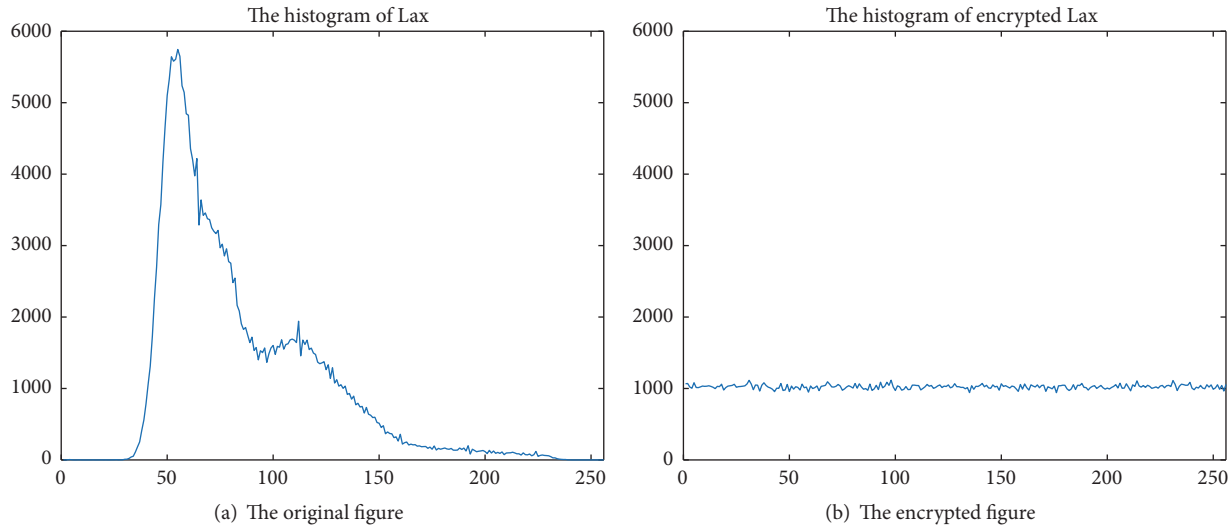

(a) The original figure

(b) The encrypted figure

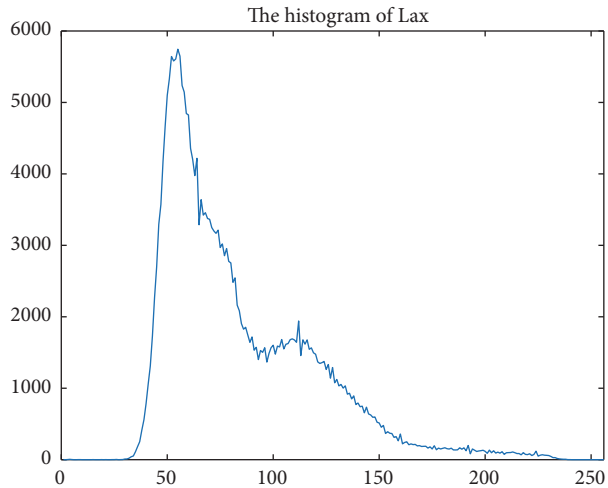

(c) The decrypted figure

Figure 34: Lax.

Table 13: NPCR and UACI between cipher-images with slightly different plain-images.

Image	NPCR and UACI of Lax			
	NPCR (1-round %)	UACI (1-round %)	NPCR (2-round %)	UACI (2-round %)
Figure 16(a)(30, 30)	1.21	0.40	99.62	33.39
Figure 16(a)(50, 50)	95.06	31.99	99.61	33.49
Figure 16(a)(80, 80)	94.92	31.87	99.58	33.41
Figure 16(a)(100, 100)	1.70	0.58	99.62	33.48

Table 14: NPCR and UACI between cipher-images with slightly different plain-images.

Image	NPCR and UACI of Boat			
	NPCR (1-round %)	UACI (1-round %)	NPCR (2-round %)	UACI (2-round %)
Figure 17(a)(30, 30)	4.83	1.60	99.59	33.47
Figure 17(a)(50, 50)	81.46	27.45	99.62	33.59
Figure 17(a)(80, 80)	80.82	27.24	99.58	33.48
Figure 17(a)(100, 100)	6.82	2.32	99.62	33.61

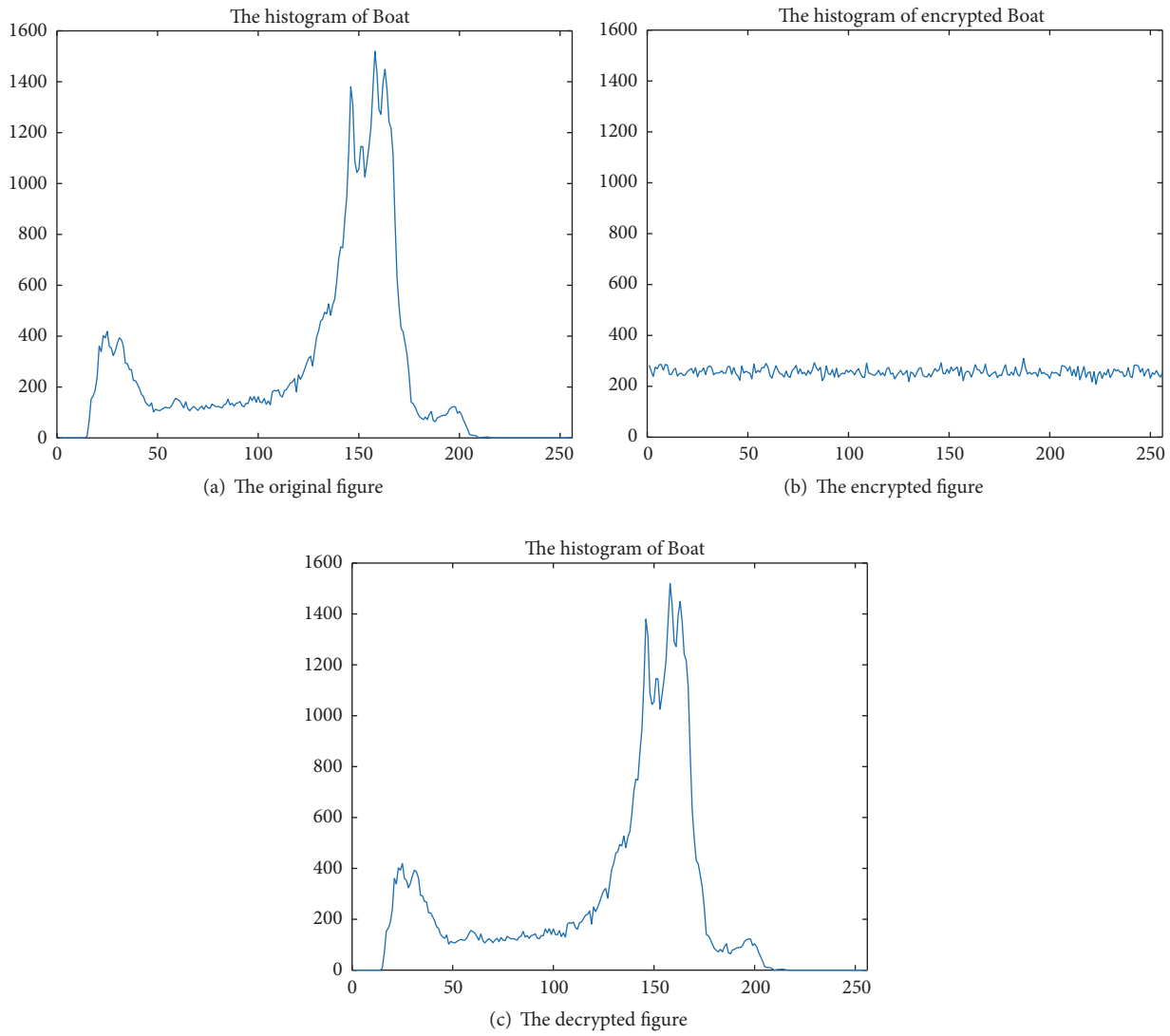

(a) The original figure

(b) The encrypted figure

(c) The decrypted figure

Figure 35: Boat.

Table 15: NPCR and UACI between cipher-images with slightly different plain-images.

Image	NPCR and UACI of Aerial			
	NPCR (1-round %)	UACI (1-round %)	NPCR (2-round %)	UACI (2-round %)
Figure 18(a)(30, 30)	1.21	0.41	99.61	33.49
Figure 18(a)(50, 50)	95.06	31.93	99.62	33.43
Figure 18(a)(80, 80)	94.91	31.88	99.61	33.53
Figure 18(a)(100, 100)	1.71	0.57	99.61	33.52

8. Conclusions

Fractional 2D-TFCDM is obtained from the 2D-TFCDM. After that, we found new chaotic dynamics behaviors from the fractionalized map. Moreover, the map can be converted into image encryption algorithm as an application. Finally, the encryption effect is analysed in 4 main aspects; we find the proposed scheme is superior to others almost anywhere in comparison. As far as we know, the proposed image encryption algorithm has never been reported before.

Conflicts of Interest

The authors declare that they have no conflicts of interest.

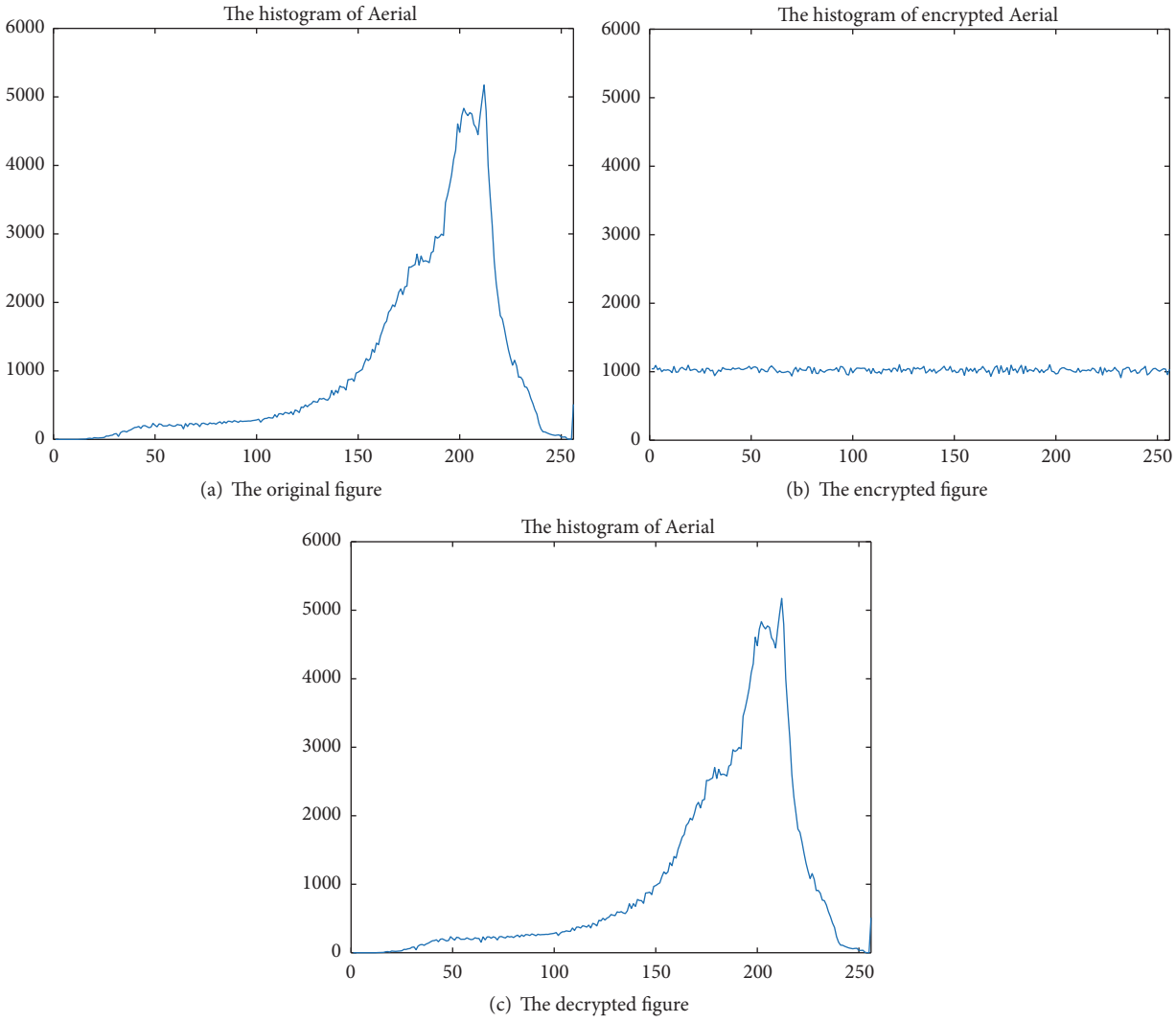

(a) The original figure

(b) The encrypted figure

(c) The decrypted figure

Figure 36: Aerial.

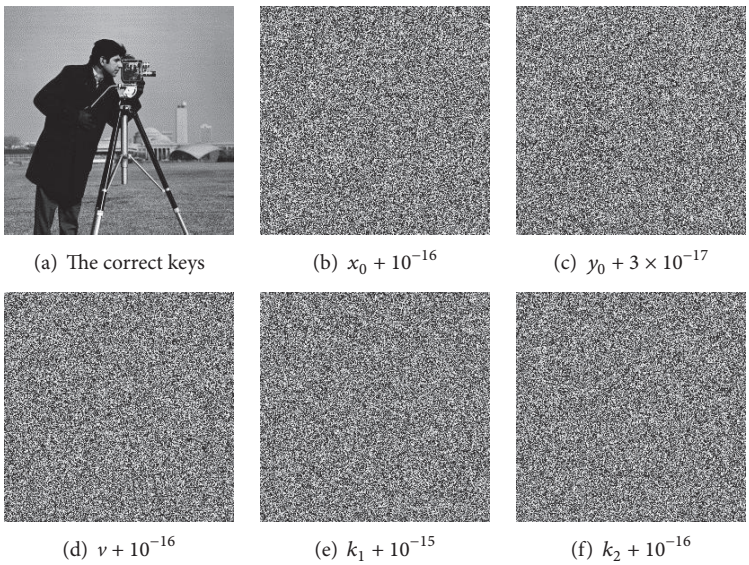

(a) The correct keys

(b) $x_0 + 10^{-16}$

(c) $y_0 + 3 \times 10^{-17}$

(d) $v + 10^{-16}$

(e) $k_1 + 10^{-15}$

(f) $k_2 + 10^{-16}$

Figure 37: The test of key sensitivity.

Table 16: Comparison of NPCR and UACI of image.

Algorithm	Image	NPCR (%)	UACI (%)
Proposed	Lena	99.60	33.48
[1]	Lena	99.61	33.53
[2]	Lena	99.6429	33.3935
[3]	Lena	99.6304	33.5989
[5]	Lena	99.932	39.520
[19]	Lena	75.62561	34.84288
[20]	Lena	99.6091	33.5038
[21]	Lena	99.6330	34.1319

Acknowledgments

The project was supported by the National Natural Science Foundation of China (Grant nos. 61072147, 11271008).

References

[1] L. Xu, X. Gou, Z. Li, and J. Li, "A novel chaotic image encryption algorithm using block scrambling and dynamic index based diffusion," *Optics and Lasers in Engineering*, vol. 91, pp. 41–52, 2017.

[2] L. Teng, X. Wang, and J. Meng, "A chaotic color image encryption using integrated bit-level permutation," *Multimedia Tools and Applications*, pp. 1–14, 2017.

[3] R. Enayatifar, A. H. Abdullah, I. F. Isnin, A. Altameem, and M. Lee, "Image encryption using a synchronous permutation-diffusion technique," *Optics and Lasers in Engineering*, vol. 90, pp. 146–154, 2017.

[4] Y. Li, C. Wang, and H. Chen, "A hyper-chaos-based image encryption algorithm using pixel-level permutation and bit-level permutation," *Optics and Lasers in Engineering*, vol. 90, pp. 238–246, 2017.

[5] S. Chakraborty, A. Seal, M. Roy, and K. Mali, "A novel lossless image encryption method using DNA substitution and chaotic logistic map," *International Journal of Security and Its Applications*, vol. 10, no. 2, pp. 205–216, 2016.

[6] N. Zhou, S. Pan, S. Cheng, and Z. Zhou, "Image compressionï¿¡Cencryption scheme based on hyper-chaotic system and 2D compressive sensing," *Optics & Laser Technology*, vol. 82, pp. 121–133, 2016.

[7] K. S. Miller and B. Ross, "Fractional difference calculus," in *Univalent functions, fractional calculus, and their applications (Kōriyama, 1988)*, Ellis Horwood Ser. Math. Appl., pp. 139–152, Horwood, Chichester, 1989.

[8] M. Bohner and A. Peterson, *Dynamic Equations on Time Scales: An Introduction with Applications*, Birkhauser, Boston, Mass, USA, 2001.

[9] F. M. Atıcı and P. W. Eloe, "Initial value problems in discrete fractional calculus," *Proceedings of the American Mathematical Society*, vol. 137, no. 3, pp. 981–989, 2009.

[10] F. M. Atici and S. Sengul, "Modeling with fractional difference equations," *Journal of Mathematical Analysis and Applications*, vol. 369, no. 1, pp. 1–9, 2010.

[11] M. T. Holm, "The Laplace transform in discrete fractional calculus," *Computers & Mathematics with Applications*, vol. 62, no. 3, pp. 1591–1601, 2011.

[12] M. D. Ortigueira, "Introduction to fractional linear systems. Part 2: discrete-time case," *IEE Proceedings Vision, Image and Signal Processing*, vol. 147, no. 1, pp. 71–78, 2000.

[13] M. D. Ortigueira, F. J. V. Coito, and J. J. Trujillo, "A new look into the discrete-time fractional calculus: Derivatives and exponentials," in *Proceedings of the 6th Workshop on Fractional Differentiation and Its Applications, FDA 2013*, pp. 629–634, France, February 2013.

[14] G.-C. Wu and D. Baleanu, "Discrete chaos in fractional delayed logistic maps," *Nonlinear Dynamics*, vol. 80, no. 4, pp. 1697–1703, 2015.

[15] G.-C. Wu and D. Baleanu, "Discrete fractional logistic map and its chaos," *Nonlinear Dynamics*, vol. 75, no. 1-2, pp. 283–287, 2014.

[16] G.-C. Wu, D. Baleanu, and S.-D. Zeng, "Discrete chaos in fractional sine and standard maps," *Physics Letters A*, vol. 378, no. 5-6, pp. 484–487, 2014.

[17] K. Araki, T. Satoh, and S. Miura, "Overview of elliptic curve cryptography," *Lecture Notes in Computer Science (including subseries Lecture Notes in Artificial Intelligence and Lecture Notes in Bioinformatics): Preface*, vol. 1431, pp. 29–49, 1998.

[18] C. Ma, *Modern Cryptography*, National Defense Industry Press, 2014.

[19] S. M. Ismail, L. A. Said, A. A. Rezk et al., "Biomedical image encryption based on double-humped and fractional logistic maps," in *Proceedings of the 6th International Conference on Modern Circuits and Systems Technologies, MOCAST 2017*, Greece, May 2017.

[20] J.-F. Zhao, S.-Y. Wang, L.-T. Zhang, and X.-Y. Wang, "Image encryption algorithm based on a novel improper fractional-order attractor and a wavelet function map," *Journal of Electrical and Computer Engineering*, vol. 2017, Article ID 8672716, 2017.

[21] P. Muthukumar, P. Balasubramaniam, and K. Ratnavelu, "A novel cascade encryption algorithm for digital images based on anti-synchronized fractional order dynamical systems," *Multimedia Tools and Applications*, pp. 1–22, 2016.

[22] G.-C. Wu, D. Baleanu, and Z.-X. Lin, "Image encryption technique based on fractional chaotic time series," *Journal of Vibration and Control*, vol. 22, no. 8, pp. 2092–2099, 2016.

[23] Z. Liu and T. Xia, "Novel two dimensional fractional-order discrete chaotic map and its application to image encryption," *Applied Computing and Informatics*, 2017.

[24] Z. Liu, T. Xia, and J. Wang, "Fractional two-dimensional discrete chaotic map and its applications to the information security with elliptic-curve public key cryptography," *Journal of Vibration and Control*, p. 107754631773471, 2017.

[25] F. M. Atici and P. W. Eloe, "A transform method in discrete fractional calculus," *International Journal of Difference Equations*, vol. 2, no. 2, pp. 165–176, 2007.

[26] T. Abdeljawad and D. Baleanu, "Fractional differences and integration by parts," *Journal of Computational Analysis and Applications*, vol. 13, no. 3, pp. 574–582, 2011.

[27] Y. Zhou, F. Chen, and X. Luo, "Existence results for nonlinear fractional difference equation," *Advances in Difference Equations*, vol. 2011, Article ID 713201, 2011.

[28] N. Koblitz, "Elliptic curve cryptosystems," *Mathematics of Computation*, vol. 48, no. 177, pp. 203–209, 1987.

[29] Y. Xiao, *Research on Elliptic Curve Cryptography*, Huazhong University of Science and Technology Press, 2006.

[30] P. Li, L. Min, Y. Hu, G. Zhao, and X. Li, "Novel two dimensional discrete chaotic maps and simulations," in *Proceedings of the*

2012 IEEE 6th International Conference on Information and Automation for Sustainability, ICIAFS 2012, pp. 159–162, China, September 2012.

[31] M. M. Liu, T. C. Xia, and J. B. Wang, "A two dimensional fractional discrete chaos combined with triangle function," *Journal of Shanghai University (Natural Science Edition)*, 2017, preprinted.

[32] G.-C. Wu and D. Baleanu, "Jacobian matrix algorithm for Lyapunov exponents of the discrete fractional maps," *Communications in Nonlinear Science and Numerical Simulation*, vol. 22, no. 1-3, pp. 95–100, 2015.

[33] F. M. Guo and L. Tu, *The Application of Chaotic Theory in Cryptography*, Beijing Institute of Technology Press, Beijing, China, 2015.

[34] D. Xiao, X. Liao, and P. Wei, "Analysis and improvement of a chaos-based image encryption algorithm," *Chaos, Solitons & Fractals*, vol. 40, no. 5, pp. 2191–2199, 2009.

[35] C. Li, S. Li, G. Chen, and W. A. Halang, "Cryptanalysis of an image encryption scheme based on a compound chaotic sequence," *Image and Vision Computing*, vol. 27, no. 8, pp. 1035–1039, 2009.

[36] R. Rhouma, E. Solak, and S. Belghith, "Cryptanalysis of a new substitution-diffusion based image cipher," *Communications in Nonlinear Science and Numerical Simulation*, vol. 15, no. 7, pp. 1887–1892, 2010.

[37] Y. Zhang, D. Xiao, W. Wen, and M. Li, "Cryptanalyzing a novel image cipher based on mixed transformed logistic maps," *Multimedia Tools and Applications*, vol. 73, no. 3, pp. 1885–1896, 2014.

[38] C. Li, L. Y. Zhang, R. Ou, K.-W. Wong, and S. Shu, "Breaking a novel colour image encryption algorithm based on chaos," *Nonlinear Dynamics*, vol. 70, no. 4, pp. 2383–2388, 2012.

[39] Y. Zhang, D. Xiao, W. Wen, and H. Nan, "Cryptanalysis of image scrambling based on chaotic sequences and Vigenère cipher," *Nonlinear Dynamics*, vol. 78, no. 1, pp. 235–240, 2014.

[40] Y. Zhang, D. Xiao, W. Wen, and M. Li, "Breaking an image encryption algorithm based on hyper-chaotic system with only one round diffusion process," *Nonlinear Dynamics*, vol. 76, no. 3, pp. 1645–1650, 2014.

[41] L. Y. Zhang, C. Li, K.-W. Wong, S. Shu, and G. Chen, "Cryptanalyzing a chaos-based image encryption algorithm using alternate structure," *The Journal of Systems and Software*, vol. 85, no. 9, pp. 2077–2085, 2012.

Hindawi
Discrete Dynamics in Nature and Society
Volume 2018, Article ID 5937572, 12 pages
https://doi.org/10.1155/2018/5937572

Research Article

Investigating a Coupled Hybrid System of Nonlinear Fractional Differential Equations

Wiyada Kumam,[1] **Mian Bahadur Zada**,[2] **Kamal Shah**,[2] **and Rahmat Ali Khan**[2]

[1]*Program in Applied Statistics, Department of Mathematics and Computer Science, Faculty of Science and Technology, Rajamangala University of Technology Thanyaburi, Thanyaburi, Pathum Thani 12110, Thailand*
[2]*Department of Mathematics, University of Malakand, Chakdara, Khyber Pakhtunkhwa, Pakistan*

Correspondence should be addressed to Wiyada Kumam; wiyada.kum@rmutt.ac.th

Received 8 December 2017; Accepted 30 January 2018; Published 20 March 2018

Academic Editor: Youssef N. Raffoul

We study sufficient conditions for existence of solutions to the coupled systems of higher order hybrid fractional differential equations with three-point boundary conditions. For this motive, we apply the coupled fixed point theorem of Krasnoselskii type to form adequate conditions for existence of solutions to the proposed system. We finish the paper with suitable illustrative example.

1. Introduction

Fractional calculus is found to be more practical and effective than the classical calculus in the mathematical modeling of several phenomena. Fractional differential equations are very important and significant part of the mathematics and have various applications in viscoelasticity, electroanalytical chemistry, and many physical problems [1–6]. A systematic presentation of the applications of fractional differential equations can be found in the book of Balachandran and Park [7]. In recent years, many works have been devoted to the study of the mathematical aspects of fractional order differential equations [8–12]. There are numerous advanced and efficient methods, which have been focusing on the existence of solution to fractional differential equations. One of the powerful tools for obtaining the existence of solutions to such equations is the fixed point methods. Many authors use fixed point theorems to prove the existence and uniqueness of solution to nonlinear fractional differential equations; see, for example, [13–17].

On the other hand, the study for coupled systems of fractional differential equations is also important as such systems occur in various problems of applied nature, for instance, [18–25]. Additionally, fixed point theory can be used to develop the existence theory for the coupled systems of fractional hybrid differential equations [13, 16, 17]. Bashiri et al. [17] discussed the existence of solution to the following system of fractional hybrid differential equations of order $p \in (0, 1)$:

$$\begin{aligned} D^p \left[x(t) - f(t, x(t))\right] &= g\left(t, y(t), I^{\alpha} y(t)\right), \\ &\text{a.e. } t \in [0, T], \ T > 0, \\ D^p \left[y(t) - f(t, y(t))\right] &= g\left(t, x(t), I^{\alpha} x(t)\right), \\ &\text{a.e. } t \in [0, T], \ T > 0, \\ x(0) &= 0, \\ y(0) &= 0, \end{aligned} \tag{1}$$

where $\alpha > 0$, and the functions $f : [0, T] \times \mathbb{R} \to \mathbb{R}$, $f(0, 0) = 0$ and $g : [0, T] \times \mathbb{R} \times \mathbb{R} \to \mathbb{R}$ satisfy certain conditions. D^p is the R-L fractional derivative of order p.

Recently, the existence of solutions for fractional differential equations involving the Caputo fractional derivative was studied in [13, 26–28]. Motivated by the work of Bashiri et al. [17], in this paper we are concerned with the existence of solutions to three-point boundary value problem for a

coupled system of hybrid fractional differential equations of order $p \in [n-1, n)$ given by

$$\begin{aligned} D^p \left[x(t) - f(t, x(t))\right] &= g\left(t, y(t), I^\alpha y(t)\right), \quad \text{a.e. } t \in [0,1], \\ D^p \left[y(t) - f(t, y(t))\right] &= g\left(t, x(t), I^\alpha x(t)\right), \quad \text{a.e. } t \in [0,1], \\ x(0) &= \delta_1 x(\eta_1), \\ y(0) &= \delta_1 y(\eta_1), \\ x(1) &= \delta_2 x(\eta_2), \\ y(1) &= \delta_2 y(\eta_2), \\ x^{(i)}(0) &= y^{(i)}(0) = 0, \quad \text{for } i = 1, 2, 3, \ldots, (n-2), \end{aligned} \tag{2}$$

where $\alpha > 0$, $0 < \eta_1 < \eta_2 < 1$, $f : [0,1] \times \mathbb{R} \to \mathbb{R}$, $f(0, x(0)) = 0$, and $g : [0,1] \times \mathbb{R} \times \mathbb{R} \to \mathbb{R}$. D^p is the Caputo fractional derivative of order p. Moreover, an example is given to illustrate the validity of the existence result.

2. Preliminaries

Throughout this manuscript $\Phi = \{\varphi: \mathbb{R}^+ \to \mathbb{R}^+$ such that $\varphi(r) < r$ for $r > 0$ and $\varphi(0) = 0\}$, $C([0,T] \times \mathbb{R}, \mathbb{R})$ denote the class of continuous functions $f : [0,T] \times \mathbb{R} \to \mathbb{R}$, and $C([0,T] \times \mathbb{R} \times \mathbb{R}, \mathbb{R})$ denote the class of functions $g : [0,T] \times \mathbb{R} \times \mathbb{R} \to \mathbb{R}$ such that

(i) the map $t \to g(t, x, y)$ is measurable for each $x, y \in \mathbb{R}$,

(ii) the map $x \to g(t, x, y)$ is continuous for each $x \in \mathbb{R}$,

(iii) the map $y \to g(t, x, y)$ is continuous for each $y \in \mathbb{R}$.

We need the following definitions which can be found in [9].

Definition 1. The Riemann-Liouville fractional integral of order $\alpha > 0$ of function $f \in L^1(R^+)$ is defined as

$$I^\alpha f(t) = \frac{1}{\Gamma(\alpha)} \int_0^t (t-s)^{\alpha-1} f(s)\, ds, \tag{3}$$

provided that the right side is pointwise defined on $(0, \infty)$.

Definition 2. Let α be a positive real number, such that $m-1 \le \alpha < m$, $m \in \mathbb{N}$, and $f^m(x)$ exists, a function of class C. Then Caputo fractional derivative of f is defined as

$${}^c D^\alpha f(t) = \frac{1}{\Gamma(m-\alpha)} \int_0^t (t-s)^{m-\alpha-1} f^m(s)\, ds, \tag{4}$$

provided that the right side is pointwise defined on $(0, \infty)$, where $m = [\alpha] + 1$ and $[\alpha]$ represents the integer part of α.

Definition 3 (see [29]). The mapping $F : X \times X \to X$ has a coupled fixed point $(x, y) \in X \times X$ if $F(x, y) = x$ and $F(y, x) = y$.

Theorem 4 (see [17]). *Let S be a nonempty, closed, convex, and bounded subset of the Banach space X and $\widetilde{S} = S \times S$. Suppose that $A : X \to X$ and $B : S \to X$ are two operators such that*

(C_1) *there exists $\varphi_A \in \Phi$ such that, for all $x, y \in X$, one has*

$$\|Ax - Ay\| \le \sigma \varphi_A(\|x - y\|), \quad \text{for some constant } \sigma > 0, \tag{5}$$

(C_2) *B is completely continuous,*

(C_3) *$x = Ax + By \Rightarrow x \in S$, for all $y \in S$.*

Then the operator $T(x, y) = Ax + By$ has at least a coupled fixed point in $\widetilde{S}$ whenever $\sigma < 1$.

Lemma 5. *The following result holds for fractional differential equations:*

$$I^\alpha \left[{}^c D^\alpha h(t)\right] = h(t) + c_0 + c_1 t + c_2 t^2 + \cdots + c_{m-1} t^{m-1}, \tag{6}$$

for arbitrary $c_i \in \mathbb{R}$, $i = 0, 1, 2, \ldots, m-1$, where $m = [\alpha] + 1$ and $[\alpha]$ represents the integer part of α.

3. Existence Results

Let us set the following notations for convenience:

$$\lambda = (1 - \delta_1)\left(1 - \delta_2 \eta_2^{n-1}\right) + (1 - \delta_2)\, \delta_1 \eta_1^{n-1}, \tag{7}$$

$$F_0 = \frac{2}{|\lambda|}\left(|f(1,0)| + \frac{1}{2} \max_{t \in [0,1]} |f(t,0)| + \max_{\eta_1 \in [0,1]} |f(\eta_1, 0)| + \max_{\eta_2 \in [0,1]} |f(\eta_2, 0)|\right). \tag{8}$$

For the forthcoming analysis, we assume that

(A_1) the function $x \to x - f(t, x)$ is increasing in $\mathbb{R}$ for all $t \in [0,1]$;

(A_2) there exists $M \ge L > 0$ such that

$$|f(t, x(t)) - f(t, y(t))| \le \frac{L|x(t) - y(t)|}{8\left(M + |x(t) - y(t)|\right)},$$

$$\frac{|f(1, \delta_2 x(\eta_2)) - f(1, \delta_2 y(\eta_2))|}{|\lambda|} \le \sup\left\{\frac{L\delta_2 |x(t) - y(t)|}{16\left(M + \delta_2 |x(t) - y(t)|\right)}\right\},$$

$$\frac{|f(\eta_1, x(\eta_1)) - f(\eta_1, y(\eta_1))|}{|\lambda|} \leq \sup\left\{\frac{L|x(t) - y(t)|}{16(M + |x(t) - y(t)|)}\right\},$$
$$\frac{|f(\eta_2, x(\eta_2)) - f(\eta_2, y(\eta_2))|}{|\lambda|} \leq \sup\left\{\frac{L|x(t) - y(t)|}{16(M + |x(t) - y(t)|)}\right\}; \tag{9}$$

(A_3) there exists a continuous function $h \in C([0, 1], \mathbb{R})$ such that

$$g(t, x(t), y(t)) \leq h(t), \quad x, y \in \mathbb{R},\ t \in [0, 1]. \tag{10}$$

Lemma 6. *If $f(0, x(0)) = 0$ and $(\partial^i f(t, x(t))/\partial t^i)|_{t=0} = 0$ for $i = 1, 2, \ldots, (n-2)$, then integral representation of the system (2) is given by*

$$\begin{aligned}
x(t) &= f(t, x(t)) + \frac{1}{\lambda}\left\{\delta_2\delta_1\eta_1^{n-1} f(\eta_2, x(\eta_2)) - \delta_1\eta_1^{n-1} f(1, x(1)) + \delta_1\left(1 - \delta_2\eta_2^{n-1}\right) f(\eta_1, x(\eta_1))\right\} \\
&\quad + \frac{1}{\lambda}\left\{(1-\delta_1)\delta_2 f(\eta_2, x(\eta_2)) - (1-\delta_1) f(1, x(1)) - (1-\delta_2)\delta_1 f(\eta_1, x(\eta_1))\right\} \cdot t^{n-1} + \frac{1}{\Gamma(p)}\int_0^t (t-s)^{p-1} g(s, y(s), I^\alpha y(s))\, ds \\
&\quad - \left\{\frac{\delta_1\eta_1^{n-1}}{\lambda} + \frac{(1-\delta_1)t^{n-1}}{\lambda}\right\}\frac{1}{\Gamma(p)} \cdot \int_0^1 (1-s)^{p-1} g(s, y(s), I^\alpha y(s))\, ds \\
&\quad + \left\{\frac{\delta_1\left(1 - \delta_2\eta_2^{n-1}\right)}{\lambda} - \frac{(1-\delta_2)\delta_1 t^{n-1}}{\lambda}\right\}\frac{1}{\Gamma(p)} \cdot \int_0^{\eta_1} (\eta_1 - s)^{p-1} g(s, y(s), I^\alpha y(s))\, ds \\
&\quad + \left\{\frac{\delta_2\delta_1\eta_1^{n-1}}{\lambda} + \frac{(1-\delta_1)\delta_2 t^{n-1}}{\lambda}\right\}\frac{1}{\Gamma(p)} \cdot \int_0^{\eta_2} (\eta_2 - s)^{p-1} g(s, y(s), I^\alpha y(s))\, ds, \\
y(t) &= f(t, y(t)) + \frac{1}{\lambda}\left\{\delta_2\delta_1\eta_1^{n-1} f(\eta_2, y(\eta_2)) - \delta_1\eta_1^{n-1} f(1, y(1)) + \delta_1\left(1 - \delta_2\eta_2^{n-1}\right) f(\eta_1, y(\eta_1))\right\} \\
&\quad + \frac{1}{\lambda}\left\{(1-\delta_1)\delta_2 f(\eta_2, y(\eta_2)) - (1-\delta_1) f(1, y(1)) - (1-\delta_2)\delta_1 f(\eta_1, y(\eta_1))\right\} \cdot t^{n-1} + \frac{1}{\Gamma(p)}\int_0^t (t-s)^{p-1} g(s, x(s), I^\alpha x(s))\, ds \\
&\quad - \left\{\frac{\delta_1\eta_1^{n-1}}{\lambda} + \frac{(1-\delta_1)t^{n-1}}{\lambda}\right\}\frac{1}{\Gamma(p)} \cdot \int_0^1 (1-s)^{p-1} g(s, x(s), I^\alpha x(s))\, ds \\
&\quad + \left\{\frac{\delta_1\left(1 - \delta_2\eta_2^{n-1}\right)}{\lambda} - \frac{(1-\delta_2)\delta_1 t^{n-1}}{\lambda}\right\}\frac{1}{\Gamma(p)} \cdot \int_0^{\eta_1} (\eta_1 - s)^{p-1} g(s, x(s), I^\alpha x(s))\, ds \\
&\quad + \left\{\frac{\delta_2\delta_1\eta_1^{n-1}}{\lambda} + \frac{(1-\delta_1)\delta_2 t^{n-1}}{\lambda}\right\}\frac{1}{\Gamma(p)} \cdot \int_0^{\eta_2} (\eta_2 - s)^{p-1} g(s, x(s), I^\alpha x(s))\, ds.
\end{aligned} \tag{11}$$

$$\begin{aligned}
x(t) &= f(t, x(t)) + \frac{1}{\lambda}\left\{\delta_2\delta_1\eta_1^{n-1} f(\eta_2, x(\eta_2)) - \delta_1\eta_1^{n-1} f(1, x(1)) + \delta_1\left(1 - \delta_2\eta_2^{n-1}\right) f(\eta_1, x(\eta_1))\right\} \\
&\quad + \frac{1}{\lambda}\left\{(1-\delta_1)\delta_2 f(\eta_2, x(\eta_2)) - (1-\delta_1) f(1, x(1)) - (1-\delta_2)\delta_1 f(\eta_1, x(\eta_1))\right\} \cdot t^{n-1} + \frac{1}{\Gamma(p)}\int_0^t (t-s)^{p-1} g(s, x(s), I^\alpha x(s))\, ds \\
&\quad - \left\{\frac{\delta_1\eta_1^{n-1}}{\lambda} + \frac{(1-\delta_1)t^{n-1}}{\lambda}\right\}\frac{1}{\Gamma(p)} \cdot \int_0^1 (1-s)^{p-1} g(s, x(s), I^\alpha x(s))\, ds \\
&\quad + \left\{\frac{\delta_1\left(1 - \delta_2\eta_2^{n-1}\right)}{\lambda} - \frac{(1-\delta_2)\delta_1 t^{n-1}}{\lambda}\right\}\frac{1}{\Gamma(p)} \cdot \int_0^{\eta_1} (\eta_1 - s)^{p-1} g(s, x(s), I^\alpha x(s))\, ds \\
&\quad + \left\{\frac{\delta_2\delta_1\eta_1^{n-1}}{\lambda} + \frac{(1-\delta_1)\delta_2 t^{n-1}}{\lambda}\right\}\frac{1}{\Gamma(p)} \cdot \int_0^{\eta_2} (\eta_2 - s)^{p-1} g(s, x(s), I^\alpha x(s))\, ds.
\end{aligned} \tag{12}$$

Proof. Applying the operator I^p on the first equation of system (2) and using Lemma 5, we obtain

$$x(t) = f(t, x(t)) + \frac{1}{\Gamma(p)}\int_0^t (t-s)^{p-1} g(s, y(s), I^\alpha y(s))\, ds + C_0 + C_1 t + C_2 t^2 + \cdots + C_{n-1} t^{n-1}. \tag{13}$$

Applying the initial conditions $x^{(i)}(0) = 0$, for $i = 1, 2, 3, \ldots, (n-2)$, we conclude that $C_1 = C_2 = \cdots = C_{n-2} = 0$. Therefore (13) becomes

$$x(t) = f(t, x(t)) + \frac{1}{\Gamma(p)} \cdot \int_0^t (t-s)^{p-1} g(s, y(s), I^\alpha y(s))\, ds + C_0 + C_{n-1} t^{n-1}. \tag{14}$$

Now, to find the values of C_0 and C_{n-1}, since $x(0) = \delta_1 x(\eta_1)$, from (14) we have

$$f(0, x(0)) + I^p g(0, y(0), I^\alpha y(0)) + C_0 = \delta_1\left\{f(\eta_1, x(\eta_1)) + \frac{1}{\Gamma(p)} \cdot \int_0^{\eta_1} (\eta_1 - s)^{p-1} g(s, y(s), I^\alpha y(s))\, ds + C_0 + C_{n-1}\eta_1^{n-1}\right\} \Longrightarrow$$

$$(1-\delta_1)C_0 - \delta_1 C_{n-1}\eta_1^{n-1} - \delta_1\left\{f(\eta_1, x(\eta_1)) + \frac{1}{\Gamma(p)} \cdot \int_0^{\eta_1} (\eta_1 - s)^{p-1} g(s, y(s), I^\alpha y(s))\, ds\right\} = 0. \tag{15}$$

Also, since $x(1) = \delta_2 x(\eta_2)$, from (14), we have

$$f(1, x(1)) + \frac{1}{\Gamma(p)} \cdot \int_0^1 (1-s)^{p-1} g(s, y(s), I^\alpha y(s))\, ds + C_0 + C_{n-1} = \delta_2\left\{f(\eta_2, x(\eta_2)) + \frac{1}{\Gamma(p)}\int_0^{\eta_2} (\eta_2 - s)^{p-1} g(s, y(s), I^\alpha y(s))\, ds + C_0 + C_{n-1}\eta_2^{n-1}\right\} \Longrightarrow \tag{16}$$

$$(1-\delta_2)C_0 + \left(1-\delta_2\eta_2^{n-1}\right)C_{n-1} + f(1, x(1)) + \frac{1}{\Gamma(p)} \cdot \int_0^1 (1-s)^{p-1} g(s, y(s), I^\alpha y(s))\, ds - \delta_2\left\{f(\eta_2, x(\eta_2)) + \frac{1}{\Gamma(p)}\int_0^{\eta_2} (\eta_2 - s)^{p-1} g(s, y(s), I^\alpha y(s))\, ds\right\} = 0.$$

Solving (15) and (16) for C_0, we get

$$\left\{\left(1-\delta_2\eta_2^{n-1}\right)(1-\delta_1) + \delta_1\eta_1^{n-1}(1-\delta_2)\right\}C_0 + \delta_1\eta_1^{n-1}\left\{f(1, x(1)) + \frac{1}{\Gamma(p)}\int_0^1 (1-s)^{p-1} g(s, y(s), I^\alpha y(s))\, ds\right\} - \delta_1\left(1-\delta_2\eta_2^{n-1}\right)\left\{f(\eta_1, x(\eta_1)) + \frac{1}{\Gamma(p)}\int_0^{\eta_1} (\eta_1 - s)^{p-1} g(s, y(s), I^\alpha y(s))\, ds\right\} - \delta_2\delta_1\eta_1^{n-1}\left\{f(\eta_2, x(\eta_2)) + \frac{1}{\Gamma(p)}\int_0^{\eta_2} (\eta_2 - s)^{p-1} g(s, y(s), I^\alpha y(s))\, ds\right\} = 0, \tag{17}$$

and using (7), we can write

$$C_0 = \frac{\delta_1\left(1-\delta_2\eta_2^{n-1}\right)}{\lambda}\left\{f(\eta_1, x(\eta_1)) + \frac{1}{\Gamma(p)}\int_0^{\eta_1} (\eta_1 - s)^{p-1} g(s, y(s), I^\alpha y(s))\, ds\right\} + \frac{\delta_2\delta_1\eta_1^{n-1}}{\lambda}\left\{f(\eta_2, x(\eta_2)) + \frac{1}{\Gamma(p)}\int_0^{\eta_2} (\eta_2 - s)^{p-1} g(s, y(s), I^\alpha y(s))\, ds\right\} - \frac{\delta_1\eta_1^{n-1}}{\lambda}\left\{f(1, x(1)) + \frac{1}{\Gamma(p)}\int_0^1 (1-s)^{p-1} g(s, y(s), I^\alpha y(s))\, ds\right\}. \tag{18}$$

Similarly, solving (15) and (16) and using (7), we obtained that

$$C_{n-1} = -\frac{(1-\delta_1)}{\lambda}\left\{f(1, x(1)) + \frac{1}{\Gamma(p)}\int_0^1 (1-s)^{p-1} g(s, y(s), I^\alpha y(s))\, ds\right\} - \frac{(1-\delta_2)\delta_1}{\lambda}\left\{f(\eta_1, x(\eta_1)) + \frac{1}{\Gamma(p)}\int_0^{\eta_1} (\eta_1 - s)^{p-1} g(s, y(s), I^\alpha y(s))\, ds\right\} + \frac{(1-\delta_1)\delta_2}{\lambda}\left\{f(\eta_2, x(\eta_2)) + \frac{1}{\Gamma(p)}\int_0^{\eta_2} (\eta_2 - s)^{p-1} g(s, y(s), I^\alpha y(s))\, ds\right\}. \tag{19}$$

Substituting the values of C_0 and C_1 in (14), we can write

$$x(t) = f(t, x(t)) + \frac{1}{\Gamma(p)} \cdot \int_0^t (t-s)^{p-1} g(s, y(s), I^\alpha y(s))\, ds + \frac{\delta_1\left(1-\delta_2\eta_2^{n-1}\right)}{\lambda}\left\{f(\eta_1, x(\eta_1)) + \frac{1}{\Gamma(p)}\int_0^{\eta_1} (\eta_1 - s)^{p-1} g(s, y(s), I^\alpha y(s))\, ds\right\} + \frac{\delta_2\delta_1\eta_1^{n-1}}{\lambda}\left\{f(\eta_2, x(\eta_2))\right.$$

$$
\begin{aligned}
&+\frac{1}{\Gamma(p)}\int_0^{\eta_2}(\eta_2-s)^{p-1}g(s,y(s),I^{\alpha}y(s))\,ds\Bigg\}\\
&-\frac{\delta_1\eta_1^{n-1}}{\lambda}\Bigg\{f(1,x(1))\\
&+\frac{1}{\Gamma(p)}\int_0^{1}(1-s)^{p-1}g(s,y(s),I^{\alpha}y(s))\,ds\Bigg\}\\
&-\frac{(1-\delta_1)}{\lambda}\Bigg\{f(1,x(1))\\
&+\frac{1}{\Gamma(p)}\int_0^{1}(1-s)^{p-1}g(s,y(s),I^{\alpha}y(s))\,ds\Bigg\}t^{n-1}\\
&-\frac{(1-\delta_2)\delta_1}{\lambda}\Bigg\{f(\eta_1,x(\eta_1))\\
&+\frac{1}{\Gamma(p)}\int_0^{\eta_1}(\eta_1-s)^{p-1}g(s,y(s),I^{\alpha}y(s))\,ds\Bigg\}\\
&\cdot t^{n-1}+\frac{(1-\delta_1)\delta_2}{\lambda}\Bigg\{f(\eta_2,x(\eta_2))\\
&+\frac{1}{\Gamma(p)}\int_0^{\eta_2}(\eta_2-s)^{p-1}g(s,y(s),I^{\alpha}y(s))\,ds\Bigg\}\\
&\cdot t^{n-1},
\end{aligned}
\tag{20}
$$

which implies that

$$
\begin{aligned}
x(t)&=f(t,x(t))+\frac{1}{\lambda}\left\{\delta_2\delta_1\eta_1^{n-1}f(\eta_2,x(\eta_2))\right.\\
&-\delta_1\eta_1^{n-1}f(1,x(1))\\
&\left.+\delta_1\left(1-\delta_2\eta_2^{n-1}\right)f(\eta_1,x(\eta_1))\right\}\\
&+\frac{1}{\lambda}\left\{(1-\delta_1)\delta_2 f(\eta_2,x(\eta_2))\right.\\
&\left.-(1-\delta_1)f(1,x(1))-(1-\delta_2)\delta_1 f(\eta_1,x(\eta_1))\right\}\\
&\cdot t^{n-1}+\frac{1}{\Gamma(p)}\int_0^{t}(t-s)^{p-1}g(s,y(s),I^{\alpha}y(s))\,ds\\
&-\left\{\frac{\delta_1\eta_1^{n-1}}{\lambda}+\frac{(1-\delta_1)t^{n-1}}{\lambda}\right\}\frac{1}{\Gamma(p)}\\
&\cdot\int_0^{1}(1-s)^{p-1}g(s,y(s),I^{\alpha}y(s))\,ds\\
&+\left\{\frac{\delta_1\left(1-\delta_2\eta_2^{n-1}\right)}{\lambda}-\frac{(1-\delta_2)\delta_1 t^{n-1}}{\lambda}\right\}\frac{1}{\Gamma(p)}\\
&\cdot\int_0^{\eta_1}(\eta_1-s)^{p-1}g(s,y(s),I^{\alpha}y(s))\,ds\\
&+\left\{\frac{\delta_2\delta_1\eta_1^{n-1}}{\lambda}+\frac{(1-\delta_1)\delta_2 t^{n-1}}{\lambda}\right\}\frac{1}{\Gamma(p)}\\
&\cdot\int_0^{\eta_2}(\eta_2-s)^{p-1}g(s,y(s),I^{\alpha}y(s))\,ds.
\end{aligned}
\tag{21}
$$

Similarly, repeating the above process with the second equation of system (2), we obtain integral equation (12). □

Now, we are in a position to present the existence theorem for the system (2).

Theorem 7. *Assume that hypotheses (A_1)–(A_3) hold. Then there exists a solution for coupled systems (2) of higher order hybrid FHDEs with three-point boundary conditions.*

Proof. Set $X = C([0,1],\mathbb{R})$ and a subset S of X defined by

$$
\begin{aligned}
&S=\{x\in X:\ \|x\|\le N\},\\
&\text{where } N\ge 7L+F_0+\frac{\|h\|_{L^1}}{\Gamma(p+1)}\left\{1+\frac{2}{|\lambda|}\left(1+\eta_1^p+\eta_2^p\right)\right\}.
\end{aligned}
\tag{22}
$$

Clearly S is a closed, convex, and bounded subset of the Banach space X. Now, since $x(t)$ is a solution of the FHDEs system (2) if and only if $x(t)$ satisfies the system of integral equations in Lemma 6, to show the existence solution of system (2) it is enough to show the existence solution of the integral equations in Lemma 6. For this, define two operators $A : X \to X$ and $B : S \to X$ by

$$
\begin{aligned}
Ax(t)&=f(t,x(t))+\frac{1}{\lambda}\left\{\delta_2\delta_1\eta_1^{n-1}f(\eta_2,x(\eta_2))\right.\\
&-\delta_1\eta_1^{n-1}f(1,x(1))\\
&\left.+\delta_1\left(1-\delta_2\eta_2^{n-1}\right)f(\eta_1,x(\eta_1))\right\}\\
&+\frac{1}{\lambda}\left\{(1-\delta_1)\delta_2 f(\eta_2,x(\eta_2))\right.\\
&\left.-(1-\delta_1)f(1,x(1))-(1-\delta_2)\delta_1 f(\eta_1,x(\eta_1))\right\}\\
&\cdot t^{n-1},\\
Bx(t)&=\frac{1}{\Gamma(p)}\int_0^{t}(t-s)^{p-1}g(s,x(s),I^{\alpha}x(s))\,ds\\
&-\left\{\frac{\delta_1\eta_1^{n-1}}{\lambda}+\frac{(1-\delta_1)t^{n-1}}{\lambda}\right\}\frac{1}{\Gamma(p)}\\
&\cdot\int_0^{1}(1-s)^{p-1}g(s,x(s),I^{\alpha}x(s))\,ds\\
&+\left\{\frac{\delta_1\left(1-\delta_2\eta_2^{n-1}\right)}{\lambda}-\frac{(1-\delta_2)\delta_1 t^{n-1}}{\lambda}\right\}\frac{1}{\Gamma(p)}\\
&\cdot\int_0^{\eta_1}(\eta_1-s)^{p-1}g(s,x(s),I^{\alpha}x(s))\,ds
\end{aligned}
$$

$$+\left\{\frac{\delta_2\delta_1\eta_1^{n-1}}{\lambda}+\frac{(1-\delta_1)\,\delta_2 t^{n-1}}{\lambda}\right\}\frac{1}{\Gamma(p)}$$

$$\cdot\int_0^{\eta_2}(\eta_2-s)^{p-1}\,g\left(s,x(s),I^{\alpha}x(s)\right)ds. \tag{23}$$

Then the operators form of system (2) is

$$\begin{aligned} x(t) &= Ax(t)+By(t), \quad t\in[0,1],\\ y(t) &= Ay(t)+Bx(t), \quad t\in[0,1]. \end{aligned} \tag{24}$$

We have to show that the operators A and B satisfy all the conditions of Theorem 4. For this, let $x, y \in X$; then we have

$$\begin{aligned} |Ax(t)-Ay(t)| &\le |f(t,x(t))-f(t,y(t))|\\ &+\left|\frac{\delta_2\delta_1\eta_1^{n-1}f(\eta_2,x(\eta_2))-\delta_1\eta_1^{n-1}f(1,x(1))+\delta_1\left(1-\delta_2\eta_2^{n-1}\right)f(\eta_1,x(\eta_1))}{\lambda}\right.\\ &\left.-\frac{\delta_2\delta_1\eta_1^{n-1}f(\eta_2,y(\eta_2))-\delta_1\eta_1^{n-1}f(1,y(1))+\delta_1\left(1-\delta_2\eta_2^{n-1}\right)f(\eta_1,y(\eta_1))}{\lambda}\right|\\ &+\left|\frac{(1-\delta_1)\,\delta_2 f(\eta_2,x(\eta_2))-(1-\delta_1)f(1,x(1))-(1-\delta_2)\,\delta_1 f(\eta_1,x(\eta_1))}{\lambda}\right.\\ &\left.-\frac{(1-\delta_1)\,\delta_2 f(\eta_2,y(\eta_2))-(1-\delta_1)f(1,y(1))-(1-\delta_2)\,\delta_1 f(\eta_1,y(\eta_1))}{\lambda}\right|\left|t^{n-1}\right| \le |f(t,x(t))-f(t,y(t))|\\ &+\delta_1\eta_1^{n-1}\left|\frac{f(1,\delta_2x(\eta_2))-f(1,\delta_2y(\eta_2))}{\lambda}\right|+\delta_1\left(1-\delta_2\eta_2^{n-1}\right)\left|\frac{f(\eta_1,x(\eta_1))-f(\eta_1,y(\eta_1))}{\lambda}\right|\\ &+\delta_2\delta_1\eta_1^{n-1}\left|\frac{f(\eta_2,x(\eta_2))-f(\eta_2,y(\eta_2))}{\lambda}\right|+(1-\delta_1)\left|\frac{f(1,\delta_2x(\eta_2))-f(1,\delta_2y(\eta_2))}{\lambda}\right|+(1-\delta_2)\\ &\cdot\delta_1\left|\frac{f(\eta_1,x(\eta_1))-f(\eta_1,y(\eta_1))}{\lambda}\right|+(1-\delta_1)\,\delta_2\left|\frac{f(\eta_2,x(\eta_2))-f(\eta_2,y(\eta_2))}{\lambda}\right| < |f(t,x(t))-f(t,y(t))|\\ &+\frac{2|f(1,\delta_2x(\eta_2))-f(1,\delta_2y(\eta_2))|}{|\lambda|}+\frac{2|f(\eta_1,x(\eta_1))-f(\eta_1,y(\eta_1))|}{|\lambda|}+\frac{2|f(\eta_2,x(\eta_2))-f(\eta_2,y(\eta_2))|}{|\lambda|}. \end{aligned} \tag{25}$$

Taking the supremum over t and using (7), we get

$$\begin{aligned} \|Ax(t)-Ay(t)\| &\le \frac{1}{2}\left\{\frac{L\|x(t)-y(t)\|}{4\left(M+\|x(t)-y(t)\|\right)}\right.\\ &+\frac{L\delta_2\|x(t)-y(t)\|}{4\left(M+\delta_2\|x(t)-y(t)\|\right)}\\ &+\frac{L\|x(t)-y(t)\|}{4\left(M+\|x(t)-y(t)\|\right)}\\ &\left.+\frac{L\|x(t)-y(t)\|}{4\left(M+\|x(t)-y(t)\|\right)}\right\}\\ &=\frac{1}{2}\left\{\frac{3L\|x(t)-y(t)\|}{4\left(M+\|x(t)-y(t)\|\right)}\right.\\ &\left.+\frac{L\delta_2\|x(t)-y(t)\|}{4\left(M+\delta_2\|x(t)-y(t)\|\right)}\right\}\le\frac{1}{2}\\ &\cdot\varphi\left(\|x(t)-y(t)\|\right). \end{aligned} \tag{26}$$

Thus A satisfies condition (C_1) of Theorem 4 with $\sigma = 1/2$ and $\varphi(r) = 3Lr/4(M+r) + L\delta_2 r/4(M+\delta_2 r)$.

Next, we show that B is compact and continuous operator on S. Let $\{x_m\}$ be a sequence in S such that $\{x_m\} \to x \in S$. Then for all $t \in [0,1]$, we have

$$\begin{aligned} \lim_{m\to\infty}Bx_m(t) &= \frac{1}{\Gamma(p)}\\ &\cdot\lim_{m\to\infty}\int_0^t(t-s)^{p-1}\,g\left(s,x_m(s),I^{\alpha}x_m(s)\right)ds\\ &-\left\{\frac{\delta_1\eta_1^{n-1}}{\lambda}+\frac{(1-\delta_1)\,t^{n-1}}{\lambda}\right\}\lim_{m\to\infty}\frac{1}{\Gamma(p)}\\ &\cdot\int_0^1(1-s)^{p-1}\,g\left(s,x_m(s),I^{\alpha}x_m(s)\right)ds\\ &+\left\{\frac{\delta_1\left(1-\delta_2\eta_2^{n-1}\right)}{\lambda}-\frac{(1-\delta_2)\,\delta_1 t^{n-1}}{\lambda}\right\}\lim_{m\to\infty}\frac{1}{\Gamma(p)} \end{aligned}$$

$$\cdot \int_0^{\eta_1} (\eta_1 - s)^{p-1} g(s, x_m(s), I^\alpha x_m(s))\, ds + \left\{ \frac{\delta_2 \delta_1 \eta_1^{n-1}}{\lambda} + \frac{(1-\delta_1)\delta_2 t^{n-1}}{\lambda} \right\} \lim_{m\to\infty} \frac{1}{\Gamma(p)} \cdot \int_0^{\eta_2} (\eta_2 - s)^{p-1} g(s, x_m(s), I^\alpha x_m(s))\, ds = \frac{1}{\Gamma(p)} \cdot \int_0^t (t-s)^{p-1} \lim_{m\to\infty} g(s, x_m(s), I^\alpha x_m(s))\, ds - \left\{ \frac{\delta_1 \eta_1^{n-1}}{\lambda} + \frac{(1-\delta_1) t^{n-1}}{\lambda} \right\} \frac{1}{\Gamma(p)} \cdot \int_0^1 (1-s)^{p-1} \lim_{m\to\infty} g(s, x_m(s), I^\alpha x_m(s))\, ds + \left\{ \frac{\delta_1 \left(1 - \delta_2 \eta_2^{n-1}\right)}{\lambda} - \frac{(1-\delta_2)\delta_1 t^{n-1}}{\lambda} \right\} \frac{1}{\Gamma(p)} \cdot \int_0^{\eta_1} (\eta_1 - s)^{p-1} \lim_{m\to\infty} g(s, x_m(s), I^\alpha x_m(s))\, ds + \left\{ \frac{\delta_2 \delta_1 \eta_1^{n-1}}{\lambda} + \frac{(1-\delta_1)\delta_2 t^{n-1}}{\lambda} \right\} \frac{1}{\Gamma(p)} \cdot \int_0^{\eta_2} (\eta_2 - s)^{p-1} \lim_{m\to\infty} g(s, x_m(s), I^\alpha x_m(s))\, ds = \frac{1}{\Gamma(p)} \int_0^t (t-s)^{p-1} g(s, x(s), I^\alpha x(s))\, ds - \left\{ \frac{\delta_1 \eta_1^{n-1}}{\lambda} + \frac{(1-\delta_1) t^{n-1}}{\lambda} \right\} \frac{1}{\Gamma(p)} \cdot \int_0^1 (1-s)^{p-1} g(s, x(s), I^\alpha x(s))\, ds + \left\{ \frac{\delta_1 \left(1 - \delta_2 \eta_2^{n-1}\right)}{\lambda} - \frac{(1-\delta_2)\delta_1 t^{n-1}}{\lambda} \right\} \frac{1}{\Gamma(p)} \cdot \int_0^{\eta_1} (\eta_1 - s)^{p-1} g(s, x(s), I^\alpha x(s))\, ds + \left\{ \frac{\delta_2 \delta_1 \eta_1^{n-1}}{\lambda} + \frac{(1-\delta_1)\delta_2 t^{n-1}}{\lambda} \right\} \frac{1}{\Gamma(p)} \cdot \int_0^{\eta_2} (\eta_2 - s)^{p-1} g(s, x(s), I^\alpha x(s))\, ds = Bx(t). \tag{27}$$

Thus the map B is continuous on S.

Let $x \in S$; then we have

$$|Bx(t)| \le \frac{1}{\Gamma(p)} \left| \int_0^t (t-s)^{p-1} g(s, x(s), I^\alpha x(s))\, ds \right| + \left| \left(\frac{\delta_1 \eta_1^{n-1}}{\lambda} + \frac{(1-\delta_1) t^{n-1}}{\lambda} \right) \frac{1}{\Gamma(p)} \right. \cdot \left. \int_0^1 (1-s)^{p-1} g(s, x(s), I^\alpha x(s))\, ds \right| + \left| \left(\frac{\delta_1 \left(1 - \delta_2 \eta_2^{n-1}\right)}{\lambda} - \frac{(1-\delta_2)\delta_1 t^{n-1}}{\lambda} \right) \frac{1}{\Gamma(p)} \right. \cdot \left. \int_0^{\eta_1} (\eta_1 - s)^{p-1} g(s, x(s), I^\alpha x(s))\, ds \right| + \left| \left(\frac{\delta_2 \delta_1 \eta_1^{n-1}}{\lambda} + \frac{(1-\delta_1)\delta_2 t^{n-1}}{\lambda} \right) \frac{1}{\Gamma(p)} \right. \cdot \left. \int_0^{\eta_2} (\eta_2 - s)^{p-1} g(s, x(s), I^\alpha x(s))\, ds \right| \le \frac{1}{\Gamma(p)} \cdot \int_0^t (t-s)^{p-1} \left| g(s, x(s), I^\alpha x(s)) \right| ds + \left\{ \frac{\left|\delta_1 \eta_1^{n-1}\right|}{|\lambda|} + \frac{\left|(1-\delta_1) t^{n-1}\right|}{|\lambda|} \right\} \frac{1}{\Gamma(p)} \int_0^1 (1-s)^{p-1} \cdot \left| g(s, x(s), I^\alpha x(s)) \right| ds + \left\{ \frac{\left|\delta_1 \left(1 - \delta_2 \eta_2^{n-1}\right)\right|}{|\lambda|} + \frac{\left|(1-\delta_2)\delta_1 t^{n-1}\right|}{|\lambda|} \right\} \frac{1}{\Gamma(p)} \cdot \int_0^{\eta_1} (\eta_1 - s)^{p-1} \left| g(s, x(s), I^\alpha x(s)) \right| ds + \left\{ \frac{\left|\delta_2 \delta_1 \eta_1^{n-1}\right|}{|\lambda|} + \frac{\left|(1-\delta_1)\delta_2 t^{n-1}\right|}{|\lambda|} \right\} \frac{1}{\Gamma(p)} \int_0^{\eta_2} (\eta_2 - s)^{p-1} \left| g(s, x(s), I^\alpha x(s)) \right| ds \le \frac{1}{\Gamma(p)} \int_0^t (t-s)^{p-1} \|h(s)\|\, ds + \frac{2}{|\lambda|\Gamma(p)} \left\{ \int_0^1 (1-s)^{p-1} \|h(s)\|\, ds + \int_0^{\eta_1} (\eta_1 - s)^{p-1} \|h(s)\|\, ds + \int_0^{\eta_2} (\eta_2 - s)^{p-1} \|h(s)\|\, ds \right\} \le \frac{\|h\|_{L^1}}{\Gamma(p)} \left\{ \int_0^t (t-s)^{p-1} ds + \frac{2}{|\lambda|} \left(\int_0^1 (1-s)^{p-1} ds + \int_0^{\eta_1} (\eta_1 - s)^{p-1} ds + \int_0^{\eta_2} (\eta_2 - s)^{p-1} ds \right) \right\} = \frac{\|h\|_{L^1}}{\Gamma(p)} \left\{ \frac{(t-s)^p}{-p} \Big|_0^t + \frac{2}{|\lambda|} \left(\frac{(1-s)^p}{-p} \Big|_0^1 + \frac{(\eta_1 - s)^p}{-p} \Big|_0^{\eta_1} + \frac{(\eta_2 - s)^p}{-p} \Big|_0^{\eta_2} \right) \right\} = \frac{\|h\|_{L^1}}{\Gamma(p)} \left\{ \frac{t^p}{p} \right.$$

$$+\frac{2}{|\lambda|}\left(\frac{1}{p}+\frac{\eta_1^p}{p}+\frac{\eta_2^p}{p}\right)\Bigg\}=\frac{\|h\|_{L^1}}{\Gamma(p+1)}\left\{t^p+\frac{2}{|\lambda|}\left(1+\eta_1^p+\eta_2^p\right)\right\}\leq\frac{\|h\|_{L^1}}{\Gamma(p+1)}\left\{1+\frac{2}{|\lambda|}\left(1+\eta_1^p+\eta_2^p\right)\right\}. \tag{28}$$

Taking the supremum over t, we get

$$\|Bx\|\leq\frac{\|h\|_{L^1}}{\Gamma(p+1)}\left\{1+\frac{2}{|\lambda|}\left(1+\eta_1^p+\eta_2^p\right)\right\},\quad\forall x\in S. \tag{29}$$

Thus B is uniformly bounded on S.

Now, let $t_1,t_2\in[0,1]$ such that $t_1\neq t_2$; then for any $x\in S$, we have

$$\begin{aligned}
\left|Bx(t_1)-Bx(t_2)\right|&=\Bigg|\frac{1}{\Gamma(p)}\\
&\cdot\int_0^{t_1}(t_1-s)^{p-1}g(s,x(s),I^\alpha x(s))\,ds\\
&-\left\{\frac{\delta_1\eta_1^{n-1}}{\lambda}+\frac{(1-\delta_1)t_1^{n-1}}{\lambda}\right\}\frac{1}{\Gamma(p)}\\
&\cdot\int_0^{1}(1-s)^{p-1}g(s,x(s),I^\alpha x(s))\,ds\\
&+\left\{\frac{\delta_1\left(1-\delta_2\eta_2^{n-1}\right)}{\lambda}-\frac{(1-\delta_2)\delta_1t_1^{n-1}}{\lambda}\right\}\frac{1}{\Gamma(p)}\\
&\cdot\int_0^{\eta_1}(\eta_1-s)^{p-1}g(s,x(s),I^\alpha x(s))\,ds\\
&+\left\{\frac{\delta_2\delta_1\eta_1^{n-1}}{\lambda}+\frac{(1-\delta_1)\delta_2t_1^{n-1}}{\lambda}\right\}\frac{1}{\Gamma(p)}\\
&\cdot\int_0^{\eta_2}(\eta_2-s)^{p-1}g(s,x(s),I^\alpha x(s))\,ds-\frac{1}{\Gamma(p)}\\
&\cdot\int_0^{t_2}(t_2-s)^{p-1}g(s,x(s),I^\alpha x(s))\,ds\\
&+\left\{\frac{\delta_1\eta_1^{n-1}}{\lambda}+\frac{(1-\delta_1)t_1^{n-1}}{\lambda}\right\}\frac{1}{\Gamma(p)}\\
&\cdot\int_0^{1}(1-s)^{p-1}g(s,x(s),I^\alpha x(s))\,ds\\
&+\left\{\frac{\delta_1\left(1-\delta_2\eta_2^{n-1}\right)}{\lambda}-\frac{(1-\delta_2)\delta_1t_1^{n-1}}{\lambda}\right\}\frac{1}{\Gamma(p)}\\
&\cdot\int_0^{\eta_1}(\eta_1-s)^{p-1}g(s,x(s),I^\alpha x(s))\,ds\\
&-\left\{\frac{\delta_2\delta_1\eta_1^{n-1}}{\lambda}+\frac{(1-\delta_1)\delta_2t_1^{n-1}}{\lambda}\right\}\frac{1}{\Gamma(p)}\\
&\cdot\int_0^{\eta_2}(\eta_2-s)^{p-1}g(s,x(s),I^\alpha x(s))\,ds\Bigg|\\
&\leq\frac{1}{\Gamma(p)}\left|\int_0^{t_1}(t_1-s)^{p-1}g(s,x(s),I^\alpha x(s))\,ds\right.\\
&\left.-\int_0^{t_2}(t_2-s)^{p-1}g(s,x(s),I^\alpha x(s))\,ds\right|\\
&\leq\frac{1}{\Gamma(p)}\left|\int_0^{t_1}(t_1-s)^{p-1}h(s)\,ds\right.\\
&\left.-\int_0^{t_1}(t_2-s)^{p-1}h(s)\,ds+\int_0^{t_1}(t_2-s)^{p-1}h(s)\,ds\right.\\
&\left.-\int_0^{t_2}(t_2-s)^{p-1}h(s)\,ds\right|\\
&\leq\frac{\|h\|_{L^1}}{\Gamma(p)}\left(\left|\int_0^{t_1}\left[(t_1-s)^{p-1}-(t_2-s)^{p-1}\right]ds\right|\right.\\
&\left.+\left|\int_{t_1}^{t_2}(t_2-s)^{p-1}\,ds\right|\right)\\
&=\frac{\|h\|_{L^1}}{\Gamma(p)}\left(\left|\frac{(t_1-s)^p}{-p}-\frac{(t_2-s)^p}{-p}\right|_0^{t_1}\right.\\
&\left.+\left|\frac{(t_2-s)^p}{-p}\right|_{t_1}^{t_2}\right)=\frac{\|h\|_{L^1}}{\Gamma(p)}\left(\left|\frac{(t_2-t_1)^p}{p}+\frac{t_1^p}{p}-\frac{t_2^p}{p}\right|\right.\\
&\left.+\left|\frac{(t_2-t_1)^p}{p}\right|\right)\leq\frac{\|h\|_{L^1}}{\Gamma(p+1)}\left(\left|t_2-t_1\right|^p+\left|t_1^p-t_2^p\right|\right.\\
&\left.+\left|t_2-t_1\right|^p\right).
\end{aligned} \tag{30}$$

Since t^p is uniformly continuous on $[0,1]$ for $n-1<p<n$, for any $\varepsilon>0$ we can find $\delta_1^*>0$ such that

$$\left|t_1^p-t_2^p\right|<\frac{\Gamma(p+1)}{3\|h\|_{L^1}}\varepsilon,\quad\text{whenever }\left|t_1-t_2\right|<\delta_1^*. \tag{31}$$

Let $\delta^*=\min\{\delta_1^*,(\Gamma(p+1)/3\|h\|_{L^1})^{1/p}\}$; then, we have

$$\left|Bx(t_1)-Bx(t_2)\right|\leq\frac{\|h\|_{L^1}}{\Gamma(p+1)}\left(\frac{\Gamma(p+1)}{3\|h\|_{L^1}}\varepsilon+\frac{\Gamma(p+1)}{3\|h\|_{L^1}}\varepsilon+\frac{\Gamma(p+1)}{3\|h\|_{L^1}}\varepsilon\right)=\varepsilon, \tag{32}$$

$$\text{whenever }\left|t_1-t_2\right|<\delta^*.$$

Thus $B(S)$ is equicontinuous and hence B is completely continuous on S.

To prove hypothesis (C_3) of Theorem 4, let $x\in X$ and $y\in S$ such that $x=Ax+By$; using (7) and (8), we have

$$
\begin{aligned}
|x(t)| &\le |Ax(t)| + |Bx(t)| \\
&= \left|f(t,x(t))\right| + \left|\frac{\delta_2\delta_1\eta_1^{n-1} f(\eta_2, x(\eta_2)) - \delta_1\eta_1^{n-1} f(1,x(1)) + \delta_1\left(1-\delta_2\eta_2^{n-1}\right) f(\eta_1, x(\eta_1))}{\lambda}\right| \\
&\quad + \left|\frac{(1-\delta_1)\delta_2 f(\eta_2, x(\eta_2)) - (1-\delta_1) f(1,x(1)) - (1-\delta_2)\delta_1 f(\eta_1, x(\eta_1))}{\lambda}\right| \left|t^{n-1}\right| \\
&\quad + \frac{1}{\Gamma(p)}\left|\int_0^t (t-s)^{p-1} g(s, x(s), I^\alpha x(s))\, ds\right| \\
&\quad + \left|\frac{\delta_1\eta_1^{n-1}}{\lambda} + \frac{(1-\delta_1)t^{n-1}}{\lambda}\right| \frac{1}{\Gamma(p)}\left|\int_0^1 (1-s)^{p-1} g(s, x(s), I^\alpha x(s))\, ds\right| \\
&\quad + \left|\frac{\delta_1\left(1-\delta_2\eta_2^{n-1}\right)}{\lambda} - \frac{(1-\delta_2)\delta_1 t^{n-1}}{\lambda}\right| \frac{1}{\Gamma(p)}\left|\int_0^{\eta_1} (\eta_1-s)^{p-1} g(s, x(s), I^\alpha x(s))\, ds\right| \\
&\quad + \left|\frac{\delta_2\delta_1\eta_1^{n-1}}{\lambda} + \frac{(1-\delta_1)\delta_2 t^{n-1}}{\lambda}\right| \frac{1}{\Gamma(p)}\left|\int_0^{\eta_2} (\eta_2-s)^{p-1} g(s, x(s), I^\alpha x(s))\, ds\right| \\
&\le \left|f(t,x(t))\right| + \frac{\left|f(\eta_2, x(\eta_2)) + f(1,x(1))\right| + \left|f(\eta_1, x(\eta_1))\right|}{|\lambda|} + \frac{\left|f(\eta_2, x(\eta_2)) + f(1,x(1))\right| + \left|f(\eta_1, x(\eta_1))\right|}{|\lambda|} \\
&\quad + \frac{\|h\|_{L^1}}{\Gamma(p+1)}\left\{1 + \frac{2}{|\lambda|}\left(1 + \eta_1^p + \eta_2^p\right)\right\}.
\end{aligned} \tag{33}
$$

This implies

$$
\begin{aligned}
|x(t)| &\le \left|f(t,x(t)) - f(t,0)\right| + \left|f(t,0)\right| \\
&\quad + 2\left(\frac{\left|f(1,0)\right|}{|\lambda|} + \frac{\left|f(\eta_1,0)\right|}{|\lambda|} + \frac{\left|f(\eta_2,0)\right|}{|\lambda|}\right) \\
&\quad + 2\left(\frac{\left|f(1,\delta_2 x(\eta_2)) - f(1,0)\right|}{|\lambda|}\right. \\
&\quad + \frac{\left|f(\eta_1, x(\eta_1)) - f(\eta_1,0)\right|}{|\lambda|} \\
&\quad \left. + \frac{\left|f(\eta_2, x(\eta_2)) - f(\eta_2,0)\right|}{|\lambda|}\right) + \frac{\|h\|_{L^1}}{\Gamma(p+1)}\left\{1\right. \\
&\quad \left. + \frac{2}{|\lambda|}\left(1 + \eta_1^p + \eta_2^p\right)\right\} \le L + 2(L + L + L) \\
&\quad + \frac{2}{|\lambda|}\left(\frac{1}{2}\left|f(t,0)\right| + \left|f(1,0)\right| + \left|f(\eta_1,0)\right|\right. \\
&\quad \left. + \left|f(\eta_2,0)\right|\right) + \frac{\|h\|_{L^1}}{\Gamma(p+1)}\left\{1\right. \\
&\quad \left. + \frac{2}{|\lambda|}\left(1 + \eta_1^p + \eta_2^p\right)\right\} \le 7L + F_0 + \frac{\|h\|_{L^1}}{\Gamma(p+1)}\left\{1\right. \\
&\quad \left. + \frac{2}{|\lambda|}\left(1 + \eta_1^p + \eta_2^p\right)\right\}.
\end{aligned} \tag{34}
$$

Taking the supremum over t on $[0,1]$, we can write

$$
\begin{aligned}
\|x(t)\| &\le 7L + F_0 \\
&\quad + \frac{\|h\|_{L^1}}{\Gamma(p+1)}\left\{1 + \frac{2}{|\lambda|}\left(1 + \eta_1^p + \eta_2^p\right)\right\} \le N.
\end{aligned} \tag{35}
$$

That is, $x \in S$. Thus condition (C_3) of Theorem 4 holds. Therefore, all the conditions of Theorem 4 are satisfied; hence the operator $T(x,y) = Ax + By$ has a coupled fixed point on $\widetilde{S}$. Consequently, system (2) has a solution defined on $[0,1]$. □

To illustrate Theorem 7, we construct the following example.

Example 8. We discuss the following hybrid fractional differential equations with three-point boundary conditions:

$$
\begin{aligned}
D^{5/2}\left[x(t) - \frac{e^{-t}|x(t)|}{11 + |x(t)|}\right] &= \frac{t^3}{3} - \left(\cos\left|y(t)\right| + \cos\left|I^{3/2} y(t)\right|\right), \\
D^{5/2}\left[y(t) - \frac{e^{-t}|y(t)|}{11 + |y(t)|}\right] &= \frac{t^3}{3} - \left(\cos|x(t)| + \cos\left|I^{3/2} x(t)\right|\right),
\end{aligned}
$$

$$
\begin{aligned}
x(0) &= \frac{1}{4}x\left(\frac{1}{4}\right),\\
y(0) &= \frac{1}{4}y\left(\frac{1}{4}\right),\\
x(1) &= \frac{1}{2}x\left(\frac{1}{2}\right),\\
y(1) &= \frac{1}{2}y\left(\frac{1}{2}\right),\\
x'(0) &= y'(0) = 0,
\end{aligned}
\tag{36}
$$

where $t \in [0,1]$, $f : [0,1] \times \mathbb{R} \to \mathbb{R}$, $f(0, x(0)) = 0$, and $g : [0,1]\times\mathbb{R}\times\mathbb{R} \to \mathbb{R}$. $D^{5/2}$ is the Caputo fractional derivative of order 5/2.

Here

$$
\begin{aligned}
\delta_1 &= \eta_1 = \frac{1}{4},\\
\delta_2 &= \eta_2 = \frac{1}{2},\\
f(t, x(t)) &= \frac{e^{-t}|x(t)|}{11 + |x(t)|},\\
g\left(t, x(t), I^{\alpha}x(t)\right) &= \frac{t^3}{3} - \left(\cos|x(t)| + \cos\left|I^{3/2}x(t)\right|\right).
\end{aligned}
\tag{37}
$$

Therefore,

$$
\begin{aligned}
\lambda &= \frac{19}{32},\\
F_0 &= \frac{2}{|\lambda|}\left(\left|f(1,0)\right| + \frac{1}{2}\max_{t\in[0,1]}\left|f(t,0)\right| + \max_{\eta_1\in[0,1]}\left|f(\eta_1,0)\right| + \max_{\eta_2\in[0,1]}\left|f(\eta_2,0)\right|\right) = 0.
\end{aligned}
\tag{38}
$$

Now, for $M = 11$ and $L = 512/19e < M$, we have

$$
\begin{aligned}
\left|f(t,x(t)) - f(t,y(t))\right| &= \left|\frac{e^{-t}|x(t)|}{11+|x(t)|} - \frac{e^{-t}|y(t)|}{11+|y(t)|}\right| \le \left|\frac{|x(t)-y(t)|+|y(t)|}{11+|x(t)-y(t)|+|y(t)|} - \frac{|y(t)|}{11+|x(t)-y(t)|+|y(t)|}\right|\\
&\le \left|\frac{|x(t)-y(t)|}{11+|x(t)-y(t)|+|y(t)|}\right|\\
&\le \frac{|x(t)-y(t)|}{11+|x(t)-y(t)|} \le \frac{(512/19e)|x(t)-y(t)|}{16\left(11+|x(t)-y(t)|\right)},
\end{aligned}
$$

$$
\begin{aligned}
&\frac{\left|f(1,\delta_2 x(\eta_2)) - f(1,\delta_2 y(\eta_2))\right|}{|\lambda|}\\
&\quad= \frac{\left|f(1,(1/2)x(1/2)) - f(1,(1/2)y(1/2))\right|}{19/32}\\
&\quad= \frac{32}{19}\left|\frac{e^{-1}|(1/2)x(1/2)|}{11+|(1/2)x(1/2)|} - \frac{e^{-1}|(1/2)y(1/2)|}{11+|(1/2)y(1/2)|}\right|,\\
&\frac{\left|f(1,\delta_2 x(\eta_2)) - f(1,\delta_2 y(\eta_2))\right|}{|\lambda|}\\
&\quad\le \frac{32}{19e}\left|\frac{\delta_2|x(1/2)-y(1/2)| + \delta_2|y(1/2)|}{11+\delta_2|x(1/2)-y(1/2)|+\delta_2|y(1/2)|} - \frac{\delta_2|y(1/2)|}{11+\delta_2|x(1/2)-y(1/2)|+\delta_2|y(1/2)|}\right|\\
&\quad\le \frac{32}{19e}\left|\frac{\delta_2|x(1/2)-y(1/2)|}{11+\delta_2|x(1/2)-y(1/2)|+\delta_2|y(1/2)|}\right|\\
&\quad\le \frac{32}{19e}\times\frac{\delta_2|x(1/2)-y(1/2)|}{11+\delta_2|x(1/2)-y(1/2)|}\\
&\quad\le \sup\left\{\frac{(512/19e)\delta_2|x(t)-y(t)|}{16\left(11+\delta_2|x(t)-y(t)|\right)}\right\}.
\end{aligned}
\tag{39}
$$

Similarly,

$$
\begin{aligned}
&\frac{\left|f(\eta_1,x(\eta_1)) - f(\eta_1,y(\eta_1))\right|}{|\lambda|}\\
&\quad\le \sup\left\{\frac{(512/19e)\delta_2|x(t)-y(t)|}{16\left(11+\delta_2|x(t)-y(t)|\right)}\right\},\\
&\frac{\left|f(\eta_2,x(\eta_2)) - f(\eta_2,y(\eta_2))\right|}{|\lambda|}\\
&\quad\le \sup\left\{\frac{(512/19e)\delta_2|x(t)-y(t)|}{16\left(11+\delta_2|x(t)-y(t)|\right)}\right\}.
\end{aligned}
\tag{40}
$$

Next,

$$
\begin{aligned}
g\left(t,x(t),I^{\alpha}x(t)\right) &= \frac{t^3}{3} - \left(\cos|x(t)| + \cos\left|I^{3/2}x(t)\right|\right)\\
&\le \frac{t^3}{3} = h(t).
\end{aligned}
\tag{41}
$$

That is, there exists a continuous function $h \in C([0,1],\mathbb{R})$ such that

$$
g\left(t,x(t),y(t)\right) \le h(t), \quad x, y \in \mathbb{R},\ t \in [0,1]. \tag{42}
$$

Finally, since

$$\|h(t)\| = \sup \int_0^1 \frac{t^3}{3} dt = \frac{1}{12},$$
$$L = \frac{512}{19e},$$
$$F_0 = 0, \tag{43}$$
$$\lambda = \frac{19}{32},$$

we can write

$$7L + F_0 + \frac{\|h\|_{L^1}}{\Gamma(p+1)} \left\{1 + \frac{2}{|\lambda|}\left(1 + \eta_1^p + \eta_2^p\right)\right\} < 70. \tag{44}$$

Thus $N \geq 70$. It follows that assumptions (A_1) and (A_2) are satisfied. Therefore, by Theorem 7 we conclude that problem (36) has a solution.

4. Conclusion

We have successfully developed appropriate conditions for existence of at least one solution to a complicated higher order coupled system of nonlinear hybrid fractional differential equations. The respective conditions have been derived by using coupled fixed point theorem of Krasnoselskii type. The obtained results were also demonstrated by a suitable example.

Conflicts of Interest

The authors declare that they have no conflicts of interest.

Authors' Contributions

All the authors have equal contribution. The first two authors designed the problem and the last two authors read and corrected its style and language and prepared the final version.

Acknowledgments

This work was financially supported by the Rajamangala University of Technology Thanyaburi (RMUTT), Pathum Thani, Thailand.

References

[1] D. Baleanu, A. C. J. Luo, and J. A. T. Machado, "Fractional dynamics and control," *Fractional Dynamics and Control*, pp. 1–313, 2012.

[2] Z. Dahmani, M. M. Mesmoudi, and R. Bebbouchi, "The foam drainage equation with time- and space-fractional derivatives solved by the Adomian method," *Electronic Journal of Qualitative Theory of Differential Equations*, pp. 1–10, 2008.

[3] W. G. Glockle and T. F. Nonnenmacher, "A fractional calculus approach to self-similar protein dynamics," *Biophysical Journal*, vol. 68, no. 1, pp. 46–53, 1995.

[4] R. Hilfer, *Applications of Fractional Calculus in Physics*, World Scientific Publishing Co., Singapore, 2000.

[5] R. Metzler, W. Schick, H. Kilian, and T. F. Nonnenmacher, "Relaxation in filled polymers: A fractional calculus approach," *The Journal of Chemical Physics*, vol. 103, no. 16, pp. 7180–7186, 1995.

[6] J. Sabatier, O. P. Agrawal, and J. A. Tenreiro MacHado, "Preface," *Advances in Fractional Calculus: Theoretical Developments and Applications in Physics and Engineering*, pp. xi–xiii, 2007.

[7] K. Balachandran and J. Y. Park, "Nonlocal Cauchy problem for abstract fractional semilinear evolution equations," *Nonlinear Analysis. Theory, Methods & Applications. An International Multidisciplinary Journal*, vol. 71, no. 10, pp. 4471–4475, 2009.

[8] O. K. Jaradat, A. Al-Omari, and S. Momani, "Existence of the mild solution for fractional semilinear initial value problems," *Nonlinear Analysis. Theory, Methods & Applications. An International Multidisciplinary Journal*, vol. 69, no. 9, pp. 3153–3159, 2008.

[9] A. A. Kilbas, H. M. Srivastava, and J. J. Trujillo, "Preface," *North-Holland Mathematics Studies*, vol. 204, no. C, pp. vii–x, 2006.

[10] B. N. Lundstrom, M. H. Higgs, W. J. Spain, and A. L. Fairhall, "Fractional differentiation by neocortical pyramidal neurons," *Nature Neuroscience*, vol. 11, no. 11, pp. 1335–1342, 2008.

[11] I. Podlubny, "Geometric and physical interpretation of fractional integration and fractional differentiation," *Fractional Calculus and Applied Analysis*, vol. 5, no. 4, pp. 367–386, 2002.

[12] S. G. Samko, A. A. Kilbas, and O. I. Marichev, *Fractional Integrals and Derivatives, Theory and Applications*, Gordon and Breach, Yverdon, Switzerland, 1993.

[13] B. Ahmad, S. K. Ntouyas, and A. Alsaedi, "Existence results for a system of coupled hybrid fractional differential equations," *The Scientific World Journal*, vol. 2014, Article ID 426438, 6 pages, 2014.

[14] A. Anber, S. Belarbi, and Z. Dahmani, "New existence and uniqueness results for fractional differential equations," *Analele Ştiinţifice ale Universităţii Ovidius Constanţa. Seria Matematică*, vol. 21, no. 3, pp. 33–41, 2013.

[15] A. Babakhani, "Existence of solution for a coupled system of fractional integro-differential equations on an unbounded domain," *Analysis in Theory and Applications*, vol. 29, no. 1, pp. 47–61, 2013.

[16] D. Baleanu, H. Khan, H. Jafari, R. A. Khan, and M. Alipour, "On existence results for solutions of a coupled system of hybrid boundary value problems with hybrid conditions," *Advances in Difference Equations*, vol. 2015, no. 1, article no. 318, 2015.

[17] T. Bashiri, S. M. Vaezpour, and C. Park, "A coupled fixed point theorem and application to fractional hybrid differential problems," *Fixed Point Theory and Applications*, vol. 2016, no. 1, article no. 23, 2016.

[18] B. Ahmad and J. J. Nieto, "Existence results for a coupled system of nonlinear fractional differential equations with three-point boundary conditions," *Computers & Mathematics with Applications*, vol. 58, no. 9, pp. 1838–1843, 2009.

[19] Y. Chen and H.-L. An, "Numerical solutions of coupled Burgers equations with time- and space-fractional derivatives," *Applied Mathematics and Computation*, vol. 200, no. 1, pp. 87–95, 2008.

[20] V. Gafiychuk, B. Datsko, and V. Meleshko, "Mathematical modeling of time fractional reaction-diffusion systems," *Journal of Computational and Applied Mathematics*, vol. 220, no. 1-2, pp. 215–225, 2008.

[21] V. Gafiychuk, B. Datsko, V. Meleshko, and D. Blackmore, "Analysis of the solutions of coupled nonlinear fractional reaction-diffusion equations," *Chaos, Solitons & Fractals*, vol. 41, no. 3, pp. 1095–1104, 2009.

[22] C. S. Goodrich, "Existence of a positive solution to systems of differential equations of fractional order," *Computers & Mathematics with Applications. An International Journal*, vol. 62, no. 3, pp. 1251–1268, 2011.

[23] M. P. Lazarević, "Finite time stability analysis of PD α-fractional control of robotic time-delay systems," *Mechanics Research Communications*, vol. 33, no. 2, pp. 269–279, 2006.

[24] S. K. Ntouyas and M. Obaid, "A coupled system of fractional differential equations with nonlocal integral boundary conditions," *Advances in Difference Equations*, vol. 2012, article no. 130, 2012.

[25] X. Su, "Boundary value problem for a coupled system of nonlinear fractional differential equations," *Applied Mathematics Letters*, vol. 22, no. 1, pp. 64–69, 2009.

[26] M. Benchohra, S. Hamani, and S. K. Ntouyas, "Boundary value problems for differential equations with fractional order and nonlocal conditions," *Nonlinear Analysis. Theory, Methods & Applications. An International Multidisciplinary Journal*, vol. 71, no. 7-8, pp. 2391–2396, 2009.

[27] X. Liu and M. Jia, "Multiple solutions of nonlocal boundary value problems for fractional differential equations on the half-line," *Electronic Journal of Qualitative Theory of Differential Equations*, pp. 1–14, 2011.

[28] S. Zhang, "Existence of solution for a boundary value problem of fractional order," *Acta Mathematica Scientia*, vol. 26, no. 2, pp. 220–228, 2006.

[29] S. S. Chang, Y. J. Cho, and N. J. Huang, "Coupled fixed point theorems with applications," *Journal of the Korean Mathematical Society*, vol. 33, no. 3, pp. 575–585, 1996.

Hindawi
Discrete Dynamics in Nature and Society
Volume 2017, Article ID 1349315, 8 pages
https://doi.org/10.1155/2017/1349315

Research Article

Two-Stage Dynamic Pricing and Advertising Strategies for Online Video Services

Zhi Li[1,2] and De-qing Tan[3]

[1]*School of Management, Tianjin Polytechnic University, Tianjin 300387, China*
[2]*College of Management and Economics, Tianjin University, Tianjin 300072, China*
[3]*School of Economics & Management, Southwest Jiaotong University, Chengdu 610031, China*

Correspondence should be addressed to Zhi Li; lizhi@tjpu.edu.cn

Received 4 May 2017; Revised 26 August 2017; Accepted 29 August 2017; Published 18 October 2017

Academic Editor: Cemıl Tunç

As the demands for online video services increase intensively, the selection of business models has drawn the great attention of online providers. Among them, pay-per-view mode and advertising mode are two important resource modes, where the reasonable fee charge and suitable volume of ads need to be determined. This paper establishes an analytical framework studying the optimal dynamic pricing and advertising strategies for online providers; it shows how the strategies are influenced by the videos available time and the viewers' emotional factor. We create the two-stage strategy of revenue models involving a single fee mode and a mixed fee-free mode and find out the optimal fee charge and advertising level of online video services. According to the results, the optimal video price and ads volume dynamically vary over time. The viewer's aversion level to advertising has direct effects on both the volume of ads and the number of viewers who have selected low-quality content. The optimal volume of ads decreases with the increase of ads-aversion coefficient, while increasing as the quality of videos increases. The results also indicate that, in the long run, a pure fee mode or free mode is the optimal strategy for online providers.

1. Introduction

Apart from text and images, video is the most important form of online media, which has been widely regarded as the future of media on the Internet. According to Cisco Visual Networking Index 2015–2020 prediction, by 2020, 82% of viewer Internet traffic will be video and total global Internet traffic will increase at 22% per year. High-quality online video service brings not only profits but also reputation and user reliability to the companies. The latter is rather more important for company's long term life cycle. For example, Youtube has attracted over a billion users all over world, because it offers free video services, selected advertising options, and a much faster streaming ability thanks to its great technologies such as Content Delivery Network (CDN) and Google File System (GFS). In other words, Youtube has paid a lot of attention to user experience and thus gains a large and stable user group, which makes Youtube one of the most famous video websites in the world. However, in 2014 Youtube annual revenue was posted at about $4 billion, which accounted for about 6% of Google's overall sales, which increased to $9 billion in 2015. This indicates that there will be a large potentiality for Youtube to be more profitable. Not only does Youtube exist, but also there are various Internet video sites such as Vimeo (US), Hulu (US), Youku (China), Dailymotion (France), Niconico (Japan), and Pandora TV (South Korea), competing in the online video market all over the world.

As the online video service has a glorious future, it is attractive and important to investigate its business models. There are several profiting modes, which mainly include three patterns: sales or redistribution of copyrights for certain films, charges for video services, and advertising revenue. In this paper, we will discuss the two latter cases dealing with online video users. Many video websites adopt the strategy of providing free video services to maximize membership. The revenues of this mode mainly depend on advertising. However, recent studies report that, with only advertising revenue, it is not sufficient for Internet-based

companies [1, 2]. According to Weiss [3], fee charge mode is necessary and becoming more popular in web content market. Hence, the strategy of combining fee charge and advertising has emerged, which has been regarded as the mainstream business model, such as Youku, the most famous video service website in China, which offers free videos with ads as well as a paid membership with a higher priority and no ads. Although the mixed strategy is popular, it also raises the problem of how to balance the revenue from fee charging and advertising. For Internet video services, higher prices result in fewer viewers, and a large amount of ads will also scare them away. In this sense, there exists a trade-off between video service price and the amount of ads.

In order to deal with this trade-off, some video websites adopt strategy that allows viewers to preview samples before buying. It might be feasible, because online video is a sort of information goods as well as experience goods, which could be valued according to viewers' perceived experience [4]. Hence, free samples are introduced into the business models with the purpose of ensuring that viewers have an actual experience with information goods [5, 6]. This humanized experience mode is helpful to set up reasonable price and ads volume for information goods. With significant increasing number of the Internet users, the pricing and advertising models have attracted attention of many researchers. Riggins [7] develops a separating equilibrium model for fee-based and ads sponsored-based websites and examines a monopolist's choice of web content price and quality. In another study, Prasad et al. [8] suggest different optimal strategies for content firms depending on the context: pure pay-per-view strategy for high income users, who are willing to pay the advertising avoidance fee, and free strategy based on advertisement for high advertising sales with low-quality content. The study derives the optimal condition for each strategy. Halbheer et al. [9] investigates digital content strategies: the sampling, paid content, and free content strategies for online publishers. Results show that the optimal strategy is determined by the relationship between advertising effectiveness and content quality. Chellappa and Shivendu [1] examine pricing and sampling strategies for digital experience goods; through a two-stage viewer piracy behavior model they obtain the optimal price and sample size. Peitz and Valletti [10] introduce the factor of viewer's favorite type into pay-tv and free-to-air models in the two-side market. The results indicate that the more sensitive the viewers are to ads the more the differentiated content should be. Kwon [11] constructs a stochastic model for online display advertising contracts and explores how pricing and contract components affect the optimal display strategies. Lin et al. [12] assert that a mixed strategy of paid and free content is most favorable for content firms in a monopoly position, and in a duopoly state, only one firm is able to employ the mixed strategy.

The papers mentioned above apply static models and optimize the maximum revenue using simple first-order and second-order conditions without considering the effect of time on the optimal strategy. However, a few papers do take into consideration the time periods in different ways and provide a dynamic analysis to study the optimal content price and the volume of ads in websites. For instance, Dewan et al. [13] develop an advertising revenue model and obtain the optimal dynamic ads volume for the manager of Internet. Kumar and Sethi [2] study dynamic pricing and advertising for web content providers and test the influence of parameters such as horizon length, cost of serving, natural growth rate, and content's utility factor on the optimal strategies. Based on the pricing strategy, Na et al. [14] categorize Korea's digital content firms' strategies into three groups: pure pay-per-view strategy, free strategy based on advertisement, and a mixed strategy; then they apply the metafrontier analysis method to estimate each group's efficiency value. As extension, our model differs from theirs by further considering the hybrid business models with the type of viewers and emotional factor varying over time. In this paper, we will introduce two business models including the fee mode and the free mode that allow viewers to select. There are two cases under consideration, the single fee mode case and the mixed fee-free mode case. In the mixed fee-free mode, viewers could maximize their utility by selecting within the two modes. Based on the emotional factor, the type of viewers, and the perceived value, we propose a model for finding the optimal dynamic fee charge and ads level over a finite time interval, to maximize the total profit of online video providers. To the best of our knowledge, it is the first analysis with a continuous time model and emotional factor in this setting. The paper is innovative and new, which firstly applies Hamilton maximum principle to solve the optimal pricing and advertising strategies for online video services.

2. The Model

Consider that the online provider offers two types of Internet video contents: high-quality content without ads requiring a fee to access and low-quality content with ads but free of charge. There will be previews for viewers to have a general judge over the video service. Assume that for high-quality and low-quality video services, the viewer's average perceived values are v_h and v_l, respectively, where $v_h > v_l > 0$ [15]. Since different viewers react differently to the same video content, they can be classified further by their types. For this model, we define high-quality type preferred viewers as those who are more sensitive to video quality; thus they have more willingness to choose the fee mode. Similarly, defined economy preferred viewers are those who are unwilling to pay for online videos but may tolerate advertising; thus they prefer to choose the free mode. Meanwhile we assume that (as well as in [16]) viewer's type θ follows a uniform distribution on $[0, 1]$, which is a factor indicating viewers' willingness to pay for service. When θ is close to 1, the viewers are more likely to choose the fee mode, and vice versa.

In this paper, the price of online video services and the amount of ads are functions of time t denoted by p_t and q_t, respectively. Based on above assumptions, define the viewer expected utility such that a viewer of type θ_h receiving from high-quality content is $U_h(t) = \theta_h v_h - p_t$ and from low-quality content is $U_l(t) = \theta_l v_l - \beta q_t$. In the free mode, viewers have to view ads that come with video content. Thus, the advertising is regarded as a nuisance that could reduce viewers' utility [17, 18]. Based on this fact, considering viewers' emotional

factor that could affect the viewing mode, we define $\beta \in (0,1)$ as a constant representing ads-aversion coefficient. When β value gets closer to 1, it means viewers are less tolerant to ads. We assume that the marginal cost of producing a product or introducing an advertisement is zero. Viewers have to view ads that come in order to access the free product. To mirror the properties of pricing and advertising strategies, let the cost of setting ads be zero [7], and the producing cost of content is negligible on Internet.

In the following part, we will introduce the single fee mode and the mixed fee-free mode, where the optimal video price and ads volume are resolved to obtain the optimal business strategies for online video services.

2.1. Case I: Fee Mode in Time Interval $(0, t_1)$. At time t, when $U_h(t) = \theta_h v_h - p_t \geq 0$, $\theta_h \geq p_t/v_h$, viewers choose the fee mode. Define the total volume of viewers as 1. Let $x_{h,t}$ be the number of viewers who have selected high-quality content. The current density of viewers $\dot{x}_{h,t} = dx_{h,t}/dt$ is expressed as

$$\begin{aligned} D_{h,t} &= \int_{p_t/v_h}^{\theta_h} d\theta = \theta_h - \frac{p_t}{v_h} = 1 - x_{h,t} - \frac{p_t}{v_h}, \\ \dot{x}_{h,t} &= 1 - x_{h,t} - \frac{p_t}{v_h}. \end{aligned} \tag{1}$$

Let $\dot{x}_{h,t} = dx_{h,t}/dt$ be the change rate of the number of high type viewers and define $\dot{x}_{h,t} = D_{h,t}$. We denote that online providers make profits over the planning horizon with length t_1, and then the profit is given as

$$\Pi_{\mathrm{I}} = \int_0^{t_1} p_t \dot{x}_{h,t} dt. \tag{2}$$

In case I, it needs to find out the optimal price p_t^* which maximizes the profit Π_{I}. The objective function for the provider is

$$J_1 = \max \int_0^{t_1} p_t \dot{x}_{h,t} dt, \tag{3}$$

This is a dynamic optimization problem, which can be solved by the modern control theory Hamiltonian Method. In the model, a dot above a variable is defined as the first derivative with respect to time. We formulate Hamiltonian function as follows:

$$H_1 = p_t \left(1 - x_{h,t} - \frac{p_t}{v_h}\right) + \lambda_{0,t} \left(1 - x_{h,t} - \frac{p_t}{v_h}\right), \tag{4}$$

where p_t is a control variable and $\lambda_{0,t}$ is a time-varying constructor variable. According to Hamiltonian principle [19, 20], the necessary conditions for the optimal control are listed as follows:

$$\begin{aligned} \frac{\partial H_1}{\partial p_t} &= 0, \\ \dot{\lambda}_{0,t} &= -\frac{\partial H_1}{\partial x_{h,t}}. \end{aligned} \tag{5}$$

Since p_t is unconstrained, the optimal price should satisfy the first-order condition $\partial H_1/\partial p_t = 0$, from which we obtain

$$p_t = \frac{v_h (1 - x_{h,t}) - \lambda_{0,t}}{2}. \tag{6}$$

From (1) and (6), the increment rate of viewers who select high-quality content $\dot{x}_{h,t}$ is given by

$$\dot{x}_{h,t} = \frac{\lambda_{0,t} + v_h (1 - x_{h,t})}{2 v_h}. \tag{7}$$

Since Lagrangian multiplier satisfies the condition $\dot{\lambda}_{0,t} = -\partial H_1/\partial x_{h,t}$, we have the following equation:

$$\dot{\lambda}_{0,t} = \frac{\lambda_{0,t} + v_h (1 - x_{h,t})}{2}. \tag{8}$$

Deduced from (7) and (8), we obtain

$$\dot{\lambda}_{0,t} = v_h \dot{x}_{h,t}. \tag{9}$$

Equation (9) is a first-order differential equation. With border conditions $x_{h,t=0} = 0$ and $\lambda_0(t_0) = 0$, final solutions are achieved as $\lambda_{0,t} = v_h(t - t_1)/(2 + t_1)$, $x_{h,t} = t/(2 + t_1)$.

We substitute the values of $\lambda_{0,t}$ and $x_{h,t}$ into (6) and derive the optimal price of online video services $p_t^* = v_h(1 + t_1 - t)/(2 + t_1)$ that could make the maximum profit in fee mode with time interval $(0, t_1)$.

2.2. Case II: Mixed Fee-Free Mode in Time Interval $(0, t_1)$. In this case, there exists both fee and free modes in online video service market. Viewers could choose any mode as their willingness. Since the newly arriving video contents are more attractive, viewers prefer to pay for the new ones. With this consideration, introduce a critical time point t_0, which divides the whole business time into two stages: in time interval $(0, t_0)$, providers employ the fee mode; in time interval (t_0, t_1), providers employ the mixed fee-free mode.

Stage 1 (fee mode $(0 \leq t \leq t_0)$). Here we make an assumption that the optimal solution for fee model is the same as case I. This assumption stands when t_1 is not infinite and for the purpose of simplifying the model. It means that in time interval $0 \leq t \leq t_0$, the optimal price of online video services is $p_t^* = v_h(1 + t_1 - t)/(2 + t_1)$.

Stage 2 (fee-free mode $(t_0 < t \leq t_1)$). At time t_0, introduce the free mode into the single fee mode in online video market, and therefore there exists both fee and free modes at the same time. The advertising in free mode will attenuate viewers' selection. In the fee mode, we adopt a scaled price of Stage 1 for Stage 2 for simplicity. Denote γ as a regular factor in (0, 1], which determines the price in Stage 2 as γp_t. For viewers, if $U_h(t) > U_l(t)$ fee mode is preferred, otherwise, free mode is better. Furthermore, we have the following results:

If $0 \leq \theta v_l - \beta q_t < \theta v_h - \gamma p_t, \theta > (\gamma p_t - \beta q_t)/(v_h - v_l) \geq 0$, viewers prefer the fee mode.

If $0 \leq \theta v_h - \gamma p_t \leq \theta v_l - \beta q_t$, $\beta q_t/v_l < \theta < (\gamma p_t - \beta q_t)/(v_h - v_l)$, viewers prefer the free mode.

It can be found that $\widetilde{\theta} = (\gamma p_t - \beta q_t)/(v_h - v_l)$ is the critical point of viewer type.

Denote $x_{l,t}$ as the number of viewers who have viewed low-quality content; thus the current densities of different viewers are defined as

$$D_{h,t} = \theta_h - \frac{\gamma p_t - \beta q_t}{v_h - v_l},$$
$$D_{l,t} = \frac{\gamma p_t - \beta q_t}{v_h - v_l} - \frac{\beta q_t}{v_l}. \tag{10}$$

Since $\dot{x}_{h,t} = D_{h,t}$, $\dot{x}_{l,t} = D_{l,t}$, we have

$$\dot{x}_{h,t} = 1 - \frac{t_0}{2 + t_0} - \frac{\gamma p_t - \beta q_t}{v_h - v_l} - x_{h,t} - x_{l,t},$$
$$\dot{x}_{l,t} = \frac{\gamma p_t - \beta q_t}{v_h - v_l} - \frac{\beta q_t}{v_l}, \tag{11}$$

where $\dot{x}_{h,t}$ is the density of arriving viewers who select fee mode and $\dot{x}_{l,t}$ is the density of viewers who select free mode. The profit of fee-free mode is given as

$$\Pi_{\mathrm{II}} = \int_{t_0}^{t_1} \left(\gamma p_t \dot{x}_{h,t} + k q_t \dot{x}_{l,t}\right) dt, \tag{12}$$

where k is the price of ads per unit. In Stage 2, it needs to find the optimal ads volume q_t^* to maximize profit Π_{II}. Over time period $t_0 < t \le t_1$, the objective function for the provider is

$$J_2 = \max \int_{t_0}^{t_1} \left(\gamma p_t \dot{x}_{h,t} + k q_t \dot{x}_{l,t}\right) dt, \tag{13}$$

subject to (14) and (15):

$$\dot{x}_{h,t} = 1 - \frac{t_0}{2 + t_0} - \frac{\gamma p_t - \beta q_t}{v_h - v_l} - x_{h,t} - x_{l,t}, \tag{14}$$

$$\dot{x}_{l,t} = \frac{\gamma p_t - \beta q_t}{v_h - v_l} - \frac{\beta q_t}{v_l}. \tag{15}$$

The Hamiltonian function is given as follows:

$$H_2 = \left(\gamma p_t + \lambda_{1,t}\right)\left(\frac{2}{2 + t_0} - \frac{\gamma p_t - \beta q_t}{v_h - v_l} - x_{h,t} - x_{l,t}\right) + \left(\lambda_{2,t} + k q_t\right)\left(\frac{\gamma p_t - \beta q_t}{v_h - v_l} - \frac{\beta q_t}{v_l}\right), \tag{16}$$

where q_t is the variable, and $p_t = v_h(1 + t_1 - t)/(2 + t_1)$ is given in Stage 1. $\lambda_{1,t}$ and $\lambda_{2,t}$ are the two constructor variables corresponding to the state variables $x_{h,t}$ and $x_{l,t}$ [20]. Based on Hamiltonian principle, q_t, $\lambda_{1,t}$, $\lambda_{2,t}$, $x_{h,t}$, and $x_{l,t}$ satisfy the following equations:

$$\frac{\partial H_2}{\partial q_t} = 0,$$
$$\dot{\lambda}_{1,t} = -\frac{\partial H_2}{\partial x_{h,t}},$$
$$\dot{\lambda}_{2,t} = -\frac{\partial H_2}{\partial x_{l,t}}. \tag{17}$$

Since q_t is unconstrained, $\partial H_2/\partial q_t = 0$, the number of ads q_t is obtained by

$$q_t = \frac{\gamma}{2\beta k\left(2 + t_1\right)}\left(\left(\beta + k\right) v_l + \left(t_1 - t\right)\left(k v_l + \beta v_h\right)\right). \tag{18}$$

Since Lagrange's equation satisfies $\dot{\lambda}_{1,t} = -\partial H_2/\partial x_{h,t}$, $\dot{\lambda}_{2,t} = -\partial H_2/\partial x_{l,t}$, we have the following equations:

$$\dot{\lambda}_{1,t} = -\frac{\partial H_2}{\partial x_{h,t}} = \gamma p_t + \lambda_{1,t},$$
$$\dot{\lambda}_{2,t} = -\frac{\partial H_2}{\partial x_{l,t}} = \gamma p_t + \lambda_{1,t}. \tag{19}$$

Through solving first-order differential equations (19) and with border condition $\lambda_{1,t} = \lambda_{2,t} = 0$, we obtain

$$\lambda_{1,t} = \lambda_{2,t} = -\frac{\gamma v_h\left(t_1 - t\right)}{2 + t_1}. \tag{20}$$

From (14), (15), (18), (20), and p_t we have the following results:

$$q_t = \frac{\gamma}{2\beta\left(2 + t_1\right)}\left(\left(\beta + k\right) v_l + \left(t_1 - t\right)\left(\beta v_h + k v_l\right)\right), \tag{21}$$

$$x_{l,t} = \frac{\gamma v_h}{2\left(v_h - v_l\right)\left(2 + t_1\right)}\left[\left(1 - \frac{\beta}{k}\right)\left(t - t_0\right) + \left(1 - \frac{\beta v_h}{k v_l}\right)\left(t_1\left(t - t_0\right) - \frac{t^2 - t_0^2}{2}\right)\right]. \tag{22}$$

In addition, from the existing results, we can resolve $x_{h,t}$ considering (6), (14), (18), (22), and the border condition $x_{h,t}(t_0) = t_0/(2 + t_1)$; the following formulation is given:

$$x_{h,t} = \frac{\gamma v_h}{2\left(v_h - v_l\right)\left(2 + t_1\right)}\left[\frac{1}{2}\left(1 - \frac{\beta v_h}{k v_l}\right) t^2 + \left(\frac{\beta v_h}{k v_l} - \frac{v_l}{v_h} - t_1 + \frac{\beta v_h}{k v_l} t_1\right) t - 2 + \left(\frac{\beta}{k} + 2\right)\frac{v_l}{v_h} - \frac{\beta v_h}{k v_l} + \left(\frac{v_l}{v_h} + \frac{\beta}{k} - 1 - \frac{\beta v_h}{k v_l}\right) t_1 + \left(1 - \frac{\beta}{k}\right) t_0 + \left(1 - \frac{\beta v_h}{k v_l}\right)\left(t_0 t_1 - \frac{t_0^2}{2}\right)\right] + C_h e^{-t} + \frac{2}{2 + t_0}, \tag{23}$$

with

$$C_h = e^{-t_0}\left(\frac{t_0}{2 + t_1} - \frac{2}{2 + t_0} - \frac{\gamma v_h}{2\left(v_h - v_l\right)\left(2 + t_1\right)}\left[\frac{1}{2}\left(1 - \frac{\beta v_h}{k v_l}\right) t_0^2 + \left(\frac{\beta v_h}{k v_l} - \frac{v_l}{v_h} - t_1 + \frac{\beta v_h}{k v_l} t_1\right) t_0 - 2 + \left(\frac{\beta}{k} + 2\right)\frac{v_l}{v_h} - \frac{\beta v_h}{k v_l} + \left(\frac{v_l}{v_h} + \frac{\beta}{k} - 1 - \frac{\beta v_h}{k v_l}\right) t_1 + \left(1 - \frac{\beta}{k}\right) t_0 + \left(1 - \frac{\beta v_h}{k v_l}\right)\left(t_0 t_1 - \frac{t_0^2}{2}\right)\right]\right). \tag{24}$$

Finally, we obtain the optimal trajectories for $x_{l,t}$, $\lambda_{1,t}$, and $\lambda_{2,t}$ in (20) and (22) and the optimal number of ads $q_t^* = (\gamma/2\beta(2+t_1))((\beta+k)v_l + (t_1-t)(\beta v_h + kv_l))$ that makes the maximization of profit.

3. The Optimal Strategy

Based on the hybrid business models discussed in the above section, we can draw the following conclusions on optimal strategies, which are useful to gain insights into factors affecting the optimal price and quantity.

3.1. The Optimal Pricing Strategy for Case I

Proposition 1. *In the single fee mode, it is optimal to set* $p_t^* = v_h(1+t_1-t)/(2+t_1)$, $0 \le t \le t_1$, *in order to attend the maximum profit.*

Proposition 1 shows that the optimal pricing strategy is determined by the relation between high-quality value and time.

Lemma 2. *The optimal price* p_t^* *is increasing as perceived value* v_h *of high-quality video increases, but it is decreasing as time t increases.*

Proof. By taking the high-quality value and time partial derivatives of the optimal price, we obtain $\partial p_t^*/\partial v_h = v_h(1+t_1-t)/(2+t_1) \ge 0$, $\partial p_t^*/\partial t = -v_h/(2+t_1) \le 0$, which supports Lemma 2. □

Lemma 2 says, as higher perceived value obtained from high-quality content video, the higher fee charge could be realized.

3.2. The Optimal Pricing-Advertising Strategy for Case II

Proposition 3. *In the mixed fee-free mode of online video market, it is optimal for online providers to adopt a paid content strategy as* $p_t^* = \gamma v_h(1+t_1-t)/(2+t_1)$, $0 \le t \le t_1$; *it is optimal to adopt a free content strategy as* $q_t^* = (\gamma/2\beta(2+t_1))((\beta+k)v_l + (t_1-t)(kv_l+\beta v_h))$, $t_0 < t \le t_1$.

Proposition 3 shows the mixed fee-free strategy with the optimal price of online video services and the optimal number of ads. This proposition is validated in Section 2 discussion by means of Hamiltonian principle. As in the benchmark case, if viewers care more about the high-quality value of online video content, it is optimal for providers to employ the fee strategy; if the viewers are not willing to pay for the online content, meanwhile, they would rather accept ads (the value of ads-aversion coefficient is small); it is optimal for providers to employ the free strategy.

Lemma 4. *The optimal number of ads* q_t^* *is increasing as either high-quality value* v_h *or low-quality value* v_l *increases, while it is decreasing as either ads-aversion coefficient* β *or time t increases.*

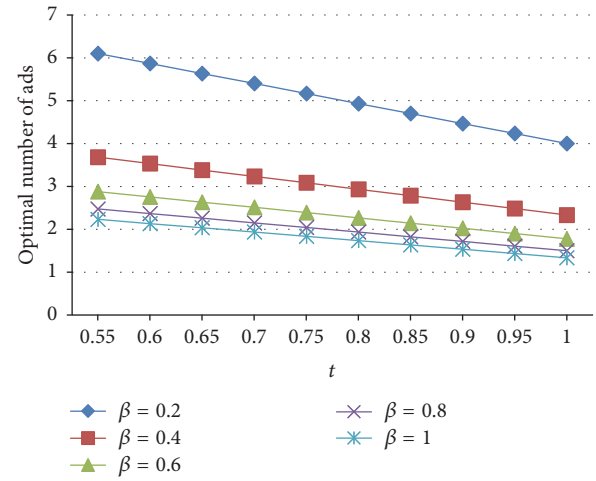

Figure 1: The optimal number of ads with respect to time t.

Proof. For the optimal number of ads q_t^*, we take the first derivative of q_t^* versus v_h, v_l, and t and then obtain $\partial q_t^*/\partial v_h = \gamma v_h(t_1-t)/2(2+t_1) \ge 0$, $\partial q_t^*/\partial v_l = (\gamma(\beta+k)+(t_1-t)k)/2\beta(2+t_1) \ge 0$, $\partial q_t^*/\partial t = -\gamma(\beta v_h + kv_l)/2\beta(2+t_1) < 0$.

Through simple transform $q_t^* = (\gamma/2\beta(2+t_1))((\beta+k)v_l + (t_1-t)(\beta v_h + kv_l)) = (\gamma/2(2+t_1))((1+k/\beta)v_l + (t_1-t)(v_h + kv_l/\beta))$, it is clear that q_t^* decreases with the increase of β. All the above can support Lemma 4. □

The result of Lemma 4 is illustrated in Figure 1 using numerical computations, where we plot the optimal ads volume with different values of β. As can be seen in Figure 1, the high ads-aversion coefficient corresponds to the low volume ads. For each curve of ads volume, the optimal number of ads is decreasing with the increase of time t. This result is rational in real online video market case. The longer the video available time lasts, the less attractive the video content is. Therefore, to get the sustainable profit in the long run, it is optimal for online providers to reduce ads volume.

Lemma 5. *The number of viewers who select low-quality content* $x_{l,t}$ *increases as time t increases, if* $kv_l > \beta v_h$, *when t is in the time interval* (t_0, t_1).

Proof. In case II Stage 2, we obtain

$$x_{l,t} = \frac{\gamma v_h}{2(v_h - v_l)(2+t_1)}\left[\left(1-\frac{\beta}{k}\right)(t-t_0) + \left(1-\frac{\beta v_h}{kv_l}\right)\left(t_1(t-t_0) - \frac{t^2-t_0^2}{2}\right)\right]. \tag{25}$$

Take the first derivative of $x_{l,t}$ with respect to t, which leads to $\partial x_{l,t}/\partial t = \gamma v_h/2(v_h-v_l)(2+t_1)[(1-\beta/k)+(1-\beta v_h/kv_l)(t_1-t)]$, given the condition $\beta/k < v_l/v_h$, and then obtain $\partial x_{l,t}/\partial t > 0$, which supports Lemma 5. □

Lemma 5 shows that, under the condition of $\beta/k < v_l/v_h$, if advertising price is high and the actual high-quality value is relatively low, viewers tend to prefer the free mode. Therefore,

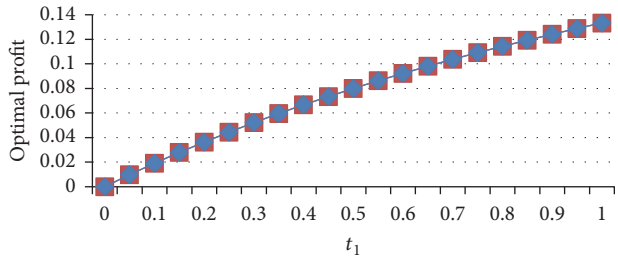

FIGURE 2: The optimal profit of case I with respect to time t_1.

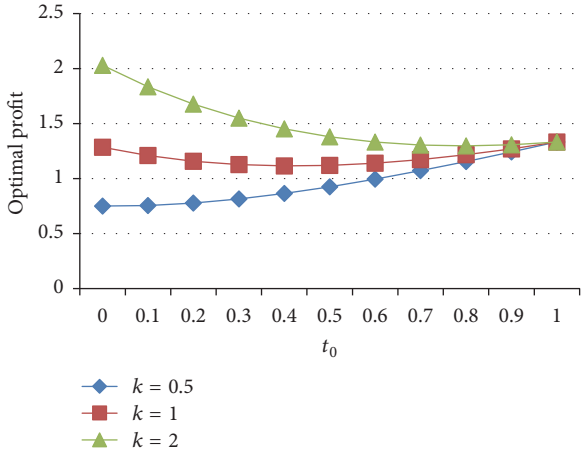

FIGURE 3: The optimal profit of case II with different ads prices k.

it is beneficial for online providers to adopt free strategy to generate advertising revenue. Taking this into account is significant for providers when fixing the optimal video price and ads volume.

To have a better understanding of parameters influence on $x_{l,t}$, we draw the curve of $x_{l,t}$ with respect to β/k and v_h/v_l in Figures 2 and 3. With generality, we set parameters values as $t_0 = 0.5$, $t_1 = 1$, and $\gamma = 0.7$. Please see the explanations in the following section.

4. The Optimal Profit

According to the Hamiltonian principle and the previous analysis, we calculate the maximum profits taking into consideration the optimal strategies of fee charge and amount of ads. For case I fee mode, the optimal profit $\Pi_I(t_1)$ equals

$$\begin{aligned}\Pi_I(t_1) &= \int_0^{t_1} p_t \dot{x}_{h,t} dt = \int_0^{t_1} \frac{v_h(1+t_1-t)}{2+t_1} \cdot \frac{1}{2+t_1} dt \\ &= \frac{v_h t_1}{2(2+t_1)}.\end{aligned} \tag{26}$$

Figure 2 reflects the changing trend of the optimal profit for case I. We observe in this figure that the optimal profit increased as the time t_1 increased, but the increase is not very sharp. When t_1 tends to infinity, the maximum profit is obtained as $\Pi_I = v_h/2$. Also, we can observe from the equation of $\Pi_I(t_1)$ that it is always optimal for online providers to adopt the single fee mode in time period t_1 when the high-quality value v_h is increasing. For case II, the mixed fee-free mode, we calculate the total profit $\Pi_{II}(t_0)$ as a function of the critical time t_0, separating into two stages. The respective profits are noted as $\Pi_{II,1}(t_0)$ and $\Pi_{II,2}(t_0)$:

$$\begin{aligned}\Pi_{II,1}(t_0) &= \int_0^{t_0} p_t \dot{x}_{h,t} dt = \int_0^{t_0} \frac{v_h(1+t_1-t)}{2+t_1} \frac{1}{2+t_1} dt \\ &= \frac{v_h(2+2t_1-t_0)t_0}{2(2+t_1)^2},\end{aligned} \tag{27}$$

and for Stage 2 profit, from the above obtained equations, we can have the following formulation:

$$\begin{aligned}\Pi_{II,2}(t_0) &= \int_{t_0}^{t_1} (\gamma p_t^* \dot{x}_{h,t} + k q_t^* \dot{x}_{l,t}) dt \\ &= \frac{\gamma^2 v_0^2}{4(v_0-v_1)(2+t_1)^2} \left((1+t_1)\left(-\frac{v_1}{v_0} - t_1 \right.\right. \\ &+ \left.\frac{\alpha v_0}{k v_1} t_1 + \frac{\alpha v_0}{k v_1}\right)(t_1 - t_0) + \left[\left(1 - \frac{\alpha v_0}{k v_1}\right)(1+t_1)\right. \\ &- \left.\left(-\frac{v_1}{v_0} - t_1 + \frac{\alpha v_0}{k v_1} t_1 + \frac{\alpha v_0}{k v_1}\right)\right] \frac{t_1^2 - t_0^2}{2} - \left(1 \right. \\ &- \left.\left.\frac{\alpha v_0}{k v_1}\right) \frac{t_1^3 - t_0^3}{3}\right) + \frac{\gamma v_0 (1+t_1)}{2+t_1} C_h \left(e^{-t_1} - e^{-t_0}\right) \\ &- \frac{\gamma v_0 C_h}{2+t_1} \left[e^{-t_1}(t_1+1) - e^{-t_0}(t_0+1)\right] \\ &+ \frac{\gamma^2 v_0 v_1 k}{4\alpha (v_0-v_1)(2+t_1)^2} \left[\left(1 - \frac{\alpha^2}{k^2}\right)(t_1 - t_0)\right. \\ &+ 2\left(1 - \frac{\alpha^2 v_0}{k^2 v_1}\right) t_1 (t_1 - t_0) - \left(1 - \frac{\alpha^2 v_0}{k^2 v_1}\right)(t_1^2 \\ &- t_0^2) + \left(1 - \frac{\alpha^2 v_0^2}{k^2 v_1^2}\right) t_1^2 (t_1 - t_0) - \left(1 - \frac{\alpha^2 v_0^2}{k^2 v_1^2}\right) \\ &\cdot t_1 (t_1^2 - t_0^2) + \left.\frac{1}{3}\left(1 - \frac{\alpha^2 v_0^2}{k^2 v_1^2}\right)(t_1^3 - t_0^3)\right].\end{aligned} \tag{28}$$

Because the formulation is complicated, we investigate numerically the influence of critical time t_0 on the total profit $\Pi_{II}(t_0)$ in case II. Without losing generality, set the total interval $t_1 = 1$, $\gamma = 0.7$, $\beta = 0.4$, $v_l = 4$, and $v_h = 8$, and t_0 belongs to $[0, t_1]$. The following shows numerically how the parameter of ads unit price k influences the optimal profit of case II of the mixed fee-free mode in Figure 3.

It can be found that no matter how the unit ads income varies, the optimal profit strategy is to take into action only one business model, either the single fee mode or the mixed fee-free mode, as the profit reaches a maximum value at the ends of the interval. The optimal profit increases as k increases. When the value of ads price k is small, it suggests that the mixed fee-free mode profiting ads revenue is less

efficient than the revenue of the single fee mode, which is supported in case $k = 0.5$ in Figure 3. Clearly, when $t_0 = 0$, there exists the mixed fee-free mode; for $t_0 = 1$, there only exists the single fee mode. Please see the optimal profit curve with $k = 0.5$; the profit at $t_0 = 0$ is less than that at $t_0 = 1$, which means the single fee mode is optimal. Conversely, when the value of ads price k is large, the mixed fee-free mode with ads revenue will create more profit. As shown in case $k = 2$ in Figure 3, $t_0 = 0$ reaches the maximum profit, which means the mixed fee-free mode outperforms in this case. At the same time, when $k = 1$, the profits at both ends of the interval are nearly equal, while the profit decreases as t_0 varying in the interval. This means, for online providers, there is no difference between the single fee mode and mixed fee-free mode. Therefore, the optimal strategy is to adopt either of them. Finally, from the above analysis, it can be concluded that the online providers should set their strategies according to the unit ads price k, but the strategy should always be one single business model.

5. Conclusion

This paper has investigated the optimal strategy for online video service business. Considering the dynamic decisions in real video market, we divide the whole period into the single fee phase and mixed fee-free phase and then, respectively, create continuous time model for each. Our models have presented a straightforward way to study the provider's pricing strategy and advertising decision based on viewers' emotional factor. There is a significant influence among applied price, ads volume, and video content quantity. In the single fee mode, we have obtained the optimal time-varying price which maximizes the profit from video service within a certain time interval. The result implies that the optimal price of online video increases with high-quality value while decreasing with time. In the mixed fee-free mode, we have found out the optimal fee and ads volume. It is beneficial for online providers to choose higher charge fee and advertising intensity. Besides, the price and the number of ads decrease as ads-aversion coefficient increases. It has turned out that, in a long run period of time, taking one strategy either fee mode or free mode is optimal for the online providers.

For future research, the following subjects can be carried out in three aspects:

(i) Accomplishment of the model: There are other factors which determine the revenue model. For example, in Ren et al. [21], the authors point out that the online popularity is a significant effecting factor on videos in online systems; in Iveroth et al. [22], competitors' price is a base factor for deciding; in Choi et al. [23], they imply that discount on price can have effect on the sales of information goods; in another study, Niu and Li [24] suggest for the Internet service providers a price model depending on the congestion of Internet.

(ii) Model validation: our time-continuous model should fit the data collected in real world, identify model coefficients, and validate other sets of data. As mentioned in Walz et al. [25], the uncertainty analysis could be carried out in two aspects: the model form uncertainty and the parameters uncertainty. The parameters standard error is investigated and the values should fall into the confidence interval. In this way, the optimal time-varying price solutions are validated.

(iii) Another path to investigate online video services is predicting and analyzing based on a fitted nonparametric model. There are several advanced regression methods to be investigated, such as multivariate adaptive regression splines (MARS) or its alternative CMARS proposed by Weber et al. [26] or RCMARS proposed by Özmen et al. [27]. The prediction model can be used for simulation and cross validation with respect to our models.

Conflicts of Interest

The authors declare that they have no conflicts of interest.

References

[1] R. K. Chellappa and S. Shivendu, "Managing piracy: Pricing and sampling strategies for digital experience goods in vertically segmented markets," *Information Systems Research*, vol. 16, no. 4, pp. 400–417, 2005.

[2] S. Kumar and S. P. Sethi, "Dynamic pricing and advertising for web content providers," *European Journal of Operational Research*, vol. 197, no. 3, pp. 924–944, 2009.

[3] T. R. Weiss, "Fees for online content proliferating, but will users buy," *Computer World*, 2002.

[4] C. Shapiro and H. R. Varian, *Information rules: A strategy guide to the network economy*, Harvard Business School Press, Boston, MA, 1998.

[5] H. K. Cheng and Q. C. Tang, "Free trial or no free trial: Optimal software product design with network effects," *European Journal of Operational Research*, vol. 205, no. 2, pp. 437–447, 2010.

[6] D. Halbheer, F. Stahl, O. Koenigsberg, and D. R. Lehmann, "Choosing a digital content strategy: How much should be free?" *International Journal of Research in Marketing*, vol. 31, no. 2, pp. 192–206, 2014.

[7] F. J. Riggins, "Market segmentation and information development costs in a two-tiered fee-based and sponsorship-based web site," *Journal of Management Information Systems*, vol. 19, no. 3, pp. 69–86, 2002.

[8] A. Prasad, V. Mahajan, and B. Bronnenberg, "Advertising versus pay-per-view in electronic media," *International Journal of Research in Marketing*, vol. 20, no. 1, pp. 13–30, 2003.

[9] D. Halbheer, F. Stahl, O. Koenigsberg, and D. R. Lehmann, "Digital content strategies," *Marketing Letters*, vol. 25, no. 3, pp. 331–341, 2013.

[10] M. Peitz and T. M. Valletti, "Content and advertising in the media: Pay-tv versus free-to-air," *International Journal of Industrial Organization*, vol. 26, no. 4, pp. 949–965, 2008.

[11] C. Kwon, "Single-period balancing of pay-per-click and pay-per-view online display advertisements," *Journal of Revenue and Pricing Management*, vol. 10, no. 3, pp. 261–270, 2011.

[12] M. Lin, X. Ke, and A. Whinston, "Vertical differentiation and a comparison of online advertising models," *Journal of*

Management Information Systems, vol. 29, no. 1, pp. 195–236, 2012.

[13] R. M. Dewan, M. L. Freimer, and J. Zhang, "Management and valuation of advertisement-supported web sites," *Journal of Management Information Systems*, vol. 19, no. 3, pp. 87–98, 2002.

[14] H. S. Na, J. Hwang, J. Y. J. Hong, and D. Lee, "Efficiency comparison of digital content providers with different pricing strategies," *Telematics and Informatics*, vol. 34, no. 2, pp. 657–663, 2017.

[15] H. L. Vogel, *Entertainment Industry Economics*, Cambridge Books, New York, NY, USA, 2015.

[16] R. Casadesus-Masanell and F. Zhu, "Strategies to fight ad-sponsored rivals," *Management Science*, vol. 56, no. 9, pp. 1484–1499, 2010.

[17] K. C. Wilbur, "A two-sided, empirical model of television advertising and viewing markets," *Marketing Science*, vol. 27, no. 3, pp. 356–378, 2008.

[18] S. P. Anderson and S. Coate, "Market provision of broadcasting: a welfare analysis," *Review of Economic Studies*, vol. 72, no. 4, pp. 947–972, 2005.

[19] D. W. Yeung and L. A. Petrosyan, *Cooperative Stochastic Differential Games*, Springer Series in Operations Research and Financial Engineering, Springer, New York, NY, USA, 2006.

[20] S. P. Sethi and G. L. Thompson, *Optimal Control Theory: Applications to Management Science and Economics*, Springer Science & Business Media, 2006.

[21] Z.-M. Ren, Y.-Q. Shi, and H. Liao, "Characterizing popularity dynamics of online videos," *Physica A: Statistical Mechanics and its Applications*, vol. 453, pp. 236–241, 2016.

[22] E. Iveroth, A. Westelius, C.-J. Petri, N.-G. Olve, M. Cöster, and F. Nilsson, "How to differentiate by price: Proposal for a five-dimensional model," *European Management Journal*, vol. 31, no. 2, pp. 109–123, 2013.

[23] H. Choi, D. Medlin, and S. Hunsinger, "The effects of discount pricing strategy on sales of software-as-a-service (SaaS): online video game market context," *Journal of Information Systems Applied Research*, vol. 10, no. 1, pp. 55–64, 2017.

[24] D. Niu and B. Li, "Congestion-aware internet pricing for media streaming," in *Proceedings of the 2014 IEEE Conference on Computer Communications Workshops, INFOCOM WKSHPS 2014*, pp. 571–576, Toronto, ON, Canada, May 2014.

[25] N. Walz, M. Burkhardt, P. Eberhard, and M. Hanss, "A Comprehensive Fuzzy Uncertainty Analysis of a Controlled Nonlinear System With Unstable Internal Dynamics," *ASCE-ASME Journal of Risk and Uncertainty in Engineering Systems, Part B: Mechanical Engineering*, vol. 1, no. 4, Article ID 041008, pp. 1–12, 2015.

[26] G. W. Weber, I. Batmaz, G. Köksal, P. Taylan, and F. Yerlikaya-Özkurt, "CMARS: A new contribution to nonparametric regression with multivariate adaptive regression splines supported by continuous optimization," *Inverse Problems in Science and Engineering*, vol. 20, no. 3, pp. 371–400, 2012.

[27] A. Özmen, G. W. Weber, I. Batmaz, and E. Kropat, "RCMARS: Robustification of CMARS with different scenarios under polyhedral uncertainty set," *Communications in Nonlinear Science and Numerical Simulation*, vol. 16, no. 12, pp. 4780–4787, 2011.